8-2005

Analysis of 2D Spatial Filtering of Simulated Muscle Action Potential Using Grid Arrays

Mohammad Moshiur Rahman
University of Tennessee - Knoxville

To the Graduate Council:

I am submitting herewith a thesis written by Mohammad Moshiur Rahman entitled "Analysis of 2D Spatial Filtering of Simulated Muscle Action Potential Using Grid Arrays." I have examined the final electronic copy of this thesis for form and content and recommend that it be accepted in partial fulfillment of the requirements for the degree of Master of Science, with a major in Electrical Engineering.

Mohammed Ferdjallah, Major Professor

We have read this thesis and recommend its acceptance:

Michael J. Roberts, Aly Fathy

Accepted for the Council:
Carolyn R. Hodges

Vice Provost and Dean of the Graduate School

(Original signatures are on file with official student records.)

To the Graduate Council:

I am submitting herewith a thesis written by Mohammad Moshiur Rahman entitled "Analysis of 2D Spatial Filtering of Simulated Muscle Action Potential Using Grid Arrays." I have examined the final electronic copy of this thesis for form and content and recommend that it be accepted in partial fulfillment of the requirement for the degree of Master of Science, with a major in Electrical Engineering.

Mohammed Ferdjallah
Major Professor

We have read this thesis
and recommend its acceptance:

Michael J. Roberts

Aly Fathy

Accepted for the Council:

Anne Mayhew
Vice Chancellor and
Dean of Graduate Studies

(Original signatures are on file with official student records)

ANALYSIS OF 2D SPATIAL FILTERING OF SIMULATED MUSCLE ACTION POTENTIAL USING GRID ARRAYS

A Thesis
Presented For the
Master of Science
Degree

The University of Tennessee, Knoxville

Mohammad Moshiur Rahman
August 2005

Dedication

This work is dedicated to my beloved parents, Mohammad Nazibur Rahman and Amina Begum and all other family members. Without their love, support and encouragement, I could not come to this point of my life.

Acknowledgement

I would like to express my sincere appreciation to my supervisor Dr. Mohammed Ferdjallah for providing me the opportunity to work with him. His constant inspiration, guidance and comments have helped me in my research as well as in course work. I would like to thank my graduate committee, Dr. Aly Fathy and Dr. Michael J. Roberts for their guidance and help. I would like to convey my special thanks to Dr. Syed K. Islam helping me in course work and providing good advices and suggestions in different situations.

I would like to thank all my group members for their continuous support. I want to specially thank Mohammad Abdul Ahad for his valuable advice and help in research, Mohmmad Alam and Mohammad Adeeb for their help in course work, S.M Shajedul Hasan for his cooperation, Abdullah Al Zaman and Omer Sezer for their help on different occasions.

Finally, I would like to acknowledge my brothers and sisters for their support and encouragement during the many years of my academic life.

Abstract

Surface grid electrode is a noninvasive technique, which can be utilized for topographic analysis of EMG signals. In this study, an innovative spatial filtering technique is proposed in the form of grid electrodes to enhance the selectivity of surface EMG signal considering the effect of intermediate tissue layers between source and recording electrode. A simulation algorithm is developed to generate complete profile of single fiber action potential (SFAP) using previously derived mathematical model and published clinical data. A multiple-layer model is investigated in order to determine the potential distribution at the skin, fat and muscle surface based on the solution of the Poisson equation in spatial frequency domain. The arbitrary constants of the solution are determined by imposing the boundary conditions. The characteristics of subcutaneous fat and skin tissues are incorporated in the SFAP model to develop a systematic approach to select an appropriate inter-electrode distance of two dimensional grid arrays in order to eliminate spatial aliasing and distortion. The minimum grid spacing is determined by satisfying the Nyquist criterion for spatial sampling. The subcutaneous tissue layers reduce the frequency contents and attenuate the amplitude of the potential distribution at muscle surface. A two dimensional spatial filter is designed by manipulating the inverse of transfer function of fat and skin in order to compensate their spatial widening effect. The inverse transfer function is approximated to represent it in the form of filter mask for a discrete grid array. This spatial filtering technique is also investigated to eliminate the effect of a particular thick anisotropic medium inside muscle.

Table of Contents

List of Tables

List of Figures

Chapter 1

Introduction

1.1 Background

A muscle is an organ specialized to produce movement of a body part. Its cells convert the chemical energy of Adenosine triphosphate (ATP) into the mechanical energy of motion and exert useful functions like movement, stability, communication, heat production etc. All these functions are shared by three different kinds of muscle named heart muscle, smooth muscle and skeletal muscle. Heart muscle makes up the wall of the heart and involves in heart contraction to pump about five liters of blood in each minute. Smooth muscle is found in the walls of all hollow organs of the body except heart. Its contraction reduces the size of the attached structures and helps to regulate the flow of blood in the arteries, flow of air through lungs, movement of food through gastrointestinal tract etc. Skeletal muscle is attached to the skeletal structure of the body. The contraction of this muscle is under volunteer control. Skeletal muscle is mainly involved in all kinds of physical movement and stability. All muscular tissue has the following characteristics:

- Excitability: When stimulated by chemical signals, stretch and other stimuli, muscle cells respond with electrical changes across the plasma membrane.
- Conductivity: The local electrical change triggers a wave of excitation that travels

along the muscle and initiates processes leading to muscle contraction.

- Contractility: Muscle tissues have the ability to shorten substantially when stimulated. This enables them to pull on bones and other tissues and create movement of the body and its parts.
- Extensibility: A muscle cell has to be extensible to stretch between contractions in order to maintain its functionality. Skeletal muscle fibers can stretch to as much as three times their contracted length.
- Elasticity: It refers to the tendency of a muscle cell to return to the original length when tension is released.

1.1.1 Anatomy of Skeletal Muscle

A typical skeletal muscle cell is about 10 to 100 μm in diameter and up to 30 cm long. Because of their extraordinary length, muscle cells are usually called muscle fibers or myofibers. The physiological structure of a muscle is presented in Figure 1.1. Each muscle fiber is surrounded by a spare layer of connective tissue called endomysium, which allows room for blood capillaries and nerve fiber to reach muscle fiber. Muscle fibers are grouped in bundles called fascicles. Each fascicle is separated from neighboring one by a connective tissue sheath called perimysium. The muscle as a whole is surrounded by another tissue layer called epimysium. The collagen fibers of the epimysium continue as a strong fibrous tendon that merges into the nearby bone. The collagen fibers possess elasticity property and they are connected with each other in a linear series. That's why; they are called series-elastic components of a muscle.

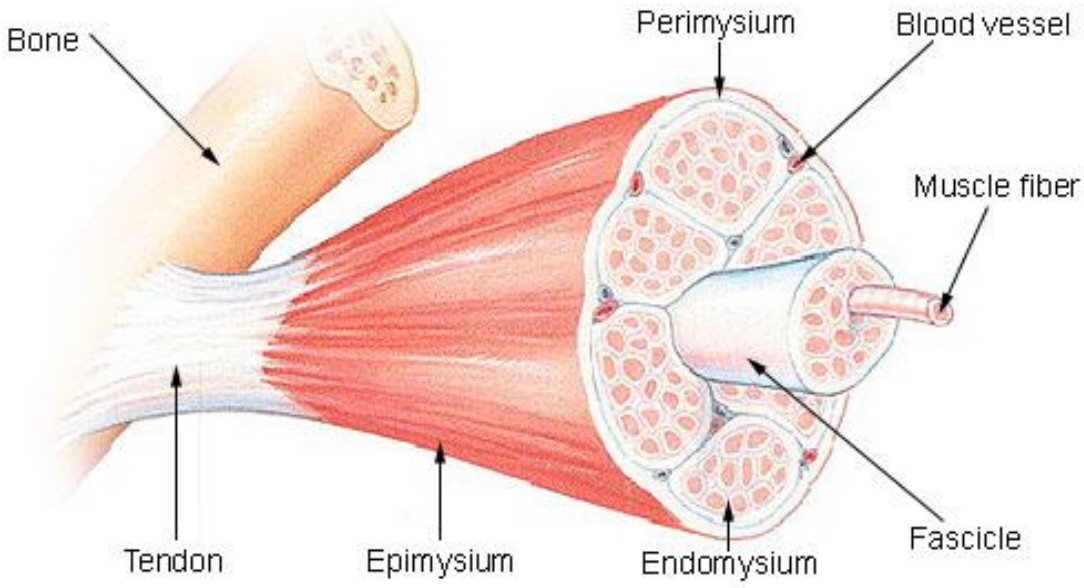

Figure 1.1: Structure of a skeletal muscle [14].

1.1.2 Muscle Fiber

Muscle fiber has a complex and tightly organized internal structure (Figure 1.2). The arrangement of the organelles and macromolecules of a muscle fiber need to be known in order to understand muscle function. Muscle fiber is originated by means of embryonic development. Several stem cells called myoblasts fuse to produce each muscle fiber by contributing nucleus. The plasma membrane of muscle fiber is called sarcolemma. It has tunnel like folded transverse (T) tubules that penetrate through the fiber and emerge on other side. The function of a T tubule is to carry electrical current from the surface of the cell to the interior when the cell is stimulated. The cytoplasm, named sracoplasm, is occupied mainly by about 1 μm diameter long protein bundles called myofibrils. Most other organelles of the cell, such as mitocondria and sarcoplasmic reticulum (SR), are located between adjacent myofibrils. The SR is a reservoir for calcium ions that can release a flood of calcium into sarcoplasm through gated channels to activate the muscle contraction process. The striated appearance of the muscle fiber is created by a pattern of alternating dark A bands and light I bands. Each A band consists of thick filaments lying side by side. The part of the A band, where thick and thin filaments overlap, is especially dark. In the middle of the A band, there is a lighter region called the H band. Thin filaments do not reach into this region. On the other hand, each light I band is bisected by a dark narrow Z disc composed of the protein. The Z disc provides anchorage for the thin filaments and elastic filaments. Each segment of myofibril from one Z disc to next is called a sarcomere, which is the functional contractile unit of the muscle fiber.

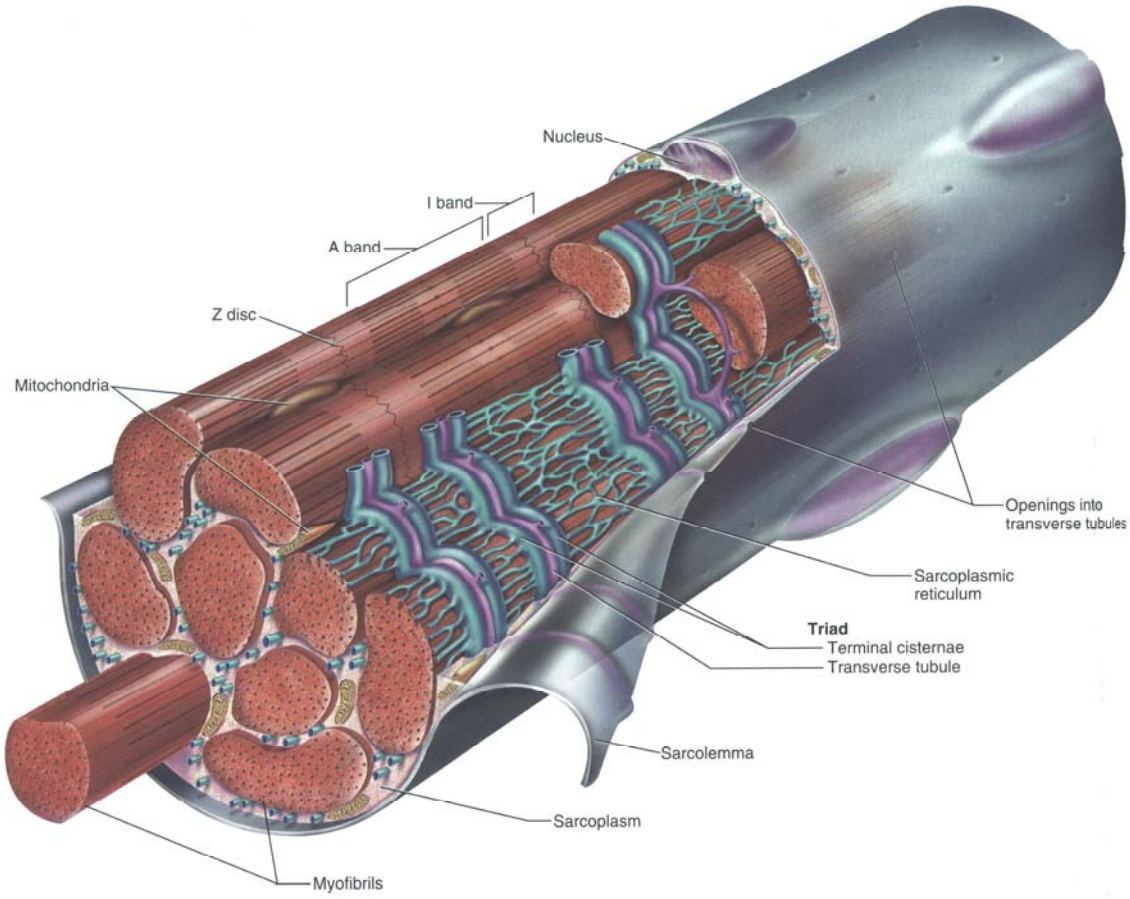

Figure 1.2: Structure of a skeletal muscle fiber [33].

1.1.3 Nerve Muscle Relationship

The skeletal muscles contract due to the stimulation of muscle fibers by motor neurons. The cell bodies of these neurons reside in the brainstem and spinal cord. The interfacing fiber between motor neuron and muscle is called axon, which is covered with myelin sheath. At the distal end, axon divides into many terminal branches. Each terminal branch innervates a muscle fiber. When a nerve signal approaches the end of an axon, it spreads out over all its terminal branches and stimulates all the muscle fibers supplied by them. So, all the excited muscle fibers contracts almost simultaneously. Since they behave as a single functional unit, one nerve fiber and all the muscle fibers innervated by it are called a motor unit (MU). Generally, the muscle fibers of a motor unit are distributed throughout muscle rather than being clustered together. A single motor unit can have 3-2,000 muscle fibers.

1.1.4 The Neuromuscular Junction

The functional connection between the terminal portion of a nerve fiber and a muscle fiber is called a neuromuscular junction. The structure and different organelles of neuromuscular junction is showed in Figure 1.3. The region of the muscle fiber, where the synaptic knob of nerve fiber is nestled on the sarcolemma called the motor end plate. A tiny gap of about 60 to 100 nm exists at the junction between the muscle and nerve cell called synaptic cleft. The synaptic vesicles reside at pre-synaptic ending store acetylcholine (ACh), which is used as a neurotransmitter substance. When a nerve impulse is received, ACh is released from synaptic vesicles. On the other hand, muscle

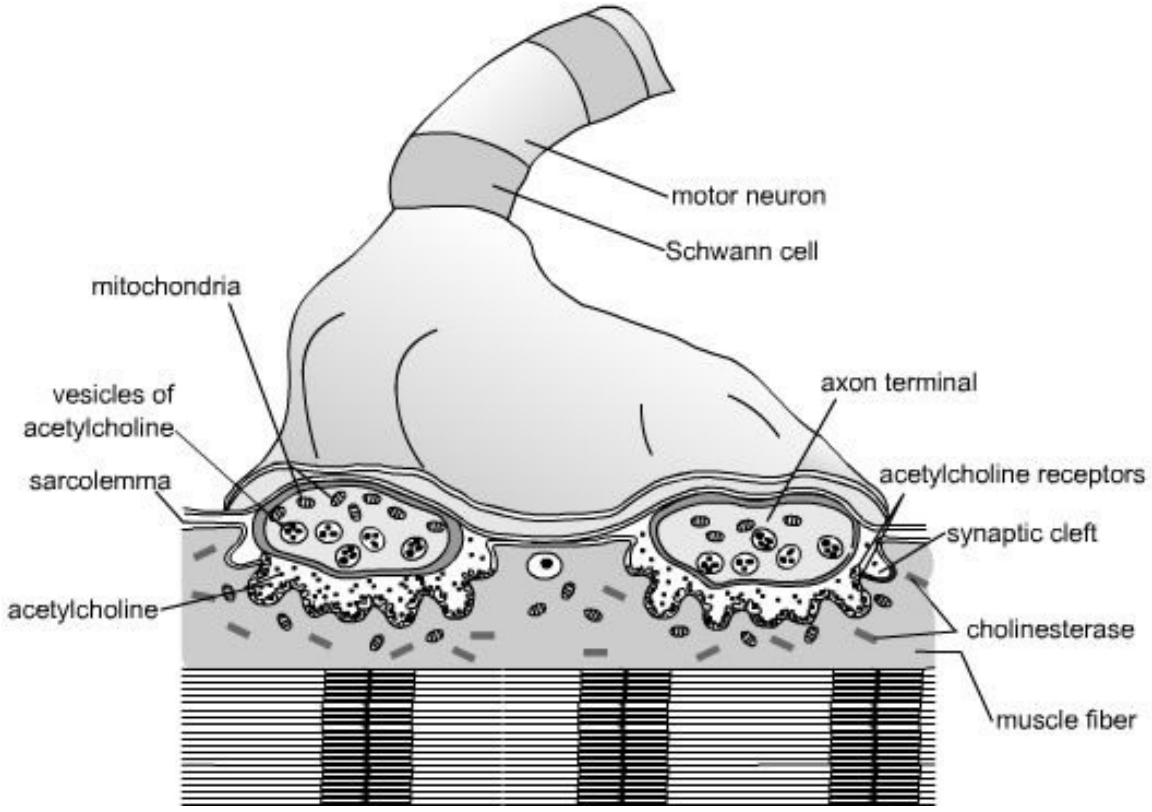

Figure 1.3: Neuromuscular junction [13].

fiber has about 50 million membrane proteins called ACh receptors, which bind the ACh released by the nerve fiber. Most of the ACh receptors are concentrated in and near the junctional folds at the end plate region. The muscle nuclei beneath the junctional folds are specifically dedicated to the synthesis of ACh receptors and other proteins of the motor endplate. The entire muscle fiber is surrounded by a basal lamina that also passes through the synaptic cleft. Both the sarcolemma and the part of basal lamina in the cleft contain an enzyme called acetylcholinesterase (AchE), which breaks down ACh, shuts down the stimulation of muscle fibers and allows a muscle to be relaxed.

1.1.5 Action Potential

The membrane of muscle and nerve fiber introduces a structural barrier to limit the movement of some ions, but permits others to diffuse freely. This selective permeability creates a potential difference across the membrane. In a resting muscle there are excess amount of sodium (Na+) and chloride (Cl-) ions in the extracellular fluid (ECF) outside the cell and excess amount of potassium (K+) ions and proteins in the intracellular fluid (ICF) within the cell. Due to this concentration gradient, K+ ions tend to diffuse or leak out of the cell into the ECF and Na+ ions tend to diffuse inside the ICF. But the membrane of the resting muscle cell is more permeable to K+ than to Na+ and prevents the negative protein from leaving the cell. The diffusion of K+ continues until the ICF reaches a negative potential with respect to the positively charged ECF. At a dynamic equilibrium condition, the potential difference across the membrane contributed by the diffusion of Na+ and K+ is called resting membrane potential. The typical value of resting potential is –70 mV to -90 mV in muscle.

When a muscle is stimulated, a change in potential distribution of the membrane takes place through some steps of electrophysiological phenomena. Initially, the nerve signal excites the synaptic vesicles of axon, which release ACh in the synaptic cleft. ACh diffuses across the synaptic cleft and binds with the receptor proteins of the muscle fiber. These bindings open ion channels in the plasma membrane through the middle of receptor protein. Each channel allows Na+ ions to diffuse quickly inside the intracellular region. The movement of positive ions overrides the negative charges in the ICF and makes the inside of the plasma membrane positive. As it inverts the polarity of the plasma membrane, this is termed as depolarization. After a short period, AchE enzyme is released, which closes the gates of Na+ ions in the membrane and opens the gates of K+ ions. Then the K+ ions rush of the intracellular region due to repulsion of Na+ and concentration gradient. The loss of positive potassium ions from the cell turns the inside of the membrane negative again. The change of inverted polarity of the membrane back to its resting condition is called repolarization. Thus, the membrane potential changes from negative resting potential to a positive value and then backs to a negative value again (Figure 1.4). This rapid fluctuation in membrane voltage is called action potential (AP). The generation of action potential in the fiber end plate is termed as excitation. Thus, the action potential is generated or the excitation occurs whenever the membrane is depolarized at or beyond a particular threshold level and follows a constant sequence of depolarization and repolarization of the membrane. The action potential generated in the end plate region is self-propagating. Action potential at one point on a plasma membrane causes another one to happen immediately in front of it, which triggers another one a little farther along and spreads like a wave over the membrane until it has moved along

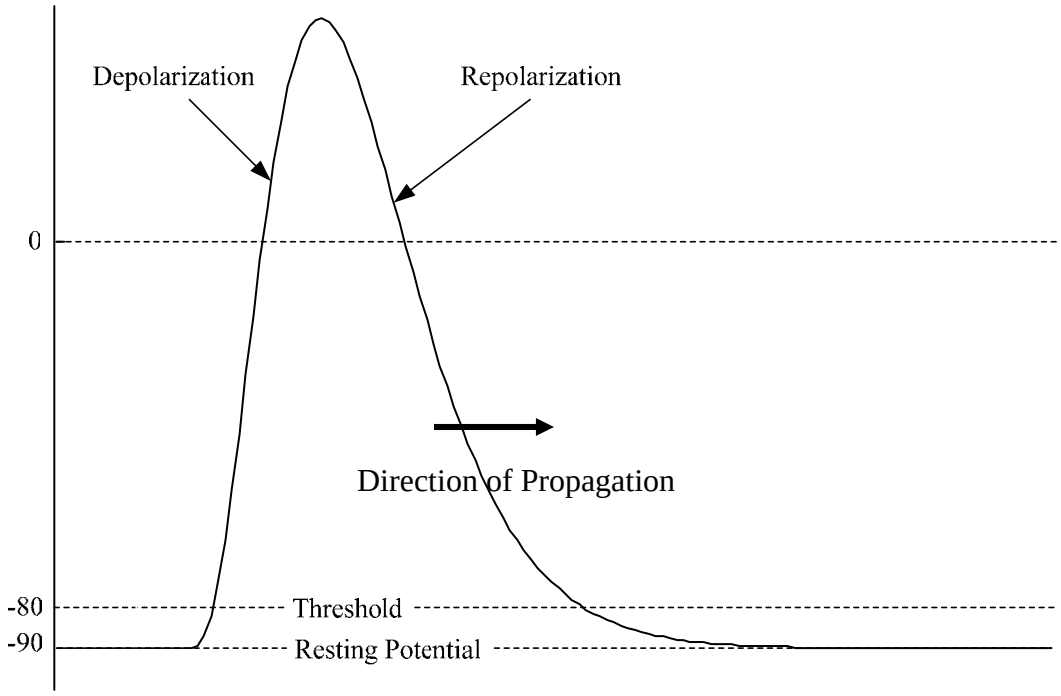

(a)

(b)

Figure 1.4: Behavior of action potential- (a) various phases of the action potential, (b) mechanism of conduction of action potential in muscle fiber.

the entire muscle fiber. The conduction speed of action potential mainly depends on the diameter of the fiber. Larger fibers conduct more rapidly than the small fibers as they have a lower resistance.

1.2 Electromyography

Electromyography (EMG) is an electrophysiological technique used to study the activity of muscle through detection and analysis of the electrical signals generated during muscular contractions. On the basis of application, electromyography can be classified in two main categories: clinical and kinesiological. Clinical or Diagnostic EMG, typically done by physiatrists and neurologists, are studies of the characteristics of the muscle bioelectric potential for amplitude, duration and phase. These are typically done to diagnosis neuromuscular disorder. The evaluation of the spontaneous discharges of relaxed muscles and the isolation of single motor unit activity are also involved in this study. Kinesiological EMG is considered as the study of muscular behavior regarding movement analysis. This study is mainly applied to analyze muscle function during biofeedback training, dynamic or static activities of sports and activities in daily livings. It helps to establish the relationship of muscle function to movement of the body segments and evaluates timing of muscle activity with regard to the movements. Additionally, some studies are attempted to examine the strength and force production of the muscles themselves. So, all kinds of studies associated with the electrical response of muscle due to nervous stimulation are performed by means of Electromyographic technique.

1.3 EMG Signal

The electrical signal that depicts the biomechanical and pathological states of musculoskeletal or neuromuscular system is called EMG signal (Figure 1.5). The measuring of EMG signal is associated with the activation of the muscle. This may be voluntary or involuntary muscle contraction. The functional unit of the muscle contraction is a motor unit, which is comprised of a single motor neuron, a myelinated axon, neuromuscular junctions and all the muscle fibers it enervates. When a muscle fiber becomes excited, the propagation of end plate potential generates an electromagnetic field and the potential at any point in the field can be measured as voltage. The motor unit action potential (MUP) is the spatial and temporal summation of the individual action potentials for all the fibers of a single motor unit. To measure EMG

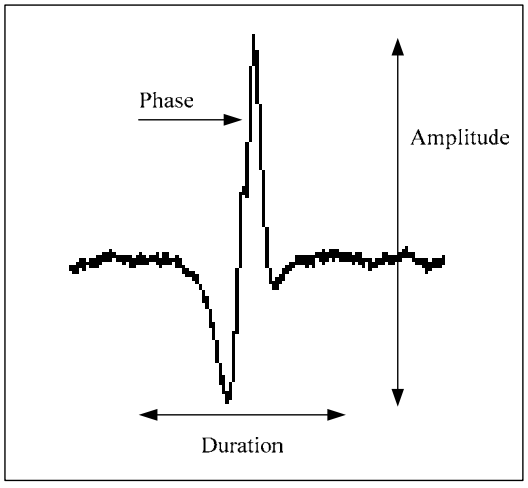

Figure1.5: Various components of a typical EMG signal.

signal a special type of device called electrode is placed close to an appropriate muscle. Therefore, the EMG signal is the algebraic summation of the motor unit action potentials within the pick-up area of the electrode. The pick-up area of an electrode will almost always include more than one motor unit as muscle fibers of different motor units are intermingled throughout the entire muscle.

1.4 EMG Instrumentation

The recording of EMG signal involves accurate and continuous detection of electrical potential distribution. Generally, the voltage and frequency ranges of EMG signal are between 0.5 μV to 10 mV and 2 to 10000 Hz respectively. Hence, the instrumentation should be precise enough to detect, process and display this tiny signal accurately. The basic instrumentation system is comprised of electrodes, amplifier, stimulator and display unit (Figure 1.6). The brief overview of different electronic components or instruments is presented below.

1.4.1 Electrodes

Electrode is the main interfacing unit between muscle or body surface and EMG machine. It serves as conductor linking the body to the electronic system. It is an electrical terminal to which a conductor can be attached to allow a current to flow. A positively charged terminal is called anode, while a negatively charged terminal is called cathode. Thus, electrode transfers the electrical signal of motor units to the electronic system. At the same time, electrode is used to transmit electrical signal to a specific

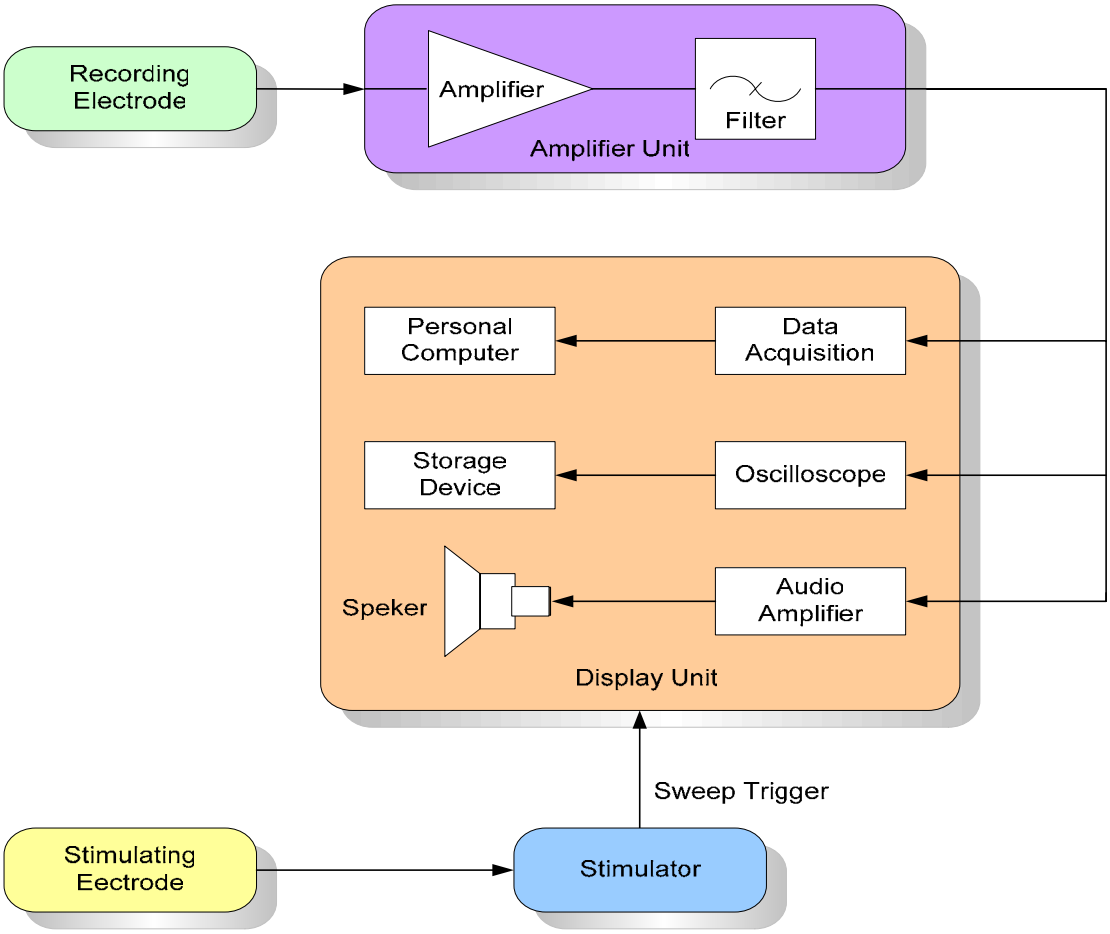

Figure 1.6: Basic components of EMG instrumentation.

muscle to stimulate involuntary contraction. So, according to application electrode can be classified in two different types: recording electrodes and stimulating electrode.

a. Recording Electrodes

Generally, three electrodes are involved in measuring of EMG signal of a specific muscle. One works as an active or exploring electrode and another one serves as an indifferent or reference electrode. The third electrode placed at some distance from the other two electrodes serves as ground. On the basis of application, mainly two types of electrodes are used to record EMG signal: surface electrode and needle electrode.

Surface electrodes, passive or active, are noninvasive small metallic discs, which can be taped to the skin. They are of different shapes and cover a wide range of surfaces of the overlying skin. The focal points of surface electrodes are greater than 50 mm^2. The impedance between electrode and the skin must be reduced to obtain a technically satisfactory recording. This can be achieved by applying conducting gel under the electrode and extensive skin preparation. Comfort and ease of use are the major advantages of surface electrodes in dynamic EMG. There are also several disadvantages of surface electrodes. The adhesive used on the surface of the body for this type of electrodes does not stick for a long time on sweaty skin. Even the electrode cannot be put on bony prominences and movement or motion creates significant problem with long term monitoring resulting in a gross change in potential. But additional tape or rough surface electrode that digs past the scaly outer layer of skin can be used to recover this problem partially sacrificing the comfort of patients.

Needle electrodes are invasive electrodes, which are inserted into tissue beneath skin by puncturing the skin on an angle. Needle electrodes are used when activity from a single or few motor units is to be recorded. The focal points of needle electrodes are usually less than 1 mm^2 and can therefore detect a small area with in the muscle. The advantages of needle electrodes are an increased bandwidth, a more specific pick-up area, ability to test deep muscles and isolation of specific muscle parts, which would be impossible to detect with a surface electrode due to cross talk. But, the needle insertion causes discomfort and the measurements are less repeatable as it is very difficult to place the needle in the same area of the muscle each time. Moreover, sometimes it may occur cramping.

b. Stimulating Electrodes

In many electro diagnostic procedures, it is necessary to stimulate nerve or muscle electrically. A rectangular pulse of current is passed for a brief period through the muscle to be stimulated by means of electrode. Stimulating electrodes are usually of the surface type. These electrodes commonly consist of two protruding metal buttons fixed in a small plastic box. The resistance of dry skin to the flow of an electric current is reduced by lightly covering the electrode with electrode jelly. The monopolar needle electrode is used to stimulate a deeply situated muscle. Any part of stimulating current may influence the potential of recording electrode. It is therefore important to limit the spread of stimulating current. This is achieved by making the impedance between stimulating electrode and ground very high, which is in turn accomplished through the use of an isolation transformer.

1.4.2 Amplifier Unit

The EMG signal picked up by recording electrode is very small in magnitude and contains undesired interference signal. The undesired signals are originated from movement artifact of electrode, harmonics of power supply and several sources, either inside or outside the patient. That's why, the recorded signal must be conditioned and amplified properly for further signal processing and display. The amplifier unit consists of several separate amplifiers. An amplifier has to meet certain features to process the detected EMG signal. The interference signals are common to both active and reference electrode. So, differential amplifier is used to reject the common mode signal. This ability of a differential amplifier is represented by common mode rejection ratio (CMRR), which can be measured by taking the ratio of differential gain and common mode gain of the amplifier. A high CMRR (typically grater than 10000) is essential for rejecting interference from electromyographic recording. Another important property of an amplifier is its input impedance. The connection between electrode-tissue junction and amplifier introduces high impedance. The effect of this high series impedance can be reduced or eliminated by making the input impedances of the amplifier many times greater than that. High input impedance of the amplifier reduces the current from the original motor unit signal preserving the magnitude of voltage. Generally the frequency range of EMG signal is from 2 to 10,000 Hz. The bandwidth of the amplifier has to cover all the frequency components of the signal. Sometimes band pass filter is included in front of amplifier to limit the frequency contents of the signal depending upon type of recording electrode. The gain of the amplifier has to be high enough to make the signal compatible for display and to operate other components of the system.

1.4.3 Display Unit

The EMG signal obtained from amplifier unit is displayed by means of an analog or digital system. The cathode ray oscilloscope helps us to visualize the instantaneous changes in bioelectric potential. The beams of electrons can be deflected in horizontal and vertical direction by applying the potential difference between suitably placed electrodes. But the electron beam of the oscilloscope has a very small mass and inertia. It cannot respond to and display instantaneous electrical signals properly. Moreover, the signal cannot be manipulated to facilitate measurement or analysis. These limitations of oscilloscope arouse the necessity to introduce digitization and signal processing technique in acquisition, store, analysis and display of EMG signal. In digital technique, software controlled data acquisition system works as an interfacing unit between amplifier unit and personal computer. It is possible to characterize any waveform as a list of numeric values or bits by means of analog to digital conversion technique. Then the digital signal is again converted into original analog signal after being processed with appropriate DSP algorithm. Different methods of digital signal processing help us to extract some specific parameters from the EMG signal, which can be correlated with physiological activities of muscle to detect diseases and apply proper medication. Some times it becomes valuable to listen to the sound generated form EMG signal along with visual display in recognizing particular signal associated with normal and abnormal muscle. Generally, the variation of frequency of EMG signal occurs within the audible range of human. The changes in frequency can be amplified and fed to a loud speaker for listening. The audio-monitor technique is really helpful, when a muscle is being examined by needle electromyography.

1.5 Review of Previous Research

EMG is an essential tool to interpret the pathological state of musculoskeletal or neuromuscular system. It is also used in the study of muscular functions during biofeedback training, activities of sports and daily livings. In particular, EMG offers valuable information concerning the timing of muscular activity and its relative intensity [3,5,22]. The advantages of surface electromyography have caught the interest of researches in different arena of muscle research. Till now numerous studies have already been performed directed towards the analytic and numerical modeling of muscle fiber action potential, detection methodology and analysis of simulated and experimental signals. The general goal is to explore new parameters regarding muscle anatomy and functionality.

Several approaches have been presented to simulate the extracellular potential by volume conduction theory [1,19,28,29,33]. In 1969, Paul Rosenfalck [33] first presented the mathematical analysis of the spread of action potential within nerve and muscle fibers. He developed the relationship between the extracellular and intracellular potential on the basis of Maxwell field equation. He modeled the intracellular potential with a mathematical expression by means of signals recorded from isolated frog muscle fibers in Ringer's solution and in air. In 1881, Andreassen et al [1] have extended this model by approximating the muscle structure with anisotropic volume conductor model. They have incorporated Bessel function in deriving the solution of extracellular medium. But they concluded that the accuracy of their model is limited by the uncertainty of the input

parameters rather than accuracy of the model itself. In 1983, Nandedkar and Stalberg [27] introduced a line source model with a simplified approach of the transfer function of the medium. They used the concept of potential produced by a point source located at the origin of cylindrical coordinate system. In 1990, Gootzen et al [13] reported the influence of the finite dimension of volume conductor and fiber length on single fiber action potential. Their described model is found to be capable of generating surface MUP, which showed a very good resemblance with measured signal. In 1999, Merletti et al [26] investigated the relationship between the parameters of active motor unit by using mathematical model of surface electromyographic signal. In 2001, Farina et al [10] proposed a new model of EMG signal generation and detection by describing volume conductor as a inhomogeneous and anisotropic medium constituted by muscle, fat and skin tissue. He presented the transfer function in the form of two-dimensional filter function. Later on most of modeling studies were focused around the precise representation of multiple layer volume conductor model [2,11,20].

Besides the modeling studies, an emphasis was given to develop detection technique in order to achieve deeper understanding of electrical phenomena taking place inside muscle. The typical monoploar or bipolar surface EMG technique reflects the compound activity of large number of motor units. But the most detailed information about structural and functional characteristics of the muscle, such as functional anatomy, excitation spread or the pattern of innervation zone can be gained from single MU action potential. To improve the spatial resolution, the surface detection technique has been extended to one and two dimensional grid array [2,24,31]. In 1979, Lynn [21] estimated

the propagation velocity of the electrical activity along muscle fiber by using a linear array. In 1987, Reucher et al [31] introduced the spatial filtering principal to electromyography by combining the signals of several recording electrodes to form one output signal. He used one-dimensional quadruple differentiating filter and double differentiating filter to improve the spatial selectivity of the signal. Masuda et al [24] improvised the concept of two-dimensional detection technique in order to eliminate the limitations of linear array. In 1997, Rau et al [30] used the high spatial resolution surface grid electrode to implement the high pass normal double differential (NDD) filter. Though this spatial filtering technique is limited to superficial motor units, it correctly identified 87% of all investigated patients with neuronal disorder. Later Disselhorst-Klug et al [6] showed a theoretical and experimental comparison of NDD, IR (Inverse rectangle) and IB (Inverse binomial) filter in order to improve the spatial resolution of surface EMG signal. In 1999, Ferdjallah et al [12] reported the effect of size and dimension of recording electrode on surface motor unit action potential. He suggested that both the peak-to-peak amplitude and mean frequency decrease with the increment of the diameter of electrode, where as the conduction velocity remains almost constant. Farina et al [7,8] introduced a systematic approach of designing spatial filter from transfer function and compared it with traditional high pass filter. He also studied on the influence of anatomical, physical and detection system parameter on surface EMG [9]. In 2004, Lapatki et al [18] opened a new era in surface detection technique by developing a thin, flexible two-dimensional multi electrode grid. This flexible grid can be cut out in any required size and can be placed on uneven surface of the body maintaining good electrical connection in the whole recording area.

1.6 Problem Statement

The enhancement of topographic imaging is a vital issue to improve clinical use of electromyography (EMG). Several applications of electromyographic imaging are especially relevant to the rehabilitation of individuals with physical disabilities. The default anatomy guide sometimes misleads to detect the exact location of infected muscle fiber prior surgery. Electromyographic imaging will provide a systematic way of assessing changes in gross muscle anatomy caused by any surgical procedures. Moreover, it will facilitate to explore unknown parameters regarding the activity of muscle. Surface grid electrode technique can be utilized for topographic analysis of EMG signals. Grid electrode increases the uptake area and provides a better picture of spatial and temporal characteristics of muscle activity. But several factors are associated with the design of grid electrodes. The detected signal is severely influenced by the material compositions, size, shape and dimension of recording electrode. Beyond these factors the total dimension of grid array directly depends on the value of inter-electrode distance. Grid spacing needs to be calculated precisely to obtain image free from spatial aliasing and distortion. The bioelectrical signal obtained at electrode is substantially affected by the conduction medium between excited muscle fiber and electrode. But two additional layers of subcutaneous fat and skin exist over the anisotropic medium of muscle. The properties of these additional layers deteriorate further the characteristics of actual surface EMG signal. This initiates the necessity of designing a filter to eliminate the effect of fat and skin. The aim of this study is to design and analyze the two-dimensional spatial filtering technique in the form of discrete grid electrode in order to

enhance the spatiotemporal image of surface EMG signal. The documentation of this research is organized in four parts.

A complete analytic muscle model is presented in chapter 2. The mathematical representations of muscle fibers and their electrophysiological behavior are developed based on the work of previous study. A simulation algorithm is developed to generate a profile of single fiber action potential (SFAP) using published anatomic and clinical data. Then the behavior of SFAP is analyzed by varying the position of recording electrode and depth of muscle fiber.

In chapter 3, a multiple-layer volume conductor model is developed incorporating the isotropic layer of fat and skin over the anisotropic medium of muscle tissue. The expression of muscle activity at each individual layer is derived by introducing boundary conditions in the solution of differential equations. The effect of fat and skin is analyzed by varying fat thickness and conductivity ratio. Then the validity of multiple-layer model is justified by comparing it with the previously derived single layer model.

In chapter 4, a systematic approach is developed to select an appropriate inter-electrode distance of two dimensional grid arrays by taking in to account relevant spatial characteristics of surface EMG signals. The required minimum inter-electrode distance is tabulated for three different level of accuracy. A two-dimensional inverse spatial filter is designed to compensate the effect of fat and skin layers. The inverse transfer function of fat and skin medium is approximated in order to determine a discrete filter with a matrix

of electrodes. The filter characteristic is determined by the weighting factors and geometrical arrangement of electrodes. Then, this spatial filter technique is extended with designing a filter mask to eliminate the effect of anisotropic muscle layer of particular thickness.

Finally, the work done in the thesis is summarized in chapter 5. This chapter also includes the discussion of the future work directions that may help to improve the performance of spatial filter and explore new field of its application.

Chapter 2

Analytic Muscle Model

2.1 Importance of Analytic Model

Electromyographic signal plays a vital role to obtain the information regarding the anatomy and physiology of skeleton muscles. In measuring EMG signal, the recording electrode detects all the bioelectric potentials generated surrounding the pick up region. This deteriorates the analysis of specific muscle or motor unit. This problem can be greatly reduced by constructing a mathematical model that incorporates the available information of the size, structure and function of the generators. A mathematical model provides a framework for the interpretation of recorded potentials and makes it possible to derive further information about the generator. More over, the analytic modeling technique, enhances the application of EMG signal, reduces the complexity of performing tedious and expensive experimental measurements and boost up the development of different DSP algorithm for post processing of measured signals. Modeling technique cannot be considered as a substitute of experimental and clinical electromyography. It interplays with various measurement activities to improve detection methodology, properties and placement of electrode, signal to noise ratio and stimulation technique to control the firing pattern of muscle fiber. So, analytic model development and simulation of EMG signal considering different physiological structure of source, properties of recording electrode and various electromechanical artifacts,

works as an important tool to accelerate research in clinical neurophysiology, rehabilitation and ergonomics.

2.2 Derivation of Analytic Model

Inside the muscle, fibers are surrounded with thin membrane and distributed in the conductive medium of extracellular fluid. To derive the potential profile generated by an excited fiber, the whole muscle can be considered as a finite volume having a current source inside it. Paul Roselkfalck first introduced the volume conductor model of muscle considering the propagation of active membrane potential as a line source [33]. Two assumptions were made in deriving the behavior of muscle fiber action potential:

- The shape of muscle fiber is almost cylindrical as the fiber radius is very small in comparison to its length.
- The potential generated inside the intracellular fluid due to excitation of muscle fiber is insensitive to the changes in the impedance of the extracellular medium.

These two assumptions are considered to develop the simplest possible model regarding the behavior of action potential generated by a single muscle fiber. A simple structure of computer muscle model is presented in Figure 2.1. The human muscle is modeled as a group of M motor units. Each motor unit, in turn, is modeled as a group of N parallel fibers distributed within its territory. The position of neuromuscular endplate divides each muscle fiber in two equal parts along its length. The action potential of a motor unit

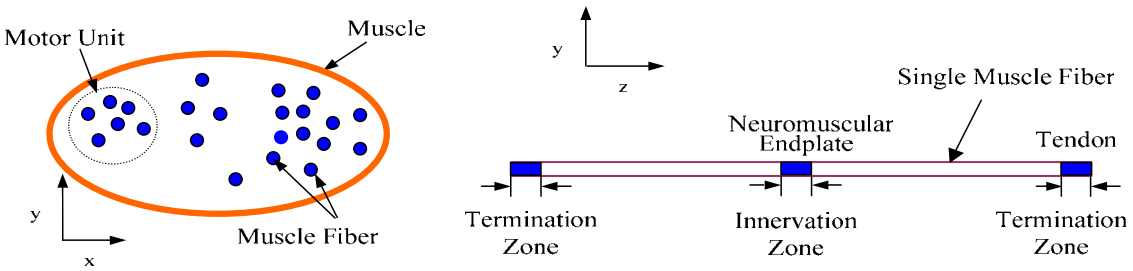

Figure 2.1: Illustration of the computer muscle model.

can be obtained by taking the summation of action potentials of each individual fiber considering their orientation inside muscle. In the same manner, it is possible to obtain the action potential of an entire muscle, which is termed as compound motor unit action potential (CMAP). The profile of CMAP for a particular muscle can only be generated by simulating the mathematical model considering muscle structure and electrophysiological parameters.

2.2.1 Mathematical Theory

Maxwell's equations, in their general form, relate the dynamic electric and magnetic fields with one another and with the electrical charges and currents present in the medium. The time-varying fields associated with electromyographic currents are considered low frequency fields, and thus, the wavelength of the harmonic fields is considerably larger than the dimensions of human muscles. Thus, the electrical field distribution can be approximated by a static field satisfying the time-varying boundary

conditions. For the case of an electrostatic medium,

$$D = \varepsilon E \tag{2.1}$$

$$\nabla . D = \rho_v \tag{2.2}$$

$$E = -\nabla \varphi \tag{2.3}$$

where D, E, φ, ρ_v, ε are electric flux density, electric field intensity, potential, volume charge density and permittivity of the medium respectively. Using Equation (2.1), (2.2) and (2.3) the relationship between field potential, φ and volume charge density, ρ_v in a homogeneous medium can be stated using Poisson's equation as:

$$\nabla^2 \varphi = -\frac{\rho_V}{\varepsilon} \tag{2.4}$$

where ∇^2 is a three dimensional differential operator, which can be expressed as:

$$\nabla^2 = \frac{\partial^2}{\partial x^2} + \frac{\partial^2}{\partial y^2} + \frac{\partial^2}{\partial z^2} \tag{2.5}$$

Electrostatic is concerned with electrical charges and field in a dielectric medium while the interest of bioelectric potential lies in currents in conducting medium. The mathematics of current flow in a volume conductor corresponds so closely with that of charges in a dielectric medium. For the case of electrophysiology, Poisson's equation can be stated as:

$$\nabla^2 \varphi = -\frac{I_V}{\sigma} \tag{2.6}$$

where I_v, σ are volume current density and conductivity of the medium respectively. In the case of muscle fiber, the sources are constrained on the membrane of the active fiber. It makes Laplace's equation valid to represent the potential field distribution in the

intracellular and extracellular medium.

$$\nabla^2 \varphi = 0 \tag{2.7}$$

Based on the assumption of quasi-stationary condition, wave propagation effects, capacitive effects and inductive effect can be ignored in the calculation of potential. But the medium surrounding the muscle fiber is not isotropic. It has different conductivity in parallel (z direction) and perpendicular (x or y direction) direction of fiber. Due to the anisotropy of the extracellular medium (i.e. parallel conductivity σ_z and perpendicular conductivity $\sigma_x = \sigma_y = \sigma_r$) field potential is expressed using modified Laplace's equation as:

$$\nabla^2 \varphi(x,y,z) = \sigma_r \left(\frac{\partial^2 \varphi(x,y,z)}{\partial x^2} + \frac{\partial^2 \varphi(x,y,z)}{\partial y^2} \right) + \sigma_z \left(\frac{\partial^2 \varphi(x,y,z)}{\partial z^2} \right) = 0 \tag{2.8}$$

$$\nabla^2 \varphi(x,y,z) = \left(\frac{\partial^2 \varphi(x,y,z)}{\partial x^2} + \frac{\partial^2 \varphi(x,y,z)}{\partial y^2} \right) + R_a \left(\frac{\partial^2 \varphi(x,y,z)}{\partial z^2} \right) = 0 \tag{2.9}$$

where $R_a = \frac{\sigma_z}{\sigma_r}$, ratio of longitudinal and radial conductivity. Assuming rotational symmetry, Equation (2.9) can be written in the cylindrical co-ordinate system as:

$$\nabla^2 \varphi(r,z) = \frac{\partial^2 \varphi(r,z)}{\partial r^2} + \frac{1}{r} \cdot \frac{\partial^2 \varphi(r,z)}{\partial r^2} + R_a \frac{\partial^2 \varphi(r,z)}{\partial z^2} = 0 \tag{2.10}$$

where $r = \sqrt{(x^2 + y^2)}$. It is only necessary to transform the distance along z-axis to spatial angular frequency, ω_z to represent Equation (2.10) in the spatial frequency domain.

$$\nabla^2 \phi(r,\omega_z) = \frac{\partial^2 \phi(r,\omega_z)}{\partial r^2} + \frac{1}{r} \cdot \frac{\partial^2 \phi(r,\omega_z)}{\partial r^2} - R_a \, {\omega_z}^2 \phi(r,\omega_z) = 0 \tag{2.11}$$

Using the modified Bessel function, I_0 and K_0, the solution of Equation (2.11) for an

infinite volume conductor can be written as [1,17]:

$$\phi(r,\omega_z) = A(\omega_z) I_0\left(r\sqrt{R_a}\,\omega_z\right) + B(\omega_z) K_0\left(r\sqrt{R_a}\,|\omega_z|\right) \tag{2.12}$$

where $A(\omega_z)$ and $B(\omega_z)$ can be solved by using boundary condition. The potential distribution is a continuous decay function with respect to the radius of the cylindrical volume and it approaches to zero at $r \to \infty$. Since $I_0 \to \infty$ for $r \to \infty$, the general solution turns into,

$$\phi(r,\omega_z) = B(\omega_z) K_0\left(r\sqrt{R_a}\,|\omega_z|\right) \tag{2.13}$$

A boundary condition is needed to solve the potential distribution in the extracellular region. In a muscle fiber, the extracellular potential is generated by the transmembrane current, flowing inward and outward during depolarization and repolarization.

2.2.2 Source Description

To describe the extracellular field, either the membrane voltage or the membrane current density may be considered to be the field source. The intracellular or membrane potential can be measured by standard microelectrode technique. A mathematical description of the membrane voltage has been suggested by Rosenfalck [33]. By means of a precise experimental setup he came up with this specific model, which can be expressed as:

$$V_m(z) = \alpha(\lambda z)^3 e^{-\lambda z} - \beta \tag{2.14}$$

where parameter α, β and λ were adjusted to give reasonable fit with experimental resting and action potentials in muscle. The factor $e^{-\lambda z}$ was chosen since later part of the phase of repolarization in a muscle fiber declines exponentially. Multiplying $e^{-\lambda z}$ by z^3

gave simulation of both the phase of depolarization and initial phase of repolarization. The generated endplate potential propagates towards the ending or tendon of muscle fiber with a conduction velocity. This propagation of potential introduced the concept of transmembrane current. At the neuromuscular endplate and muscle fiber endings, the transmembrane current is constrained by the excitation and extinction principles. However, far from the neuromuscular endplate and the fiber endings, the transmembrane current is proportional to the second derivative of the intracellular potential [1,33]:

$$\begin{aligned} i_m(z) &= \frac{\sigma_i a}{2} \frac{\partial^2 V_m(z)}{\partial z^2} \\ &= \frac{\sigma_i a}{2} \alpha \lambda^2 (\lambda z) \cdot \left[6 - 6\lambda z + (\lambda z)^2\right] e^{-\lambda z} \end{aligned} \tag{2.15}$$

where, σ_i is the intracellular conductivity and a is the radius of fiber. The transmembrane current is considered as discrete point sources along the axis of muscle fiber.

2.2.3 Solution for Extracellular Potential

The boundary condition at the interface of intracellular and extracellular medium can be expressed by membrane current, I_m to get the solution of field potential:

$$\left.\frac{\partial \phi(r, \omega_z)}{\partial r}\right|_{r=a} = -\frac{I_m(\omega_z)}{\sigma_r} \tag{2.16}$$

Introducing the boundary condition in Equation (2.13), the value of $B(\omega_z)$ can be obtained as:

$$B(\omega_z) = \frac{I_m(\omega_z)}{\sigma_r \sqrt{R_a}|\omega_z| K_1\left(a\sqrt{R_a}|\omega_z|\right)} \tag{2.17}$$

where $K_0^{'} = -K_1$. Inserting the expression of $B(\omega_z)$, obtained from boundary condition,

in Equation (2.13) the solution of extracellular potential for an infinite volume conductor can be written as:

$$\phi(r,\omega_z)=\frac{I_m(\omega_z)}{\sigma_r}\frac{K_0\left(r\sqrt{R_a}\,|\omega_z|\right)}{\sqrt{R_a}|\omega_z|K_1\left(a\sqrt{R_a}|\omega_z|\right)} \tag{2.18}$$

Taking the inverse Fourier transform, the extracellular potential distribution in space domain can be expressed as:

$$\varphi(r,z)=\frac{1}{2\pi\sigma_r}\int_{-\infty}^{\infty}\frac{K_0\left(r\sqrt{R_a}\,|\omega_z|\right)}{\sqrt{R_a}|\omega_z|K_1\left(a\sqrt{R_a}|\omega_z|\right)}I_m(\omega_z)\,e^{-i\,\omega_z z}\,d\omega_z \tag{2.19}$$

To calculate the potential distribution, at first it is necessary to obtain the expression for source current $i_m(z)$. Then $\varphi(r,\omega_z)$ can be calculated for a specific position of recording electrode with respect the muscle fiber by using the discrete Fourier transform of transmembrane current and evaluating Bessel functions K_0, K_1. Again inverse Fourier transform of $\phi(r,\omega_z)$ readily provides $\varphi(r,z)$. These processes can be carried out adopting the algorithm of Fast Fourier Transform (FFT). Though above procedure involves moderate calculation load, it might be helpful for the understanding of extracellular field to have simple expressions that do not involve Fourier transform. For simplification Equation (2.18) can be divided into two parts as:

$$\phi(r,\omega_z)=H(r,\omega_z)\cdot I_m(\omega_z) \tag{2.20}$$

where $H(r,\omega_z)=\frac{1}{\sigma_r}\frac{K_0\left(r\sqrt{R_a}\,|\omega_z|\right)}{\sqrt{R_a}|\omega_z|K_1\left(a\sqrt{R_a}|\omega_z|\right)}$

$H(r,\omega_z)$ can be termed as weighting function or transfer function of the volume conductor in the spatial frequency domain. So, in the space domain extracellular

potential can be expressed as a convolution between the membrane current and weighting function.

$$\begin{aligned}\varphi(r,z) &= i_m(z) * h(r,z) \\ &= \int_{-\infty}^{\infty} i_m(s).h(r,z-s)ds\end{aligned} \tag{2.21}$$

The behavior of different parts of $H(r,\omega_z)$ can be analyzed to develop a simplified expression for *h(r,z)*. In the frequency domain the intracellular potential is limited to frequencies below 10 kHz and $I_m(\omega_z)=0$ for $|a\omega_z|>0.44$ [1]. So, it is unimportant to consider the weighting function beyond this limit. Introducing this condition, weighting function can be approximated as:

$$H(r,\omega_z)=\frac{1}{\sigma_r}\frac{aK_0(r'|\omega_z|)}{a'|\omega_z|K_1(a'|\omega_z|)} \quad for\ |a'\omega_z|\le 0.44 \tag{2.22}$$

where $a'=a\sqrt{R_a}$ and $r'=r\sqrt{R_a}$. From the behavior of the first order modified Bessel function (Figure 2.2) it is found that the value $a'|\omega_z|K_1(a'|\omega_z|)\to 1$ for $|a'\omega_z|\to 0$ and changes from 1 to 0.86 due to the variation of $|a'\omega_z|$ up to 0.44 for any value of radius. So, ignoring around 14% error it can be assumed that $a'|\omega_z|K_1(a'|\omega_z|)\approx 1$ for $|a'\omega_z|\le 0.44$. This approximation turns the weighting function as:

$$H(r,\omega_z)\approx\frac{1}{\sigma_r}aK_0(r'|\omega_z|) \tag{2.23}$$

Taking the inverse Fourier transform,

$$h(r,z)\approx\frac{1}{2\pi}\int_{-\infty}^{\infty}\frac{a}{\sigma_r}K_0(r'|\omega_z|)e^{-i\,\omega_z z}d\omega_z \tag{2.24}$$

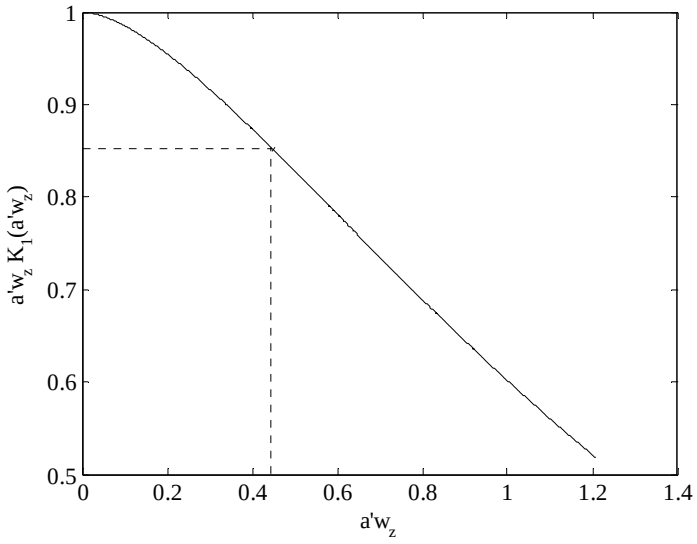

Figure 2.2: Behavior of modified first order Bessel function, K_1.

As $H(r,\omega_z)$ is real and even, $h(r,z)$ should be real and even function.

$$\begin{aligned} h(r,z) &= \frac{a}{\sigma_r \pi}\int_0^{\infty} K_0(r'\omega_z)\cos(z\,\omega_z)\,d\omega_z \\ &= \frac{a}{\sigma_r \pi r'}\int_0^{\infty} K_0(q)\cos\left(\frac{qz}{r'}\right)dq \end{aligned} \tag{2.25}$$

This integral can be evaluated using the properties of modified Bessel function as [1,35]:

$$\int_0^{\infty} K_0(q)\cos\left(\frac{qz}{r'}\right)dq = \frac{\pi}{2\sqrt{1+\left(\frac{z}{r'}\right)^2}} \tag{2.26}$$

Insertion of this solution results the expression of weighting function in space domain as:

$$h(r,z) = \frac{a}{2\sigma_r}\,\frac{1}{\sqrt{r^2 R_a + z^2}} \tag{2.27}$$

This simplified model of weighting function converts the profile of potential recorded at the surface of the medium with cylindrical anisotropy as:

$$\varphi(r,z)=\frac{a}{2\sigma_r}\int_{-\infty}^{\infty}\frac{i_m(s)}{\sqrt{r^2R_a+(z-s)^2}}ds \tag{2.28}$$

But the length of muscle fiber is finite. Inserting the relationship between transmembrane current and membrane potential, the potential distribution for a finite volume conductor can be expressed as:

$$\varphi(r,z)=\frac{\sigma_i a^2}{4\sigma_r}\int_{z_1}^{z_2}\frac{\alpha\lambda^2(\lambda s)\cdot\left[6-6\lambda s+(\lambda s)^2\right]e^{-\lambda s}}{\sqrt{r^2R_a+(z-s)^2}}ds \tag{2.29}$$

To account for the finite dimensions of muscle fibers and volume conductor distortions, the excitation and the extinction of the action potential are described as current sources at the neuromuscular endplate and fiber endings. These compensating current sources are calculated such as the total current is zero over the active part of the fiber.

$$\int_{fiber} i_m(z)dz=0 \tag{2.30}$$

Single fiber model is a convenient way to explore the issues related to the volume conduction only. But the influence of fiber distribution, motor unit type and location, motor unit firing pattern and synchronization must be considered for interpreting surface electromyographic signals.

2.3 Single Fiber Action Potential Modeling Algorithm

The muscle fibers of the motor unit are assumed to be cylindrical and lie parallel to each other. The neuromuscular endplate is located roughly at the center of the muscle fiber. The membrane potential propagates from the neuromuscular endplate in both directions along the muscle fiber with a conduction velocity. Thus, the surface potential distribution is caused by two sources traveling in opposite direction from neuromuscular junction to the endings of fiber. The conduction velocity of action potential is calculated as a linear function of the fiber diameter by using an empirical formula proposed by Nandedkar and Stalberg [27].

$$v_c = 2.2 + 0.05(d - 25) \tag{2.31}$$

where d is the diameter of fiber in μm and v_c is the conduction velocity in m/s. Few sequential steps are involved in algorithm development of single fiber action potential (SFAP).

The algorithm regarding the simulation of SFAP starts from a time sampling frequency, f_s defined by the user. The spatial sampling frequency is deduced from f_s and mean conduction velocity v_c to produce the spatial resolution as:

$$\Delta z = \frac{v_c}{f_s} \cdot 1000 \tag{2.32}$$

where f_s in Hz, v_c in m/s and Δz in mm. Total number of sampling points, *Npt* for left or right side of the fiber (as they are considered equal) is deduced by dividing the half of fiber length $L_{0.5f}$ with the spatial sampling resolution. The default value of potential

duration is considered 5 ms to calculate the total sampling points, *Nev* of intracellular potential and transmembrane current. The sampled source current $i_m(z)$ is obtained from the analytic model of intracellular potential. The parameters of this analytical model obtained from Roselfalck's mathematical formulation [33], where: α=96, λ=1 and β=90. These values represent the equation as:

$$V_m(z) = 96z^3e^{-z} - 90 \tag{2.33}$$

Afterward, Nandedkar and Stalberg [27] proposed a modified version of this model by introducing λ=2 in Equation (2.14) in order to obtain better match with experimental data.

$$V_m(z) = 768z^3e^{-2z} - 90 \tag{2.34}$$

Though this modification matched amplitude of intracellular potential and its second derivative, it did not able to maintain the rise time and duration of the simulated signal with actual one (Figure 2.3). To fit the analytic model of intracellular potential with the experimental data is also a matter of research interest, but beyond this study. That's why Rosenfalck's parameters are used in each simulation study, which depict the source current as:

$$i_m(z) = \frac{\sigma_i a}{2} 96z\left[6 - 6z + (z)^2\right]e^{-z} \tag{2.35}$$

The transfer function of the volume conductor model depends on the positions of source, $S(x_0,y_0,z_0)$ and the recording electrode, $E(x_e,y_e,z_e)$. As the position of the point source is moving with a conduction velocity, the instantaneous position of source can be represented as $S(x_0,y_0,z_0+m\Delta z)$, where *m* varies from 0 to *Npt*. So, the transfer function of the medium with cylindrical anisotropy can be described as:

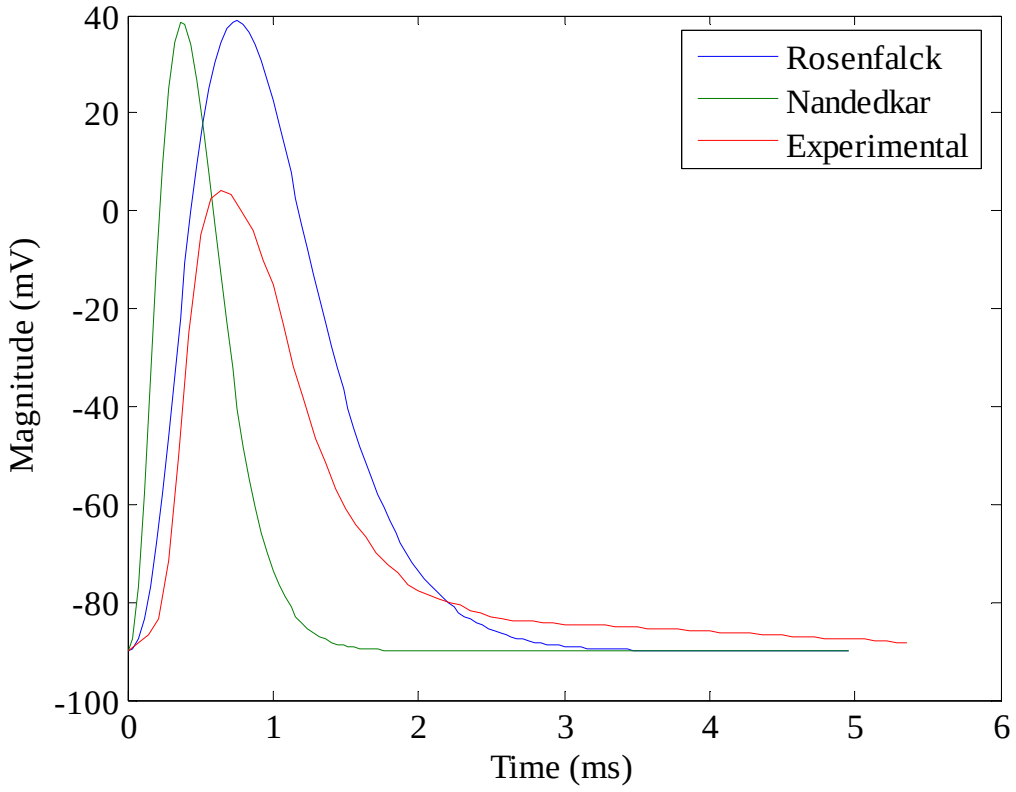

Figure 2.3: Comparison of Rosenfalck's and Nandedkar's model of membrane potential V_m with experimental data recorded by Ludin.

$$h(x, y, z(t)) = \frac{a}{2\sigma_r} \frac{1}{\sqrt{R_a\left[(x_e - x_0)^2 + (y_e - y_0)^2\right] + (z_e \pm z_0(t))^2}} \tag{2.36}$$

Here, $\pm$ sign is used in front of $z_0(t)$ to consider the transfer function for both side of the muscle fiber across the endplate region. The number of discrete values in $h(x,y,z(t))$ of each side of the fiber is equal to Npt. So, the length of discrete convolution between $h(x,y,z(t))$ and $i_m(z(t))$ is $Npt+Nev-1$. The convolution result provides the generated potential, V_1 due to the propagation of transmembrane current. Fast Fourier Transform (FFT) technique can be used to make the convolution faster. This will be really helpful in simulating CMAP.

A compensation technique needs to be incorporated to introduce the effect of excitation and extinction of transmembrane current. These effects are described as current sources at the neuromuscular endplate and fiber endings. The discrete integral of i_m at each step is multiplied by $h(x,y,z_0)$ and $h(x,y\ ,z_0+Npt\,\Delta z)$ in order to get compensation at the endplate, V_2 and the tendon, V_3 respectively. Then the computation of the final single fiber extracellular potential,

$$V_{SFAP}(z,t) = V_3 + V_2 - V_1 \tag{2.37}$$

Accuracy of the result produced by the above algorithm mainly depends on a correct discrete derivative of the intracellular potential. The discrete integral of i_m may not be equal to zero due to the sampling effect, which may provide erroneous estimation of V_1, V_2 and V_3.

2.4 Simulation Results

Single fiber action potential is simulated by adopting published physiological parameters of human muscle. The parameters used for the simulated fiber are: fiber length = 325 mm, diameter = 0.06 mm, radius of innervation zone = 5 mm. So, the distance between endplate and tendon is 163 mm. The sampling frequency is considered 25 kHz, which is well above the Nyquist requirement. The anisotropic characteristics of the medium are represented by using following values: radial conductivity, σ_r =0.063 Sm^{-1}, longitudinal conductivity, σ_z =0.33 Sm^{-1} and intracellular conductivity, σ_i = 1.01 Sm^{-1}. The muscle fiber is considered parallel to the z axis and the position of point source is started from $S(x_0=0,y_0=0,z_0=0)$, which moves along the fiber with conduction velocity, v_c (Figure 2.4). The behavior of transfer function of the cylindrical medium directly depends on the position of recording electrode.

Figure 2.5 shows different components involved in computation of extracellular potential recorded by an electrode placed at $E(x_e$=0 mm, y_e=10 mm, z_e=20 mm) with respect to the origin *S*. As the source current moves along the fiber axis towards tendons, it is quite obvious that transfer function, $h(t)$ will be maximum when the source and electrode are in same z plane. The result of convolution between the transfer function and transmembrane current, the electrophysiological effect of neuromuscular junction and tendon are presented sequentially. Finally the total extracellular potential is the summation of the signals positioned in both directions of the fiber after end effect compensation. Figure 2.6 depicts the complete potential profile and its frequency

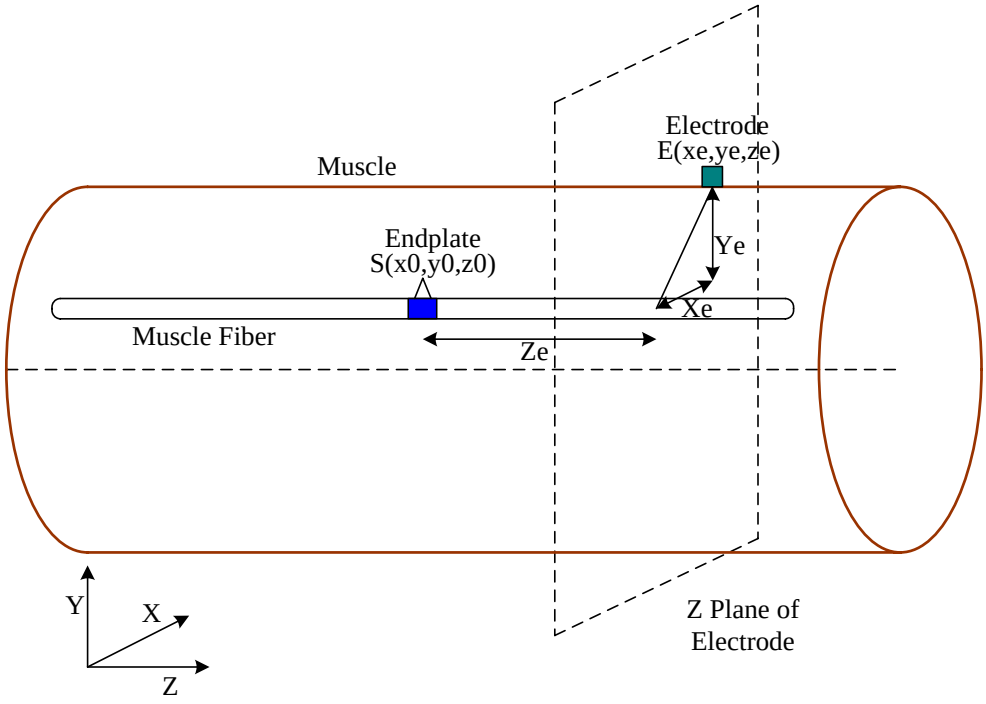

Figure 2.4: Schematic representation of muscle fiber and position of electrode.

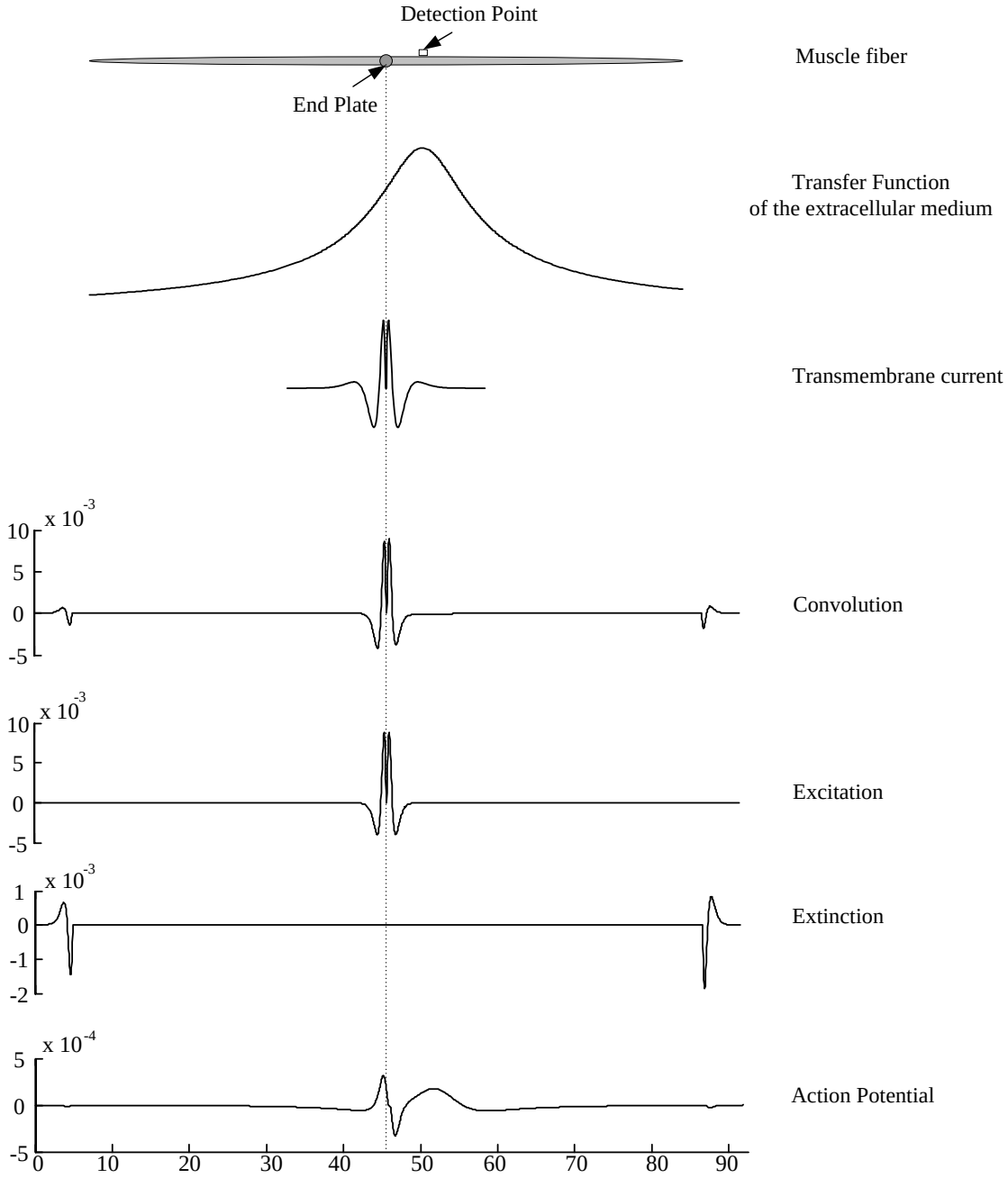

Figure 2.5: Different components involved in computation of extracellular potential generated by a fiber located at a depth of 10 mm inside the muscle.

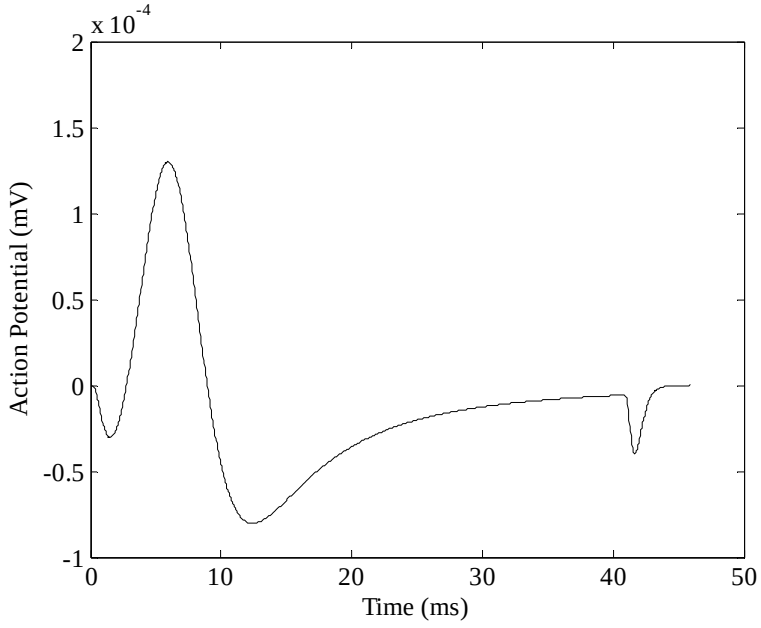

(a)

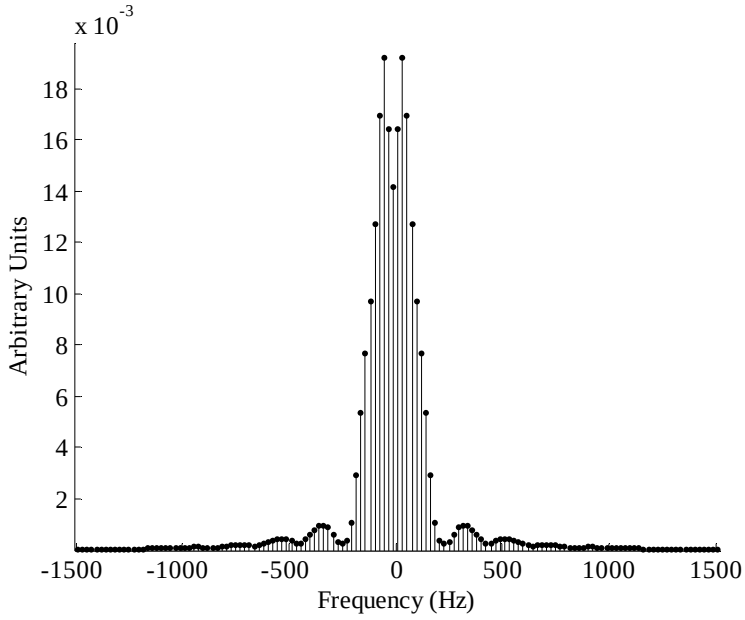

(b)

Figure 2.6: Simulated action potential generated by a fiber at the depth of 10 mm within the muscle- (a) complete profile and (b) frequency spectrum.

contents. It clearly shows that frequencies below 500 Hz play the dominating role in surface EMG signal.

Figure 2.7 shows the variation extracellular potential distribution with the depth of muscle fiber considering longitudinal and radial position of the electrode fixed at Z_e=20 mm and X_e=0 mm respectively. SFAP is simulated by varying Y_e from 5 mm to 10 mm. The figure clearly illustrates the attenuation effect of the extracellular medium of the muscle. This effect introduces the limitation on allowable depth of muscle fiber in surface electromyography. Action potential of the fiber located close to the electrode subjects to high rate of change, consequently contains higher frequency components than that of fiber located far away from the electrode.

The shape of the EMG signal varies depending upon the position of the electrode. Figure 2.8 presents the variation of detected SFAP signals when the position of electrode is changed parallel to the length of the muscle fiber located at 10 mm depth from the muscle surface. The position perpendicular to the center of endplate is marked as the reference point. From this reference point EMG signals are detected at Z_e= 0 mm, 5 mm, 10 mm, 15 mm, 20 mm and 25 mm distant along the fiber considering X_e=0 mm. As can be seen from the figure, the peak values of the signals shifted spatially with the spatial change of the position of electrodes. At first the peak magnitude declines up to a certain level, then it starts to increase. There are also some variations in the shape of the individual signals. The signals detected at Z_e=0 mm, 5 mm and 10 mm have only two phases. One part has positive values and other part has negative values. But all other signals have three

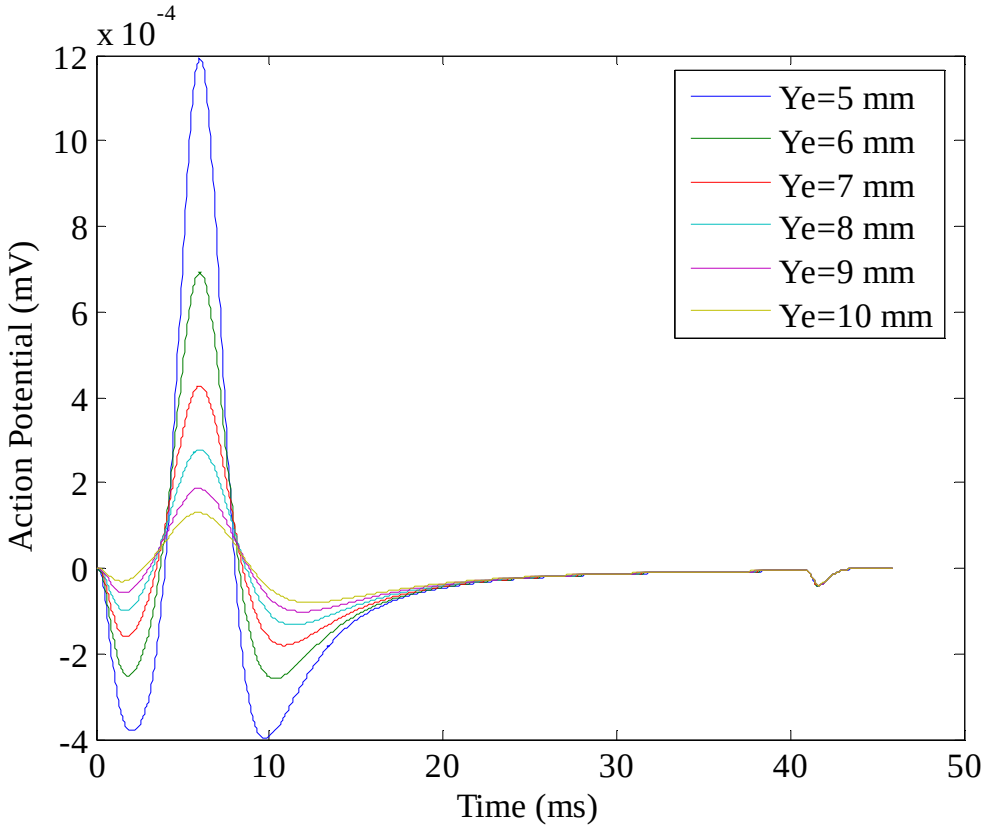

Figure 2.7: Variation of SFAP signals with depth of fiber inside muscle.

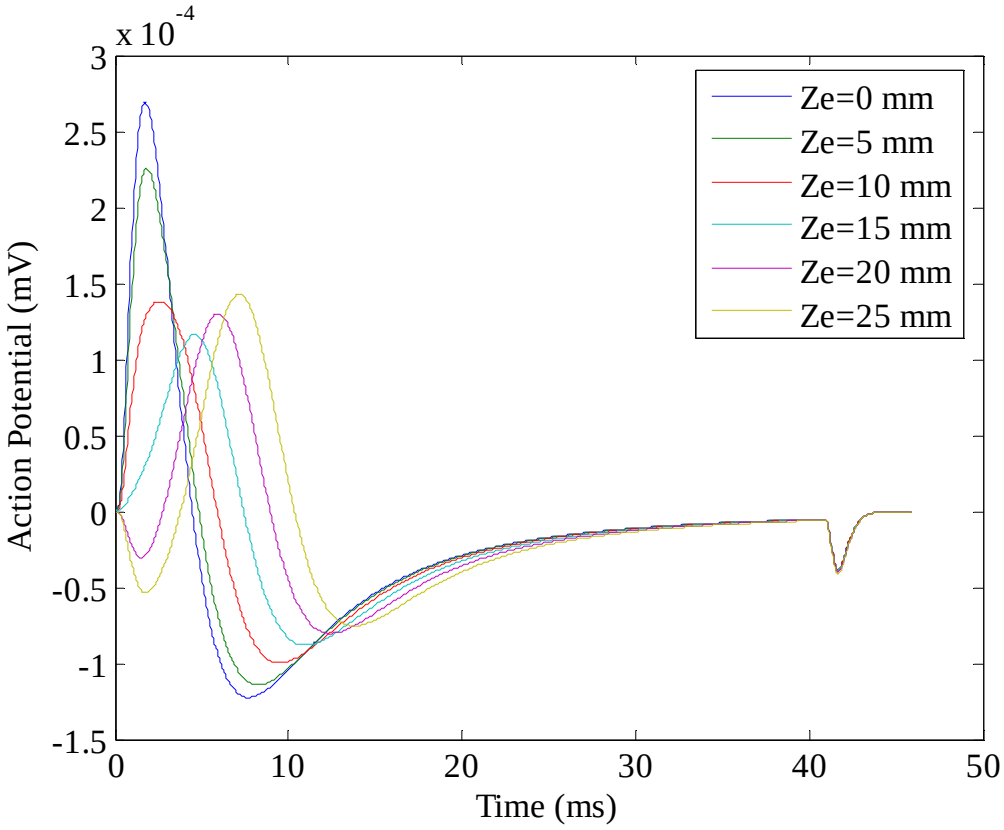

Figure 2.8: Variation of SFAP signals with different spatial position of electrode.

phases, two in the negative side and one in the positive side. So, the shape of the signal is changed from biphasic to triphasic with the spatial variation of electrode.

The variation of SFAP signal with the radial movement of the electrode along x direction is illustrated in Figure 2.9. Here the SFAP signals are detected at X_e=0 mm, 5 mm, 10 mm, 15 mm, 20 and 25 mm radial distant from the reference point considering Y_e=10 mm and Z_e=20 mm. According to the figure, there is a sharp change in the peak magnitude of the signals. The magnitude decreases with the radial increment of the position of the electrode. But there is a spatial movement among the signals, which can be considered negligible with respect the variation of the magnitude. The shape of the signal is changed from triphasic to biphasic with the radial movement of electrodes.

To systematically design effective, reliable, and accurate EMG topographical mapping and processing techniques, a muscle computer model is designed to perform simulation of SFAP. Few special cases regarding the change in the position of the electrode are briefly discussed. Dilation effect dominates while the electrode is moved along the fiber (in z direction). Where as magnitude variation plays a vital role in radial movement (in x direction) of the electrode. These observations are very helpful to understand the behavior of EMG signal in the surface grid electrode.

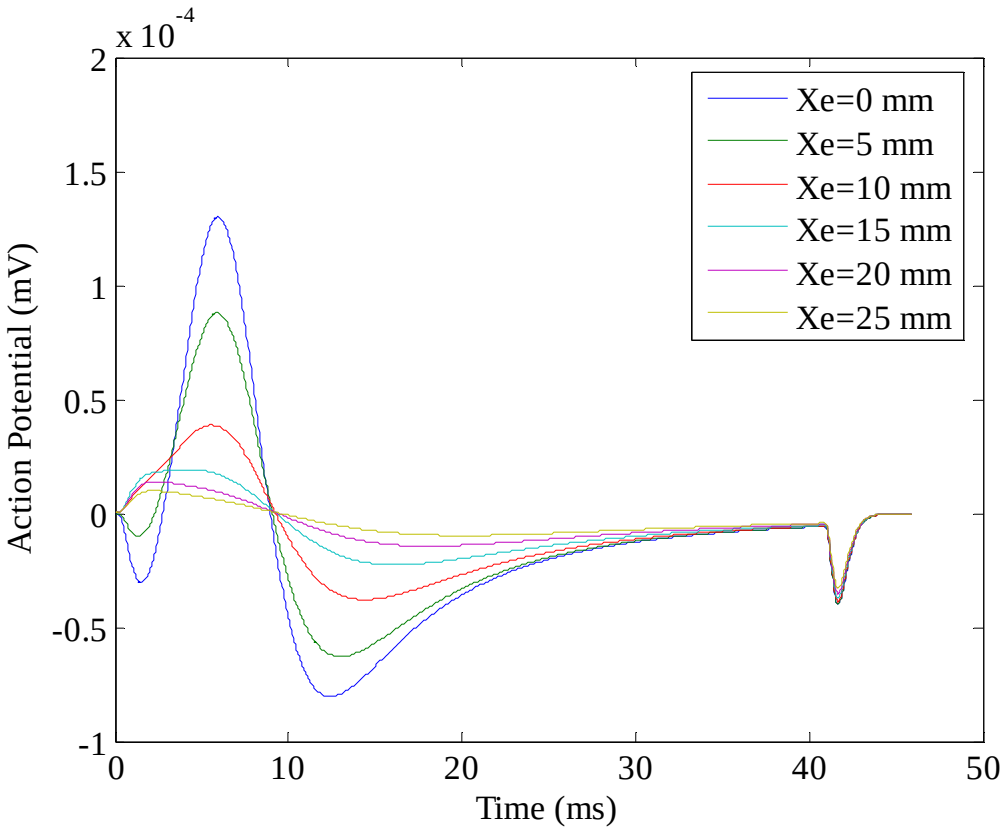

Figure 2.9: Variation of SFAP signals with different radial positions of electrode.

Chapter 3

Multiple-layer Volume Conductor Model

3.1 Significance of Multiple-layer Model

Surface Electromyography (SEMG) is a noninvasive electrophysiological technique. The conventional SEMG signal consists of accumulated bioelectric activities of a large number of muscle fibers, which are located in a complex geometric arrangement inside the muscle and are excited in a complex interference pattern. SEMG becomes popular in clinical diagnosis due to ease of use and less stress to patient. It has found many applications in the fields of neurology, kinesiology, and the sports and rehabilitation sciences. In SEMG, the recording electrode is placed on the skin surface. The intermediate tissues act as a conductive medium for generated potential distribution. So, the behavior of SEMG signal is considerably influenced by the composition and conductivity of tissues between bioelectric source and the recording electrode.

The analytic model presented in previous chapter is based on the volume conduction theory. Only the anisotropic medium of muscle is considered to picture the electrophysiological phenomena that take place inside muscle. But two additional tissue layers of fat and skin exist between muscle and surface electrode. Though the composition and conductivity of fat and skin layers are different in nature, both mediums are isotropic. The existence of these subcutaneous layers substantially effect the potential

profile generated by an excited muscle fiber. In fact, these two layers may constitute the major part of the intermediate tissue for superficial sources. So, the properties of fat and skin tissues need to be incorporated to represent the conduction medium more appropriately in surface detection technique. The proper understanding of volume conduction aspects is also essential for the correct interpretation of experimental result. In this chapter, a multiple layer volume conductor model of muscle is developed in order to accurately simulate the potential distribution at the skin surface, irrespective of position of recording electrode.

3.2 Derivation of Mathematical Model

According to muscle anatomy, each muscle cell or fiber is distributed inside the extracellular fluid with a specific orientation. The extracellular medium possesses different conductivity along longitudinal and radial direction of fiber. The layers of fat and skin tissues lie above the muscle and possess same conductivity along longitudinal and radial direction. These three layers can be taken to represent a large inner cylinder of muscular tissue, an intermediate layer of subcutaneous fat and an outer layer of relatively well conducting skin. To reproduce volume conducted potential distribution properly, it is essential that the geometry of the model reflect the recording configuration of the experiment. Figure 3.1 depicts the structural model of three layers volume conductor. The outermost layer consists of air with zero conductivity. The radiuses of muscle, fat and skin surface are r1, r2 and r3 with respect to the center of the volume. As SEMG signals are dominated by the superficial motor units, the model should support the use of

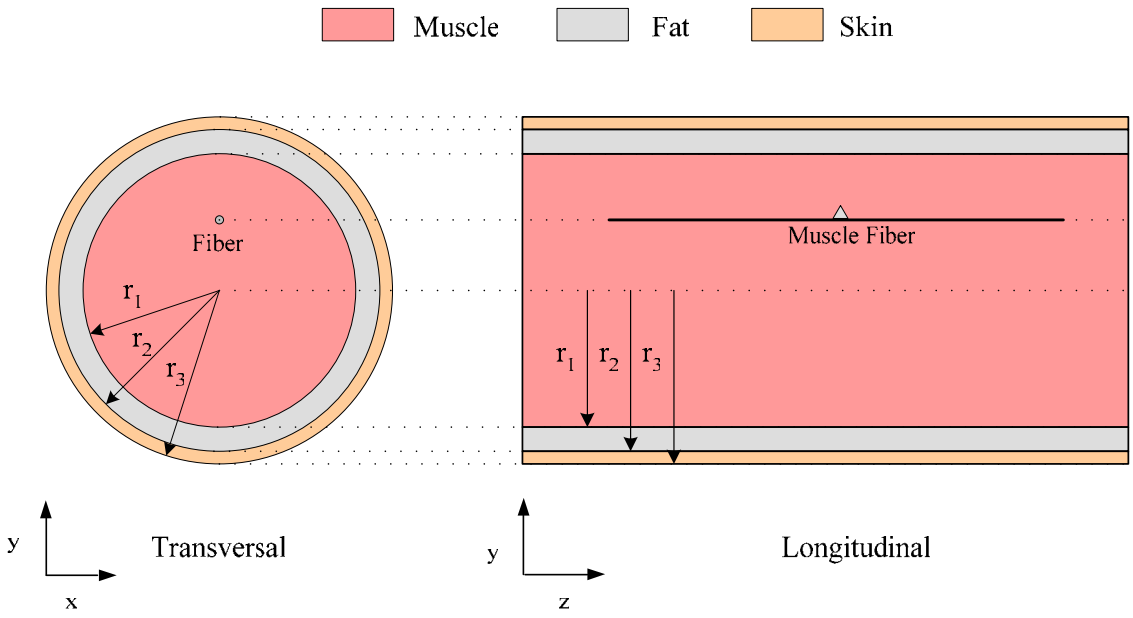

Figure 3.1: Transversal and longitudinal view of three-layered cylindrical volume conductor muscle model with eccentric source

eccentric sources. There also exists limitation regarding the depth of measurable sources. After a certain depth, the magnitude the conducted bioelectric signal becomes too small to be measured. At that condition, the noise signal generated from electromechanical artifacts becomes dominant. To develop the simulation model the position of muscle fiber is considered parallel along z-axis in the superficial area of muscle.

The existence of current inside the volume conductor implies the presence of an electric field and this current source is confined on the membrane of the active muscle fiber. In the electrophysiological problem, even under time varying condition, the electric field behaves like a static field at each instant of time. Considering these conditions, the

distribution of electrophysiological potential generated by an excited muscle fiber, can be represented by Laplace's equation. The potential distribution will be different inside different layers of the model. In previous chapter (Equation 2.9), it is proved that the behavior of potential field inside the anisotropic muscle region can be expressed as:

$$\left(\frac{\partial^2}{\partial x^2}+\frac{\partial^2}{\partial y^2}+R_a\frac{\partial^2}{\partial z^2}\right)\varphi_{muscle}(x,y,z)=0 \tag{3.1}$$

Both the fat and skin layers are isotropic, i.e. $\sigma_x=\sigma_y=\sigma_z$. This property converts the potential distribution in fat and skin layers as:

$$\left(\frac{\partial^2}{\partial x^2}+\frac{\partial^2}{\partial y^2}+\frac{\partial^2}{\partial z^2}\right)\varphi_{fat\ \&\ skin}(x,y,z)=0 \tag{3.2}$$

Equation (3.1) and (3.2) are partial differential equations, which can be solved by introducing boundary conditions at the interface. In the multiple layer muscle model, current can be considered continuous along y direction and electric field can be considered continuous along x and z direction at the interface of two different layers. If medium 1 and medium 2 are interfaced at $y=y_1$, then the boundary conditions can be expressed as:

$$\sigma_1\frac{\partial\varphi_1}{\partial y}\bigg|_{y=y_1}=\sigma_2\frac{\partial\varphi_2}{\partial y}\bigg|_{y=y_1},\ \frac{\partial\varphi_1}{\partial x}\bigg|_{y=y_1}=\frac{\partial\varphi_2}{\partial x}\bigg|_{y=y_1}\ and\ \frac{\partial\varphi_1}{\partial z}\bigg|_{y=y_1}=\frac{\partial\varphi_2}{\partial z}\bigg|_{y=y_1} \tag{3.3}$$

But, in the two dimensional spatial frequency domain, Equation (3.1) and (3.2) convert into ordinary differential equations as,

$$\left(\frac{\partial^2}{\partial y^2}-\omega_x^2-R_a\omega_z^2\right)\phi_{muscle}(\omega_x,y,\omega_z)=0 \tag{3.4}$$

$$\left(\frac{\partial^2}{\partial y^2} - \omega_x^2 - \omega_z^2\right)\phi_{fat\ \&\ skin}(\omega_x, y, \omega_z) = 0 \tag{3.5}$$

For a particular depth of muscle fiber the potential distribution varies along x and z direction. Therefore, it is judicial to consider the spatial frequency analysis along x and z direction. Moreover, it reduces the calculation load and complexity of solution. Representing the anisotropic and isotropic frequency distribution by $\omega_{ya} = \sqrt{\omega_x^2 + R_a\omega_z^2}$ and $\omega_y = \sqrt{\omega_x^2 + \omega_z^2}$ Equation (3.4) and (3.5) can be expressed as:

$$\left(\frac{\partial^2}{\partial y^2} - \omega_{ya}^2\right)\phi_{muscle}(\omega_x, y, \omega_z) = 0 \tag{3.6}$$

$$\left(\frac{\partial^2}{\partial y^2} - \omega_y^2\right)\phi_{fat\ \&\ skin}(\omega_x, y, \omega_z) = 0 \tag{3.7}$$

Spatial frequency distribution ω_{ya} and ω_y can be considered constants to derive the potential at different levels along y direction. Then the solutions of these ordinary differential equations can be written as,

$$\phi_{muscle}(\omega_x, y, \omega_z) = A_1 e^{y\omega_{ya}} + B_1 e^{-y\omega_{ya}} \tag{3.8}$$

$$\phi_{fat\ \&\ skin}(\omega_x, y, \omega_z) = A_2 e^{y\omega_y} + B_2 e^{-y\omega_y} \tag{3.9}$$

where the value of A_1,B_1,A_2,B_2 can be derived by adopting boundary conditions.

To solve the individual potential distribution in muscle, fat and skin layers due to an excited eccentric muscle fiber, the total volume conduction region is divided into five

layers along y-z plane (Figure 3.2). As the surface detection technique mainly subjects to the fibers located close to the skin, the region beyond the location of muscle fiber can be considered an infinite anisotropic muscle layer. The layers are numbered from bottom to top sequentially. Layer 1 and layer 2 are anisotropic muscle layers. The muscle fiber, which is considered as a line source, exists at the interface of these two layers. For simplicity, the top level of layer 2 is considered as reference level, which represents the muscle surface with respect to electrode. Layer 3 and layer 4 denote the isotropic medium of fat and skin respectively. Layer 5 is an infinite layer resides in air medium with zero conductivity. With respect to reference level, y=0, muscle fiber is located at y=-y_0, the interface of fat-skin layers and skin-air layers are located at y=d_1 and y=d_2 respectively. So, the thickness of fat layer, $t_f = d_1$ and the thickness of skin, $t_s = d_2$-d_1. The condition of potential decay to zero for $y \to \pm\infty$ can be imposed for two outermost layers (layer 1 and layer 5). Using the approach presented in Equation (3.8) and Equation (3.9), the solution of potential distribution in each layer can be expressed as:

$$\phi_1(\omega_x, y, \omega_z) = A_1 e^{y\omega_{ya}} \tag{3.10}$$

$$\phi_2(\omega_x, y, \omega_z) = A_2 e^{y\omega_{ya}} + B_2 e^{-y\omega_{ya}} \tag{3.11}$$

$$\phi_3(\omega_x, y, \omega_z) = A_3 e^{y\omega_y} + B_3 e^{-y\omega_y} \tag{3.12}$$

$$\phi_4(\omega_x, y, \omega_z) = A_4 e^{y\omega_y} + B_4 e^{-y\omega_y} \tag{3.13}$$

$$\phi_5(\omega_x, y, \omega_z) = B_5 e^{-y\omega_y} \tag{3.14}$$

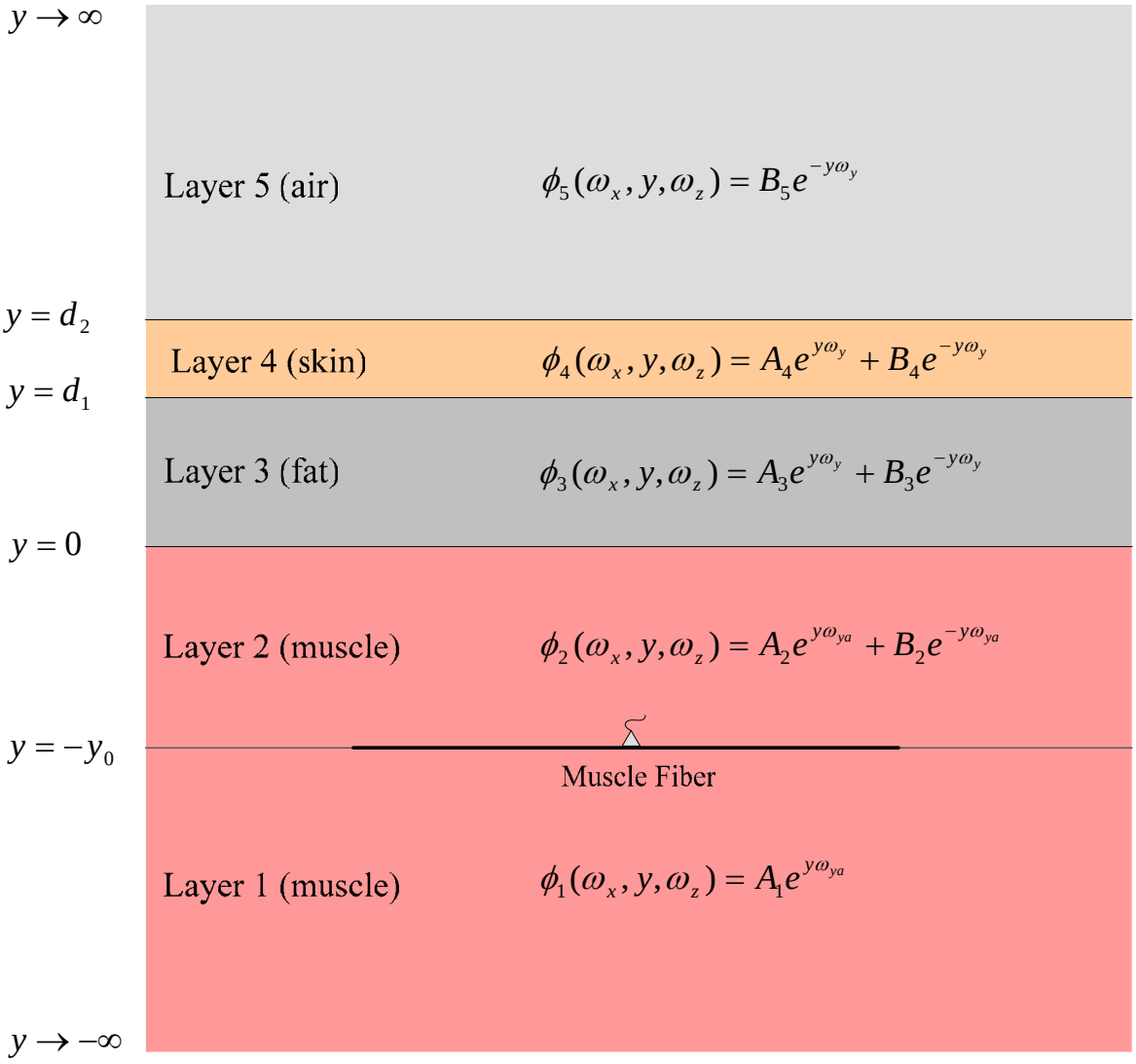

Figure 3.2: Five layer medium model along y-z plane for the calculation of potential distribution at different medium.

There are four boundaries in a volume conductor consists of five layers. In the spatial frequency domain these boundary conditions are:

$$\sigma_1 \left.\frac{\partial \phi_1(\omega_x, y, \omega_z)}{\partial y}\right|_{y=-y0} - \sigma_2 \left.\frac{\partial \phi_2(\omega_x, y, \omega_z)}{\partial y}\right|_{y=-y0} = I_m(\omega_z) \tag{3.15}$$

$$\phi_1(\omega_x, y, \omega_z)\big|_{y=-y0} = \phi_2(\omega_x, y, \omega_z)\big|_{y=-y0} \tag{3.16}$$

$$\sigma_2 \left.\frac{\partial \phi_2(\omega_x, y, \omega_z)}{\partial y}\right|_{y=0} = \sigma_3 \left.\frac{\partial \phi_3(\omega_x, y, \omega_z)}{\partial y}\right|_{y=0} \tag{3.17}$$

$$\phi_2(\omega_x, y, \omega_z)\big|_{y=0} = \phi_3(\omega_x, y, \omega_z)\big|_{y=0} \tag{3.18}$$

$$\sigma_3 \left.\frac{\partial \phi_3(\omega_x, y, \omega_z)}{\partial y}\right|_{y=d_1} - \sigma_4 \left.\frac{\partial \phi_4(\omega_x, y, \omega_z)}{\partial y}\right|_{y=d_1} \tag{3.19}$$

$$\phi_3(\omega_x, y, \omega_z)\big|_{y=d_1} = \phi_4(\omega_x, y, \omega_z)\big|_{y=d_1} \tag{3.20}$$

$$\left.\frac{\partial \phi_4(\omega_x, y, \omega_z)}{\partial y}\right|_{y=d_2} = 0 \tag{3.21}$$

$$\phi_4(\omega_x, y, \omega_z)\big|_{y=d_2} = \phi_5(\omega_x, y, \omega_z)\big|_{y=d_2} \tag{3.22}$$

Here $I_m(\omega_z)$ represents the Fourier transform of the transmembrane current in spatial frequency domain, σ_1 and σ_2 are the radial conductivity of muscle, σ_3, and σ_4 are radial conductivity of fat and skin layers. Following simplification can be adopted regarding the radial conductivity of different layers,

$$\sigma_1 = \sigma_2 = \sigma_r, \quad R_b = \frac{\sigma_3}{\sigma_2} \quad and \quad R_c = \frac{\sigma_4}{\sigma_3} \tag{3.23}$$

Eight unknown values, A_1, A_2, B_2, A_3, B_3, A_4, B_4, and B_5 can be determined by using eight boundary conditions. Implementation of boundary conditions in aforementioned volume conduction model results following eight liner equations,

$$A_1 e^{-y0\omega_{ya}} - A_2 e^{-y0\omega_{ya}} + B_2 e^{y0\omega_{ya}} = \frac{I_m}{\sigma_r \omega_{ya}} \tag{3.24}$$

$$A_1 e^{-y0\omega_{ya}} - A_2 e^{-y0\omega_{ya}} - B_2 e^{y0\omega_{ya}} = 0 \tag{3.25}$$

$$A_2\omega_{ya} - B_2\omega_{ya} - A_3 R_b\omega_y + B_3 R_b\omega_y = 0 \tag{3.26}$$

$$A_2 + B_2 - A_3 - B_3 = 0 \tag{3.27}$$

$$A_3\,\omega_y\, e^{d_1\omega_y} - B_3\,\omega_y\, e^{-d_1\omega_y} - A_4\,R_c\,\omega_y\, e^{d_1\omega_y} + B_4\,R_c\,\omega_y\, e^{-d_1\omega_y} = 0 \tag{3.28}$$

$$A_3\, e^{d_1\omega_y} + B_3\, e^{-d_1\omega_y} - A_4\, e^{d_1\omega_y} - A_4\, e^{-d_1\omega_y} = 0 \tag{3.29}$$

$$A_4\,\omega_y\, e^{d_2\omega_y} - B_4\,\omega_y\, e^{-d_2\omega_y} = 0 \tag{3.30}$$

$$A_4\, e^{d_2\omega_y} + B_4\, e^{-d_2\omega_y} - B_5\, e^{-d_2\omega_y} = 0 \tag{3.31}$$

Eight coefficients can be evaluated from above equations by means of techniques involved in linear algebra. Substitution of these coefficients provides the potential distribution for each value of the y coordinate. At the surface of muscle, fat and skin layers the values of y are 0 mm, d_1 mm and d_2 mm respectively. At those positions potential distribution in 2D spatial frequency domain can be expressed as:

$$\phi(\omega_x,0,\omega_z) = \frac{I_m(\omega_z)}{\sigma_r} e^{-y0\omega_{ya}} \frac{(1+R_c)\cosh(\omega_y(t_f+t_s)) + (1-R_c)\cosh(\omega_y(t_f-t_s))}{\alpha_1(\omega_y,\omega_{ya},R_c,t_f,t_s) + \alpha_2(\omega_y,\omega_{ya},R_c,t_f,t_s)} \tag{3.32}$$

$$\phi(\omega_x, d_1, \omega_z) = \frac{2I_m(\omega_z)}{\sigma_r} e^{-y0\omega_{ya}} \frac{\cosh(\omega_y, t_s)}{\alpha_1(\omega_y, \omega_{ya}, R_c, t_f, t_s) + \alpha_2(\omega_y, \omega_{ya}, R_c, t_f, t_s)} \tag{3.33}$$

$$\phi(\omega_x, d_2, \omega_z) = \frac{2I_m(\omega_z)}{\sigma_r} e^{-y0\omega_{ya}} \frac{1}{\alpha_1(\omega_y, \omega_{ya}, R_c, t_f, t_s) + \alpha_2(\omega_y, \omega_{ya}, R_c, t_f, t_s)} \tag{3.34}$$

where α_1 and α_2 for a specific value of frequency are,

$$\alpha_1(\omega_y, \omega_{ya}, R_c, t_f, t_s) = (1 + R_c)\cosh\{\omega_y(t_f + t_s)\}\left[\omega_{ya} + R_b\,\omega_y \tanh\{\omega_y(t_f + t_s)\}\right]$$

$$\alpha_2(\omega_y, \omega_{ya}, R_c, t_f, t_s) = (1 - R_c)\cosh\{\omega_y(t_f - t_s)\}\left[\omega_{ya} + R_b\,\omega_y \tanh\{\omega_y(t_f - t_s)\}\right]$$

Thus the behavior of potential distribution can be obtained at the surface of muscle, fat and skin. The derived equations are in agreement with the work done by Farina *et al*. [7]. Though the fat and skin layers are source free region, they have some effects on the potential distribution at muscle surface. If the source is considered as an impulse of current, Equation (3.32) will represent the Fourier transform of the transfer function of muscle tissue. In the same way, Equation (3.34) will provide the transfer function of muscle and isotropic tissues together. So, the transfer function of the isotropic layers of fat and skin can be obtained by dividing the total transfer function with the transfer function of muscle tissues. In reverse way, the total transfer function of the intermediate tissue layers can be considered as a cascade of transfer function of anisotropic and isotropic medium. The solution of potential distribution in the space domain can be obtained by taking the two dimensional inverse Fourier transform.

3.3 Simulation of 2D Potential Distribution

To simulate the two dimensional potential distribution at different layer physiological parameters of human muscle, sampling frequency and profile of transmembrane current are considered same as previous chapter. The conductivity ratios between muscle and fat layers and fat and skin layers are taken as R_b=0.5 and R_c=20 respectively [7]. The product of sampling interval in time and the conduction velocity at membrane of fiber defines the sampling interval in spatial domain, which in turn determines the bandwidth in spatial frequency domain. Same bandwidth and frequency interval are considered along both z (parallel to fiber) and x (perpendicular to fiber) directions. Thus a two-dimensional frequency matrix is generated to represent the frequency contents along z and x directions. Using this frequency matrix, the 2D transfer functions of muscle tissues and subcutaneous fat and skin layers are calculated for a particular depth of fiber with respect to the muscle surface and specific values of fat and skin thickness. As the muscle fiber is assumed parallel to the skin surface, the transmembrane current will propagate only along z direction. The spatial frequency spectrum of transmembrane current is obtained adopting FFT technique. The multiplication of Fourier transform of transmembrane, I_m with the 2D transfer function of the medium, $H(\omega_x,\omega_z)$ results 2D potential distribution, $\phi(\omega_x,y,\omega_z)$ in spatial frequency domain. Then the two-dimensional IFFT technique is utilized to generate the potential distribution with respect to the spatial variation along x and z direction (assuming the surface of skin is almost flat) irrespective of location of recoding electrode.

3.4 Effect of Fat and Skin Layers

The effect of subcutaneous fat and skin layers are analyzed by simulating the potential distribution at different layers. Emphasis has been given on the characteristics and comparative approaches of different simulated signals rather than magnitude. Figure 3.3 represents the two-dimensional signal in spatial frequency domain obtained on the muscle and on the skin from a fiber parallel to skin at a depth of y_0=2 mm in the muscle, with the fat thickness, t_f=3 mm and skin thickness, t_s=1 mm. From this figure it is clear that the isotropic fat and skin layer behaves as a low pass filter, which reduces the frequency contents of the signal. Figure 3.4 shows the behavior of these signals in the two-dimensional spatial domain. It reveals that the isotropic layers cause attenuation and spatial widening of the signal. So, spatial widening in the space domain corresponds the compression in frequency domain. Signals along z-direction and x-direction are plotted in Figure 3.5 and Figure 3.6 respectively to analyze fat and skin effect along two directions individually. To depict the behavior in z direction spatial frequency is varied along the center frequency of x direction. On the other hand, for the signal in x direction the spatial frequency in z direction is kept constant at the value where the spectrum of transmembrane current contains maximum magnitude. Both attenuation and spatial widening effect exists in two directions. The normalized signals at muscle and skin are plotted in Figure 3.7 along z direction and x direction separately. It shows that the characteristics of spatial widening effect are almost similar in both directions.

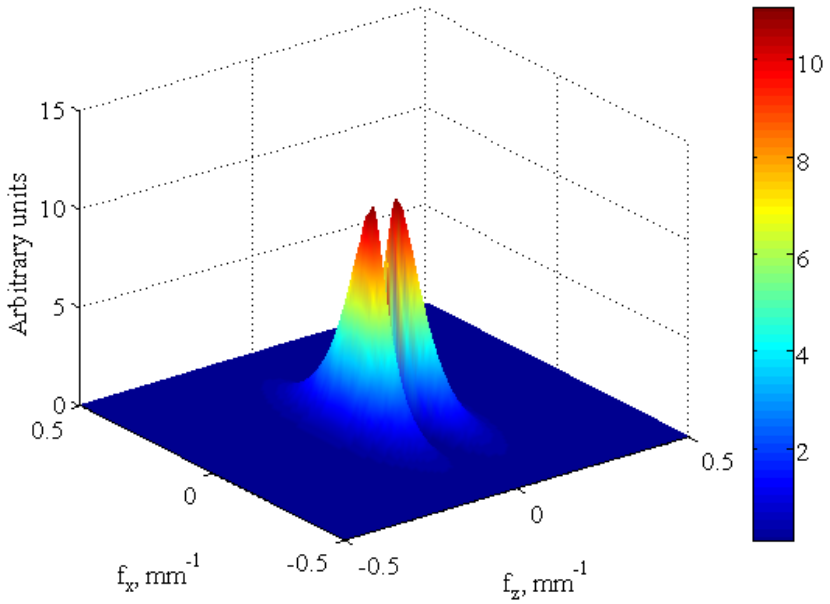

(a)

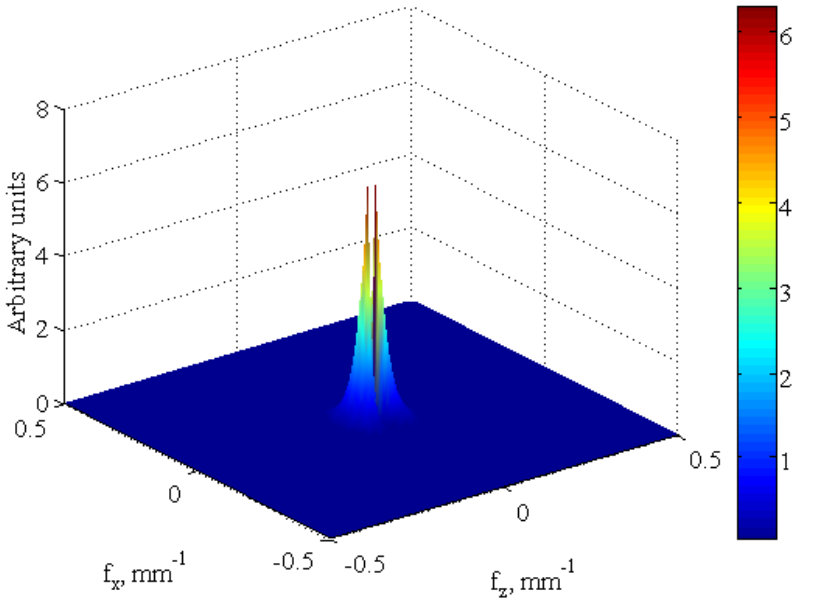

(b)

Figure 3.3: Simulated potential distribution at the top of muscle, y=0 (a) and at the top of skin, $y=d_2$ (b), in spatial frequency domain generated by a fiber located at a depth of 2 mm inside muscle with a fat and skin layers of thickness 3 mm and 1 mm respectively.

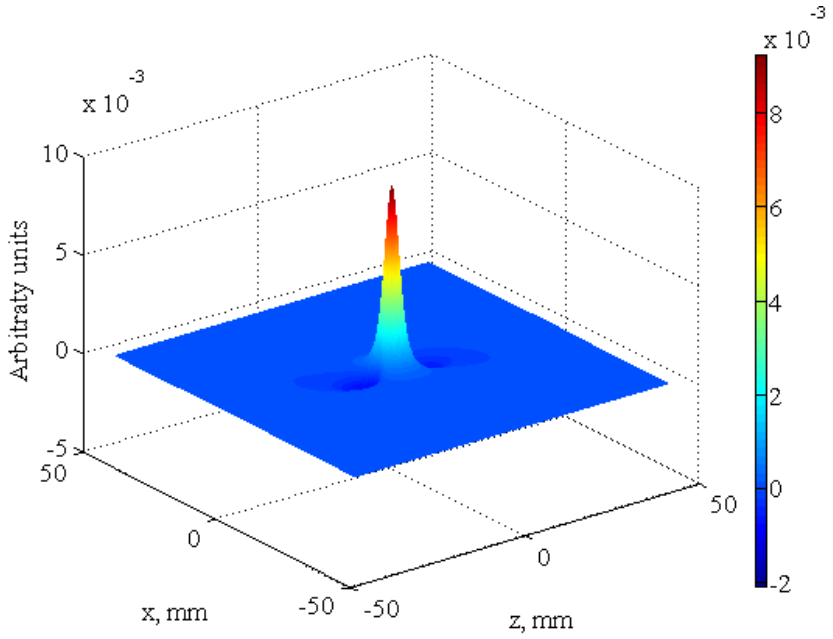

(a)

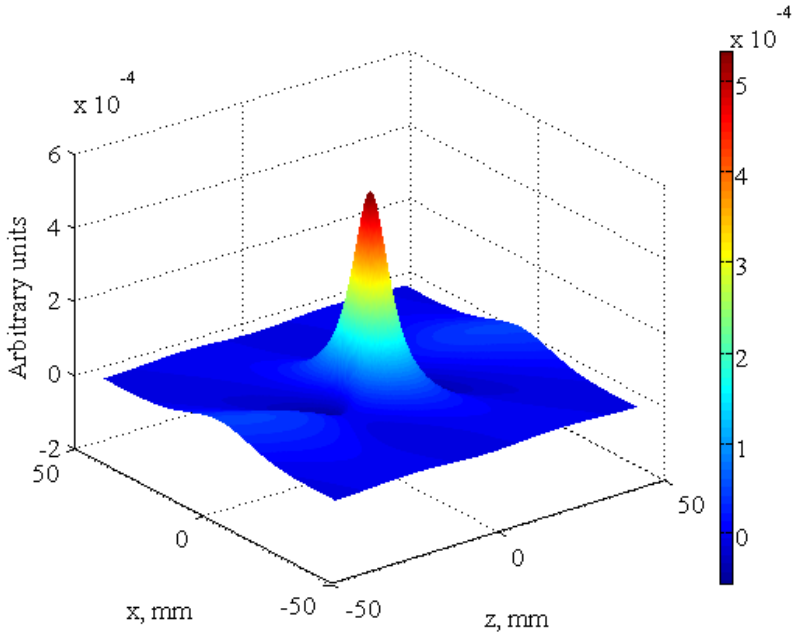

(b)

Figure 3.4: Simulated potential distribution at the top of muscle, y=0 (a) and at the top of skin, $y=d_2$ (b), in two dimensional spatial domain generated by a fiber located at a depth of 2 mm inside muscle with a fat and skin layers of thickness 3 mm and 1 mm respectively.

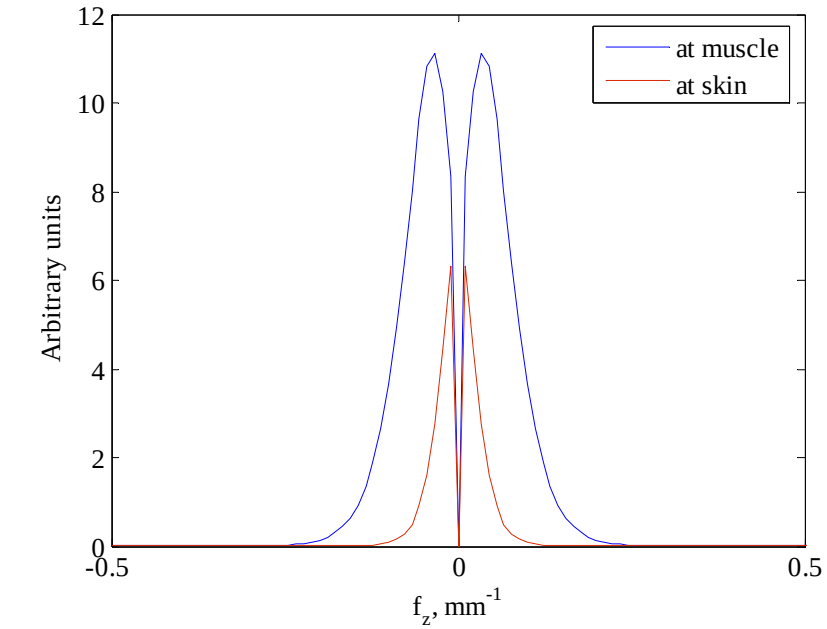

(a)

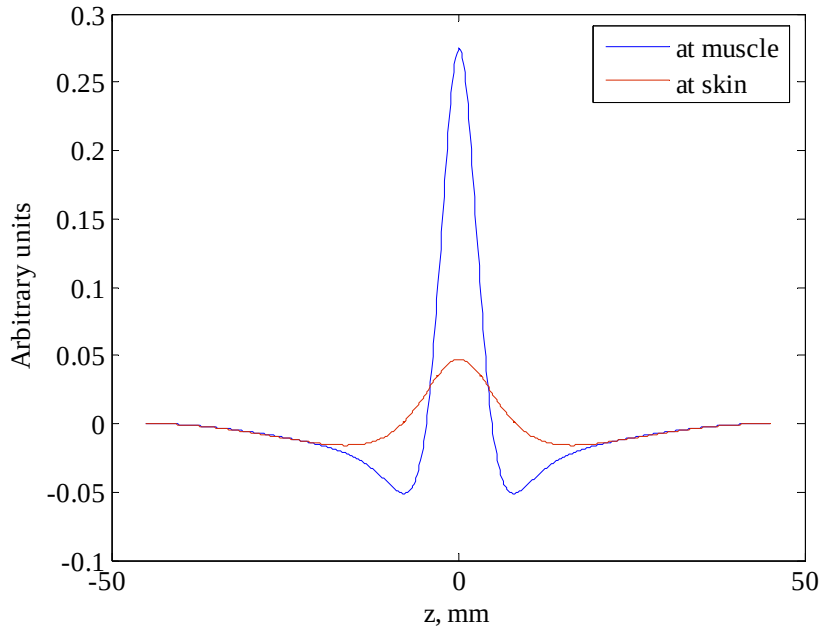

(b)

Figure 3.5: Comparison between signals detected at muscle and skin surface in spatial frequency (a) and spatial (b) domain along z direction (parallel to the fiber) only.

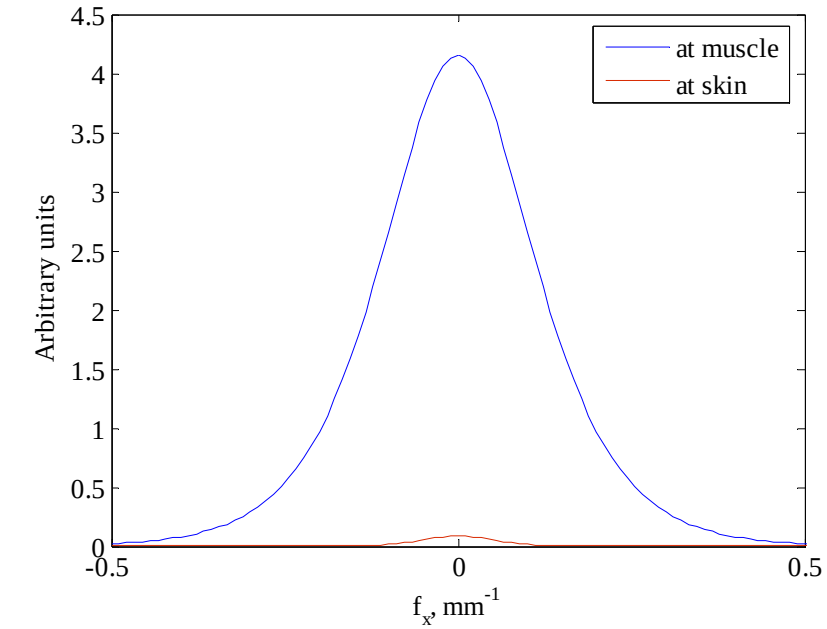

(a)

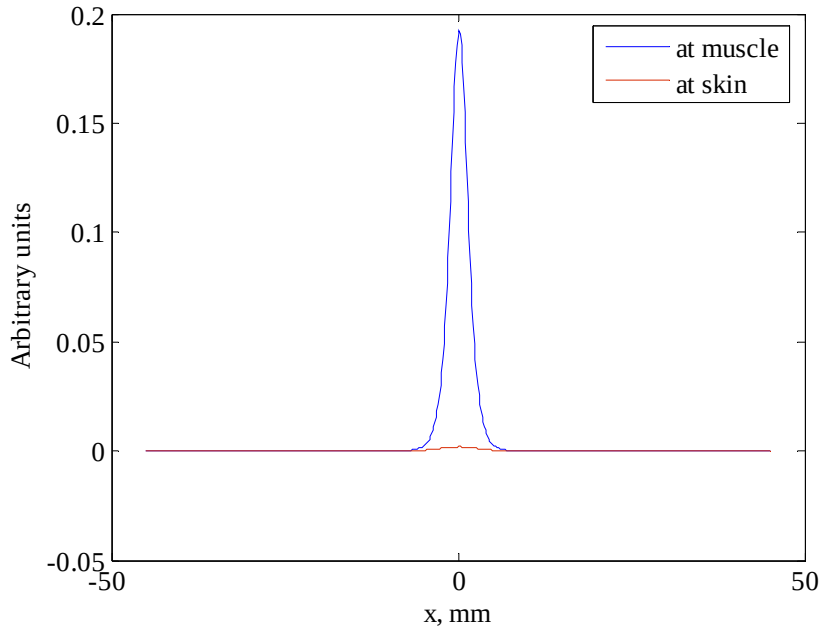

(b)

Figure 3.6: Comparison between signals detected at muscle and skin surface in spatial frequency (a) and spatial (b) domain along x direction (perpendicular to the fiber) only.

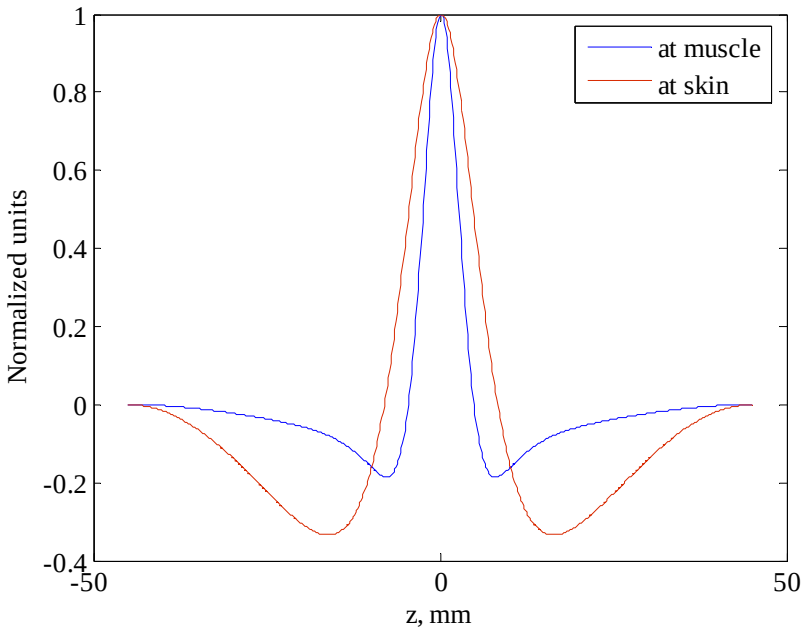

(a)

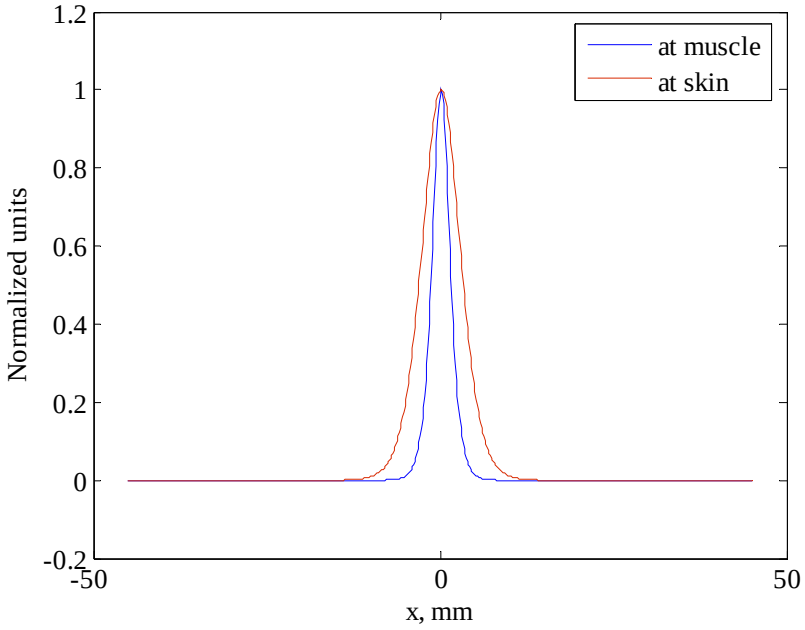

(b)

Figure 3.7: Spatial widening effect of isotropic layers along z direction (a) and x direction (b).

The thickness of fat layer, t_f and conductivity ratio between fat and skin layers, R_c of human muscle may vary for the case of normal and obese people. That's why, the effect of variation of these two parameters are analyzed for the potential distribution at skin. Figure 3.8 shows the characteristics of potential distribution along x direction with the variation of fat thickness, t_f form 3 mm to 9 mm considering R_c=20. The location of the source and other electrophysiological parameters are kept unchanged. The variation of thickness introduces substantial attenuation effect on the magnitude of the signal. The amplitude of the signal drastically decreases with small increment of fat thickness. Simulation plot resulting form the variation of conductivity ratio, R_c from 12 to 20, keeping the fat and skin thickness fixed at 3 mm and 1 mm respectively is presented in Figure 3.9. Though the amplitude of the signal also decreases with the increment of R_c, the attenuation is considerably less than that obtained with the variation of fat thickness. The spatial variation of the normalized signals with fat thickness and conductivity ratio are presented in Figure 3.10. The normalized potential signals clearly show some spatial widening effect with the increment of fat thickness. The rate of decrease of the signal along x direction is smaller for larger value of fat thickness. But, there is almost negligible spatial widening effect at different values of R_c.

3.5 Comparison with Single Layer Model

One of the advantages of the multiple-layer model is that it can easily be converted into single layer model by converting the thickness of other layers to zero. The behavior of potential distribution at the top of the muscle surface, results from the derived multiple

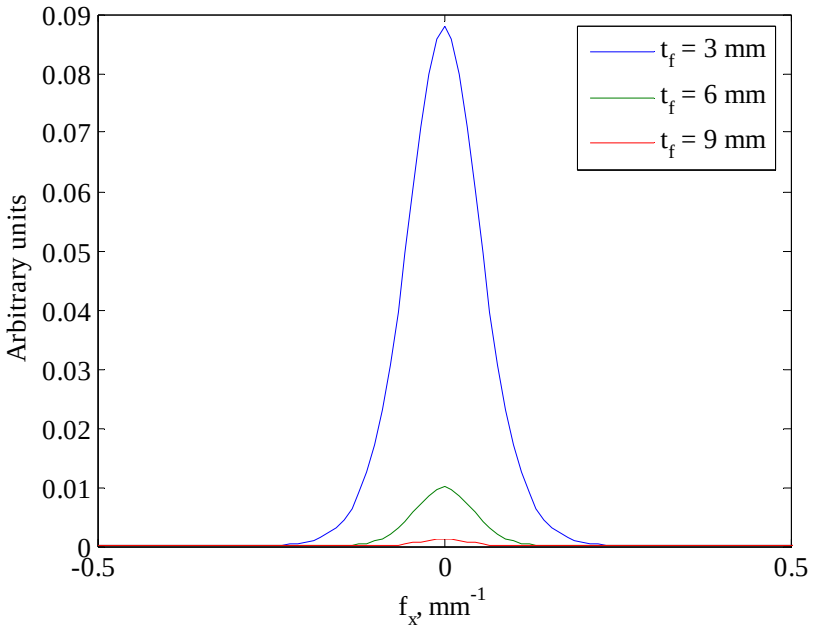

(a)

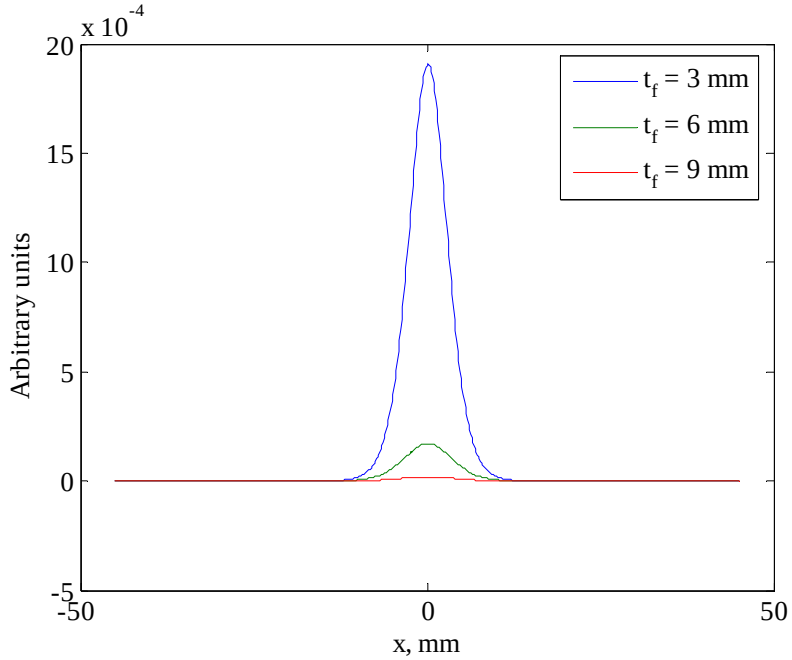

(b)

Figure 3.8: Characteristics of potential distribution in spatial frequency domain (a) and spatial domain (b) along x direction with the variation of fat thickness with R_c=20.

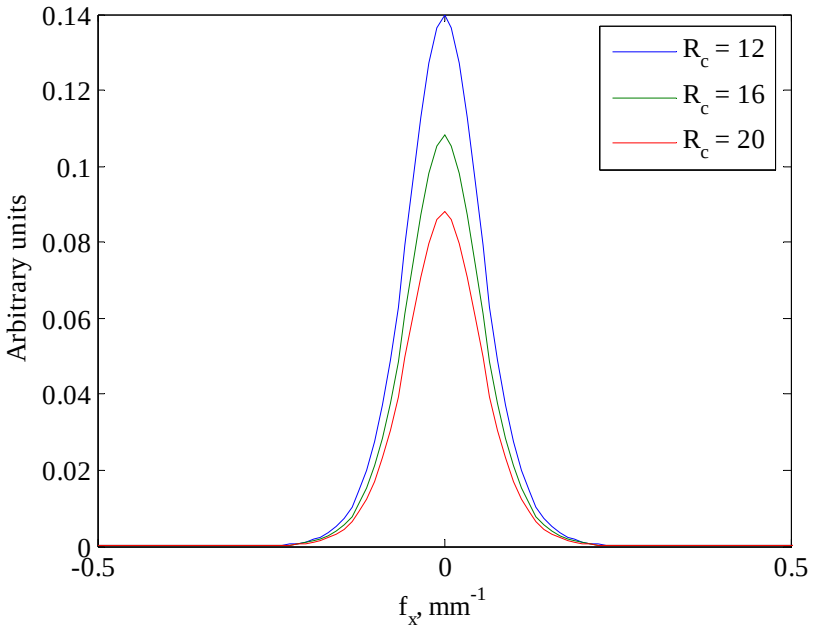

(a)

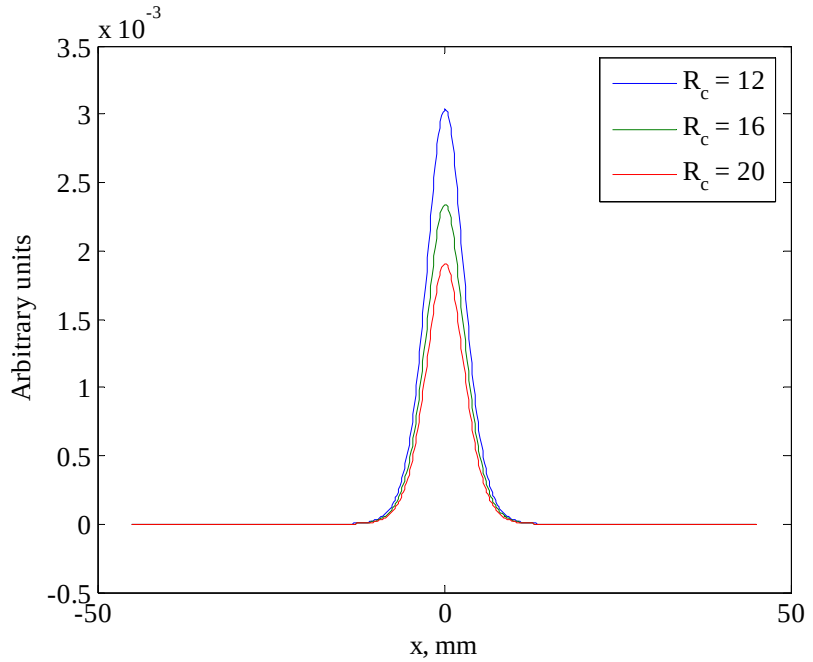

(b)

Figure 3.9: Characteristics of potential distribution in spatial frequency domain (a) and spatial domain (b) along x direction with the variation of conductivity ratio R_c for fat thickness 3 mm and skin thickness 1 mm.

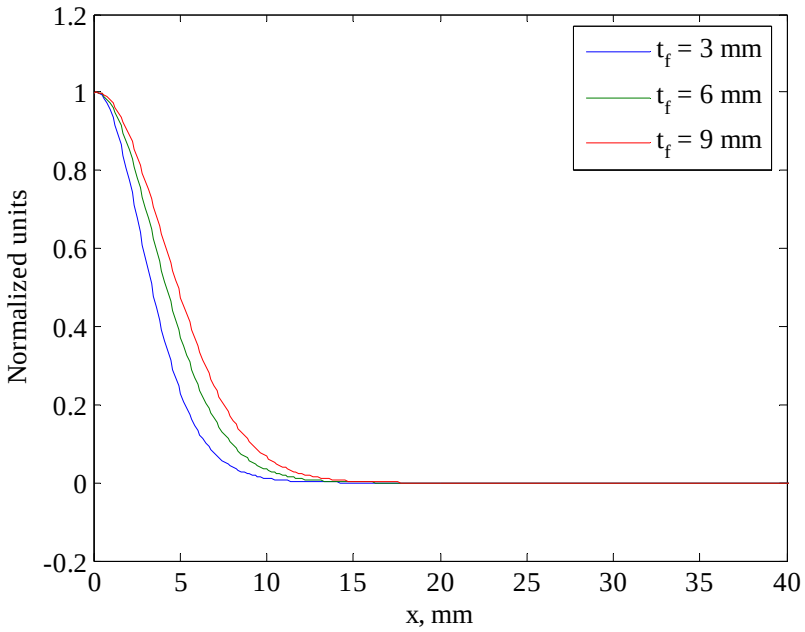

(a)

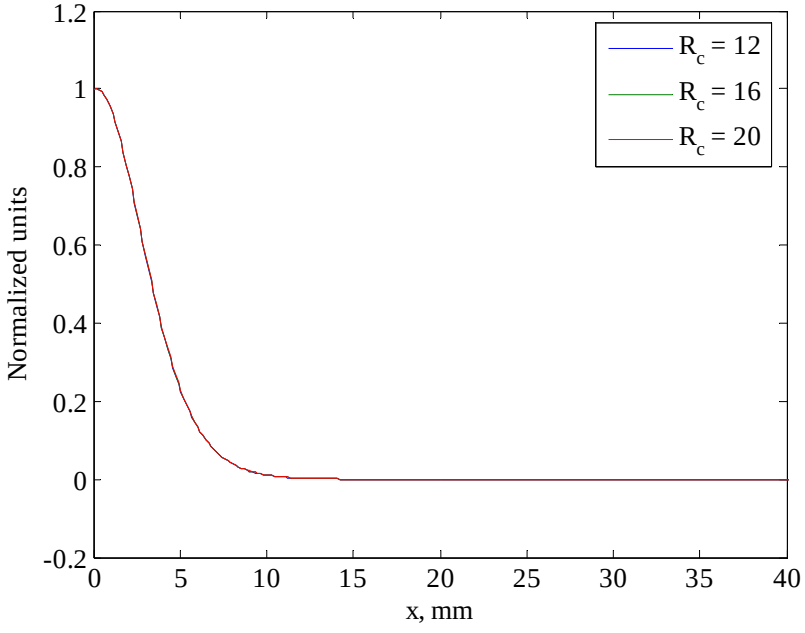

(b)

Figure 3.10: Effect of spatial widening with the variation of fat thickness, t_f (a) and conductivity ratio, R_c (b) in spatial domain along x direction.

layer-model is presented in Equation (3.32). If the values of fat and thickness are turned into zero, then the equation will become,

$$\varphi(\omega_x, \omega_z) = \frac{I_m(\omega_z)}{\sigma_r\, \omega_{ya}} e^{-y0\, \omega_{ya}} \tag{3.36}$$

To compare this model equation with single layer one-dimensional model, variation can be considered only along the length of fiber by substituting ω_x with zero.

$$\varphi(\omega_z) = \frac{I_m(\omega_z)}{\sigma_r \sqrt{R_a}\, \omega_z} e^{-y0\, \omega_z} \tag{3.37}$$

According the Rosenfalck's volume conduction model described in previous chapter, the profile of potential distribution at muscle surface generated by a single fiber located at a depth of y_o mm inside the muscle can be represented as:

$$\varphi(\omega_z) = \frac{I_m(\omega_z)}{\sigma_r \sqrt{R_a}\, \omega_z} \frac{K_0\left(y_0 \sqrt{R_a}\, \omega_z\right)}{K_1\left(a \sqrt{R_a}\, \omega_z\right)} \tag{3.38}$$

Simulation of both potential distributions in the spatial domain for the same physiological parameters and position of muscle fiber are presented in Figure 3.11. Both signals are plotted in normalized unit for better comparison of shape. The characteristics of both signals are almost same except a small spatial variation. This comparison clearly validates the approach of multiple-layer volume conductor model.

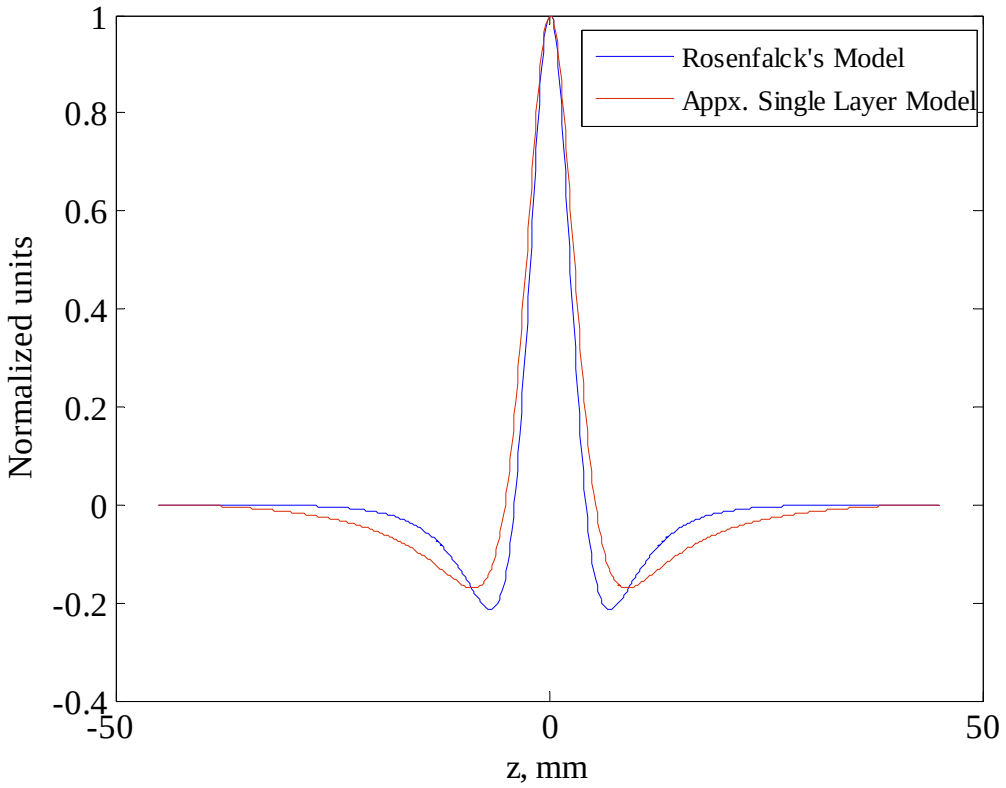

Figure 3.11: Comparison between potential distributions simulated by using Rosenfalck's single layer model and single layer model approximated from multiple layer model considering t_f and t_s equal to zero.

Chapter 4

Design of Grid Spacing and 2D Spatial Filter

4.1 Concept of Grid Electrode

The topographical study of surface electromyography is a matter of great interest in different arena of muscle research in clinical neurophysiology, rehabilitation and ergonomics. Recently, it has been evolved in different directions regarding the type of electrode and detection methodology depending upon the character of neuromuscular investigation. SEMG technique was introduced in muscle diagnosis by means of single bipolar surface electrode. But this method provides limited information on the electrical activity of a single motor unit (MU). EMG signals recorded from discrete sites provide only a limited picture of the actual muscular electrical activity in the vicinity of the recording electrode. In single-channel EMG recording, the electrical events originating in the MU are measured as a time varying signal. Only certain spatial properties of the MU are reflected in the temporal characteristics of SEMG signal such as its duration. To eliminate these limitations, the noninvasive technique has been extended with the design of linear and two dimensional electrode arrays and grids. Linear array electrode can be used to estimate muscle conduction velocity (MCV) of electrical activity along the muscle fiber [21]. But it never became a widely accepted clinical diagnostic tool due to its limitation in addressing most of the clinically relevant issues regarding the properties of MU. Two dimensional multi electrode grids cover a larger pick up area of the muscle

and add spatial information that is largely independent on temporal information [18]. The most common utilization of multi-electrode is represented by the detection of the innervation or motor endplate region [23]. The enhancement of the activity of superficial MUs [31] and the estimation of MU size and location [32] represent some of the challenging applications of 2D grid array.

4.2 Grid Spacing

The potential distribution on the skin generated by an active muscle provides a deeper understanding of electrical phenomena taking place inside the muscle tissue and may reveal some clinical information about the muscle structure. To achieve this goal measured potential will have to be free from spatial aliasing and distortion. In this regard, noninvasive multi-electrode technique can be implemented by determining appropriate dimension and grid spacing of surface electrode. Larger inter electrode distance will cause spatial aliasing and smaller spacing will cause spatial over sampling without increasing the information content of the sampled signals. Proper calculation of grid spacing considering the depth of muscle fibers is really a vital one for accurate detection of SEMG signals.

To obtain an adequate resolution in the spatial domain, the inter-electrode distance (IED) of grid electrode has to high enough to meet the spatial version of Nyquist criterion. The highest temporal frequency components of the SEMG can be considered around 400 Hz [2]. According to Nyquist criterion, the minimum sampling frequency of the propagating

action potential is 800 Hz, which results maximum sampling interval of 1.25 ms. Assuming a constant conduction velocity over the fiber of 4 m/s, the propagating component should be sampled with a maximum IED of 5 mm. This calculation is based on the worst-case scenario. The frequency contents of the SEMG signal vary with the location of active muscle fiber and properties of volume conduction medium. Therefore, it is necessary to develop a systematic approach to select an appropriate inter-electrode distance of the two dimensional grid arrays by taking into account the relevant spatial characteristics of SEMG signals.

4.2.1 Design Methodology

Requirement of grid spacing is directly related to the volume conductor model of single fiber action potential (SFAP) signal. The equation of SFAP can be represented as a spatial convolution between the transmembrane current and the transfer function of the volume conductor. The peak value of the transfer function of the muscular medium declines as the distance between the observation point and line source increases. Thus, only the transfer or weighting function can be considered in calculation of grid spacing. Two different approaches of transfer function are used to analyze and establish the theoretical concept of grid spacing. In the spatial domain (approach 1), the impulse response of the volume conductor is a filter function calculated as the potential of a unit current line source within a medium with cylindrical anisotropy. For an observation point (x,y,z) and a current line source located at $(x_o,y_o,z_o(t))$ in a medium with cylindrical anisotropy, the impulse response of the volume conductor can be written as:

$$h_{muscle}(x,y,z) = \frac{a}{2\sigma_r} \frac{1}{\sqrt{R_a\, r^2 + (z - z_0(t))^2}} \tag{4.1}$$

where $r = \sqrt{\{(x - x_0)^2 + (y - y_0)^2\}}$

Implementing boundary condition in the solution of modified Laplace equation the form of weighting function is obtained in the spatial frequency domain (approach 2), which can be written as:

$$H_{muscle}(x,y,\omega_z) = \frac{1}{\sigma_r} \frac{K_0\left(r\sqrt{R_a}\,|\omega_z|\right)}{\sqrt{R_a}\,|\omega_z|\,K_1\left(a\sqrt{R_a}\,|\omega_z|\right)} \tag{4.2}$$

The weighting function in spatial domain can also be calculated by taking the inverse FFT of the Equation (4.2).

The isotropic layers of subcutaneous fat and skin provide an adverse effect in measuring the activity of muscle. The layers of fat and skin cause an attenuation and spatial widening of the SEMG signals and consequently limit the depth of measurable action potential of MU beneath the skin. The potential distributions at the surface of different layers are derived in previous chapter. The theoretical transfer function of the fat and skin in spatial frequency domain can be obtained by dividing the potential at the top of skin by the potential at muscle surface.

$$H_{fat\&skin}(\omega_x,\omega_z) = \frac{2}{(1+R_c)\cosh\left(\omega_y\left(t_f + t_s\right)\right) + (1-R_c)\cosh\left(\omega_y\left(t_f - t_s\right)\right)} \tag{4.3}$$

The distance between consecutive electrodes is more sensitive along z direction, due to the propagation of intracellular action potential along the fiber. The IED along x direction can be assumed same as z direction in order to maintain the symmetrical shape

of grid electrode. That's why, only the spatial variation of transfer function along z direction is considered in this study. The transfer function of fat and skin is incorporated with the transfer function of muscle (volume conductor model) to analyze the combined effect on spatial aliasing and grid electrode spacing.

$$H_{total}(\omega_z) = H_{muscle}(\omega_z) \times H_{fat\&skin}(\omega_z) \tag{4.4}$$

The total transfer function of intermediate tissue layers behaves as a low pass filter. The spatial characteristic of the filter depends on the depth of active fiber inside muscle. The patterns of spatial transfer function for different distance with respect to muscle surface are simulated using both approaches. To measure the spatial cut off frequency, each signal is passed through second order Butterworth low pass filters having different cutoff frequencies. The error between the filtered and original values of normalized signal is considered as the criterion for calculating cut off frequency. The definition of average and maximum error functions can be mentioned as:

$$Error_{avg} = \sqrt{\Delta t \sum_{i=1}^{N} \left(h_{n_i} - hf_{n_i}\right)^2} \times 100 \tag{4.5}$$

$$Error_{\max} = \sqrt{\left(h_{n_i} - hf_{n_i}\right)^2_{\max}} \times 100 \tag{4.6}$$

where h_n is the normalized transfer function, hf_n is the filtered value and Δt is the sampling interval. Average error function is selected to set the level of accuracy in worst-case condition. Thus, error values are calculated at different depth of muscle fibers for a range of normalized cutoff frequencies of Butterworth filter. Three different limits of error – 1%, 5% and 10% are used for judicial justification of spatial cut off frequency. To ensure the rapid changes in the potential distribution over the skin surface can be

recorded, the density of the electrode has to be high enough to meet the spatial version of Nyquist criterion. Minimum spatial frequency should be equal the twice of the spatial cut off frequency. The inverse of Nyquist frequency represents the minimum required inter-electrode distance for a particular direction and distance.

4.2.2 Simulation Results

Simulations are performed adopting electrophysiological parameters of muscle and behaviors of source same as previous chapters. The sampling frequency, muscle fiber diameter and length are also kept unchanged. Figure 4.1 shows the profile of normalized impulse response of the medium for a fiber located at a depth of 2 mm from the muscle surface. The effect of isotropic layers of fat and skin is incorporated for two different cases of thickness (generally normal and obese people) for direct comparison. The thickness of skin is considered 1 mm and the thickness of fat considered 3 mm for normal people and 8 mm for obese people. The conductivity ratio between fat and skin layer, R_c is considered 20. The figure illustrates the spatial widening effect of fat and skin layers on the transfer function of volume conductor model for a particular muscle fiber.

The combined transfer function of the volume conductor model is analyzed in both space (approach 1) and spatial frequency domain (approach 2) for comparison. The profiles of transfer functions are calculated by varying the depth of a muscle fiber from 1 mm to 50 mm with respect to the muscle surface. Each transfer function is passed through a second order low pass Butterworth filter having a normalized frequency range from 0.001 to 0.999. The average percentage of errors are calculated for the whole set of cutoff

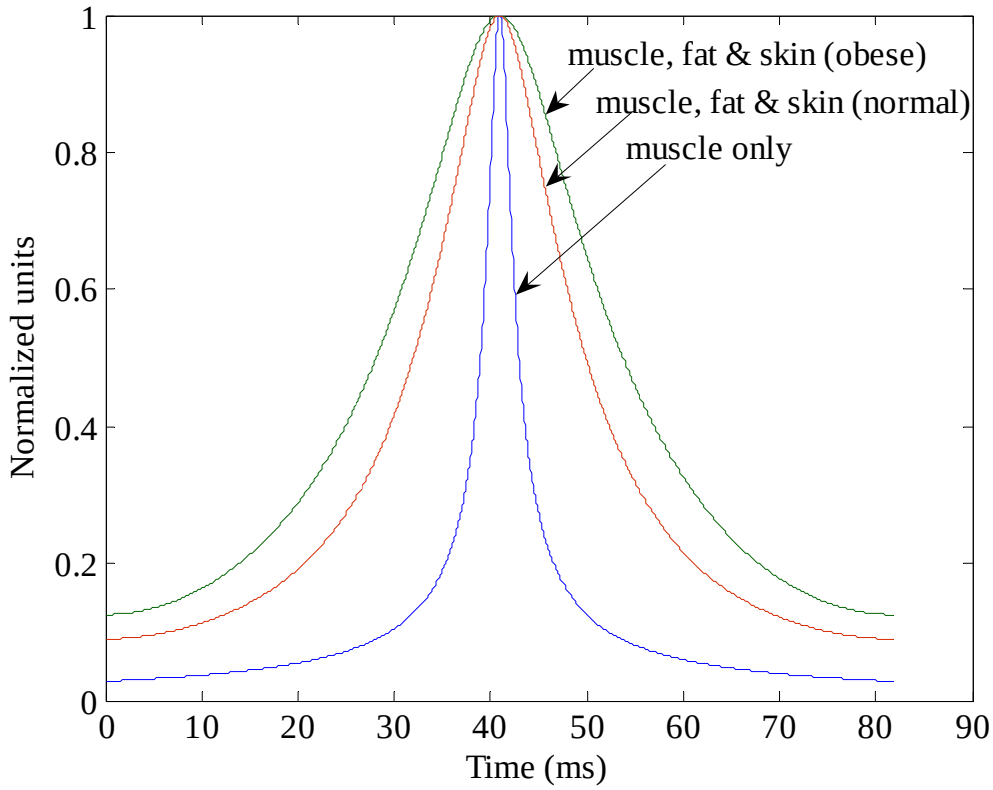

Figure 4.1: The transfer function of the SFAP model for a muscle fiber located 2 mm deep inside muscle - at the top of muscle and at the surface of skin for normal people (t_f =3 mm and t_s =1 mm) and obese people (t_f =8 mm and t_s =1 mm).

frequencies. Thus a two-dimensional error matrix is obtained with the variation of normalized cutoff frequency in one direction and the depth of fiber in other direction. From this error matrix spatial cutoff frequencies are picked up only for 1%, 5% and 10% error level for a particular depth of fiber. Table 4.1 and Table 4.2 show the variation of spatial cut off frequency and corresponding required minimum inter-electrode distance (IED) with the depth of active fiber inside the muscle for three different set of error level between the filtered and original values of normalized transfer function for the case of normal and obese people respectively. Required IED values are very sensitive when the position of fiber is very close to the muscle surface. But it increases with the depth of muscle and the rate is higher initially, then it decreases towards a certain steady state value. This behavior directly depends upon the shape and nature of transfer function of volume conductor. Figure 4.2 shows the profile of spatial cutoff frequency as a function of the distance of the location of active fiber inside the muscle. The curves simulated using the transfer function obtained from both space and spatial frequency domain show almost same characteristics, which depict the accuracy of the approximation.

4.2.3 Required Grid Spacing

The volume conductor muscle model is utilized to demonstrate an innovative methodology in designing 2D surface grid electrode. The presence of subcutaneous fat and skin layers play a significant role in this matter. The isotropic nature of skin and fat layers not only spread the signal spatially but also incorporate severe attenuation upon its amplitude. So it is worthy to set a trade off between these two phenomena to determine a practically allowable grid spacing to measure the activity of the deepest fiber inside the

Table 4.1: Variation of spatial cut off frequency and required inter-electrode distance with the depth of muscle fiber from muscle surface considering the effect of subcutaneous tissue layers for normal people (Thickness of fat = 3 mm, Thickness of skin = 1 mm).

Distance (mm)	Approach 1						Approach 2					
	Spatial Cut Off frequency, f_s (1/mm)			Required Minimum IED, d_e (mm)			Spatial Cut Off frequency, f_s (1/mm)			Required Minimum IED, d_e (mm)		
	Error			Error			Error			Error		
	1%	5%	10%	1%	5%	10%	1%	5%	10%	1%	5%	10%
1	2.167	0.481	0.237	0.231	1.04	2.106	2.086	0.456	0.225	0.24	1.097	2.22
5	1.811	0.388	0.194	0.276	1.29	2.576	1.636	0.344	0.169	0.306	1.455	2.957
10	1.567	0.331	0.162	0.319	1.509	3.08	1.368	0.281	0.138	0.366	1.777	3.625
15	1.405	0.287	0.144	0.356	1.739	3.471	1.199	0.244	0.119	0.417	2.053	4.201
20	1.281	0.262	0.131	0.39	1.905	3.81	1.086	0.219	0.106	0.46	2.282	4.708
25	1.18	0.244	0.119	0.424	2.053	4.201	1.005	0.206	0.1	0.497	2.424	4.995
30	1.099	0.225	0.113	0.455	2.22	4.428	0.943	0.187	0.094	0.53	2.668	5.319
35	1.037	0.212	0.106	0.482	2.354	4.708	0.9	0.181	0.088	0.556	2.758	5.689
40	0.981	0.2	0.1	0.51	2.498	4.995	0.856	0.169	0.081	0.584	2.957	6.159
45	0.931	0.187	0.094	0.537	2.668	5.319	0.825	0.162	0.081	0.606	3.08	6.159
50	0.887	0.181	0.088	0.564	2.758	5.689	0.8	0.156	0.081	0.625	3.2	6.159

Table 4.2: Variation of spatial cut off frequency and required inter-electrode distance with the depth of muscle fiber from muscle surface considering the effect of subcutaneous tissue layers for obese people (Thickness of fat = 8 mm, Thickness of skin = 1 mm).

Distance (mm)	Approach 1						Approach 2					
	Spatial Cut Off frequency, f_s (1/mm)			Required Minimum IED, d_e (mm)			Spatial Cut Off frequency, f_s (1/mm)			Required Minimum IED, d_e (mm)		
	Error			Error			Error			Error		
	1%	5%	10%	1%	5%	10%	1%	5%	10%	1%	5%	10%
1	1.786	0.381	0.187	0.28	1.311	2.668	1.749	0.369	0.187	0.286	1.356	2.668
5	1.549	0.325	0.162	0.323	1.54	3.08	1.455	0.3	0.15	0.344	1.665	3.33
10	1.387	0.287	0.144	0.361	1.739	3.471	1.262	0.256	0.125	0.396	1.95	3.996
15	1.268	0.262	0.131	0.394	1.905	3.81	1.137	0.231	0.113	0.44	2.162	4.428
20	1.174	0.237	0.119	0.426	2.106	4.201	1.049	0.212	0.106	0.477	2.354	4.708
25	1.099	0.225	0.113	0.455	2.22	4.428	0.981	0.2	0.1	0.51	2.498	4.995
30	1.037	0.212	0.106	0.482	2.354	4.708	0.925	0.187	0.094	0.541	2.668	5.319
35	0.987	0.2	0.1	0.507	2.498	4.995	0.881	0.175	0.088	0.568	2.854	5.689
40	0.937	0.187	0.094	0.534	2.668	5.319	0.844	0.169	0.081	0.593	2.957	6.159
45	0.893	0.181	0.088	0.56	2.758	5.689	0.818	0.162	0.081	0.611	3.08	6.159
50	0.862	0.175	0.088	0.58	2.854	5.689	0.793	0.156	0.075	0.63	3.2	6.66

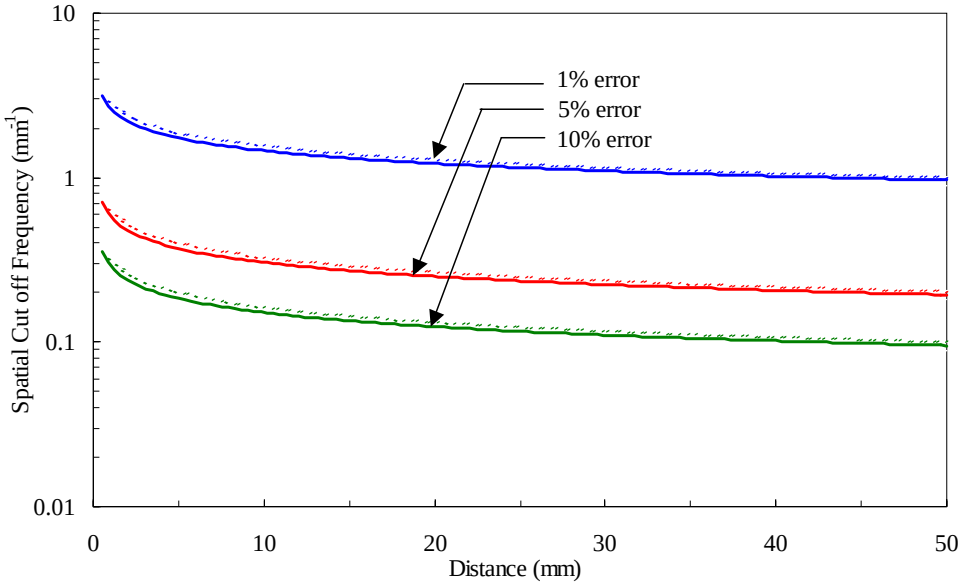

(a)

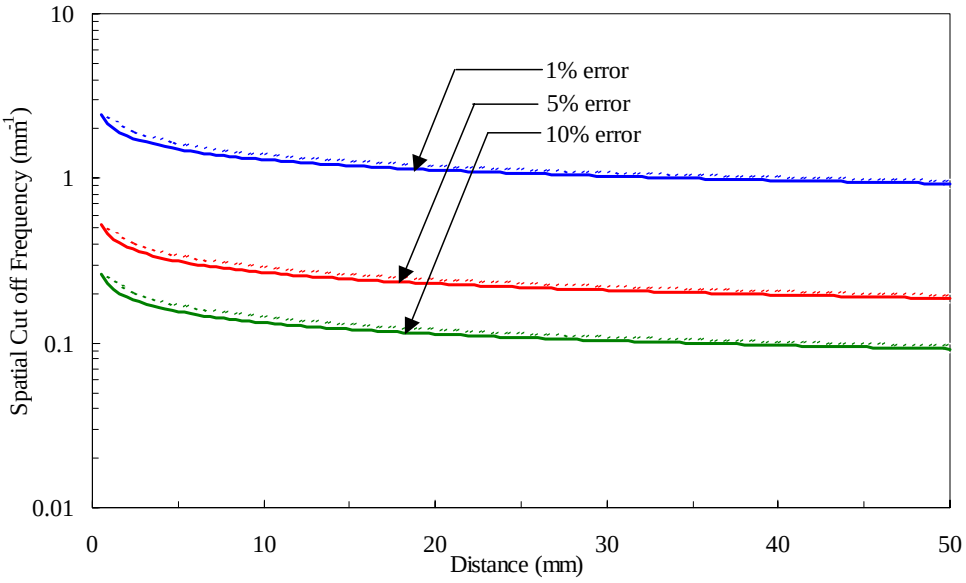

(b)

Figure 4.2: Spatial cut off frequency as a function of the distance of depth of muscle fiber considering the effect of subcutaneous tissue layers for normal people (a) and obese people (b) at 1%, 5% and 10% error level considering average error using approach1 (solid line) and approch2 (break line).

muscle considering the limitation of SEMG signals. The muscle fibers located closer to the electrode subject to high rate of change in amplitude and phase. This effect reduces the required minimum inter-electrode distance to meet the Nyquist criterion for spatial sampling. The values of required IED increases almost linearly with the increment of the depth of muscle fiber due to the continuous reduction of the average slope of the transfer function of the medium. Simulation result shows that the minimum IED for the muscle fiber located at 1 mm and 30 mm inside the muscle are 2.6 mm and 5.3 mm respectively for 10% error level. For the case of an entire muscle the grid spacing should meet the requirement of the closest muscle fiber to eliminate spatial aliasing and distortion. As a whole, the selection of grid spacing in the range 2.5~3 mm is an ideal choice for the topographic imaging of SEMG signals.

4.3 Spatial Filter

Surface electrode detects the compound activity of a large number of motor units. But, it is important to reduce the detection volume for specific and accurate electrophysiological analysis of a single motor unit. The concept of implementing spatial filter in the form of one or two dimensional grid electrode array was introduced to overcome this inherent limitation of surface detection technique [4,31]. The purpose of spatial filter is to enhance the spatial selectivity of the recorded signal. In image processing, spatial filters are used to enhance edges in the picture. An edge in image corresponds to an amplitude step in the spatial electromyographic surface potential. The spatial frequency content of the SEMG signal moves towards lower frequencies as the distance from the source

increases [8]. So, the selectivity can be improved by designing selective high pass spatial filter. In surface electromyography, spatial filtering is performed by taking the weighted summation of signals detected at electrodes. The spatial resolution of the electrode array has to satisfy the Nyquist criterion of spatial sampling, which is discussed in previous section. Geometrical arrangement and number of required electrode depends on the type of filter. Different types of filter correspond to different type of filter mask. Three types of spatial high pass filter are commonly used in different research activities on SEMG signal as well as in image processing- normal double differentiating (NDD), inverse rectangle (IR) and inverse binomial (IB) filter. These filters are defined by following filter mask:

$$M_{NDD} = \begin{bmatrix} 0 & -1 & 0 \\ -1 & 4 & -1 \\ 0 & -1 & 0 \end{bmatrix}, \quad M_{IR} = \frac{1}{9}\begin{bmatrix} -1 & -1 & -1 \\ -1 & 8 & -1 \\ -1 & -1 & -1 \end{bmatrix} and \quad M_{IB2} = \frac{1}{16}\begin{bmatrix} -1 & -2 & -1 \\ -2 & 12 & -2 \\ -1 & -2 & -1 \end{bmatrix}$$

NDD filter is obtained by taking second spatial derivative in two dimensions. It represents the discrete Laplace operator, which is well suited for detection of edges perpendicular to the direction of differentiation [6]. Another approach to get high pass filter is the inversion of smoothing filter. The difference between the unfiltered and the smoothed signal contains only high frequency components. Rectangle filter and binomial filter are well known smoothing filter having isotropic transfer function [16]. Thus, IR and IB filter masks are obtained by the inversion of rectangle and binomial filter. For a discrete grid electrode array the transfer function of the filter in spatial frequency domain can be derived from filter mask using following equation [10],

$$H_{filter}(\omega_x,\omega_z) = \sum_{m=-K}^{K}\sum_{n=-L}^{L} M_{filter}(m,n)e^{-i\omega_x m d_x} e^{-i\omega_x n d_z} \quad (4.7)$$

where K and L are number of columns right or left and number of rows above or below the center of the electrode array respectively, M_{filter} is the spatial filter mask and d_x and d_z are inter-electrode distance in x and z direction respectively. Considering 2.5 mm inter-electrode distance, the transfer functions of NDD, IR and IB2 filters are plotted in Figure 4.3. The figure shows that transfer function of NDD filter becomes anisotropic at higher spatial frequencies. IR filter shows a higher isotropy compared to the NDD filter and IB2 filer exhibits the behavior of an almost complete isotropic filter.

4.3.1 Concept of Filter to Eliminate Fat and Skin Effect

The effect of spatial widening and attenuation of subcutaneous tissue layers of fat and skin limits the application of surface detection of EMG signal. From simulation, it is found that the transfer function of isotropic tissue layers behaves as a low pass filter (Figure 4.4). It hinders the detection of the high frequency components of action potential generated by superficial muscle fibers and consequently, causes a blurring effect on surface potentials. To compensate this effect a spatial high pass filter can be designed with the aim of inverting the transfer function of fat and skin layers [7]. The high pass filter needs to be implemented in the form of filter mask to develop a two-dimensional discrete spatial grid filter. The bandwidth of the spatial filter has to be equal to or smaller than the half of the inverse of the IED. So, the practical limitations for the IED and the number of electrodes have to be considered to implement a discrete filter with a matrix of electrode.

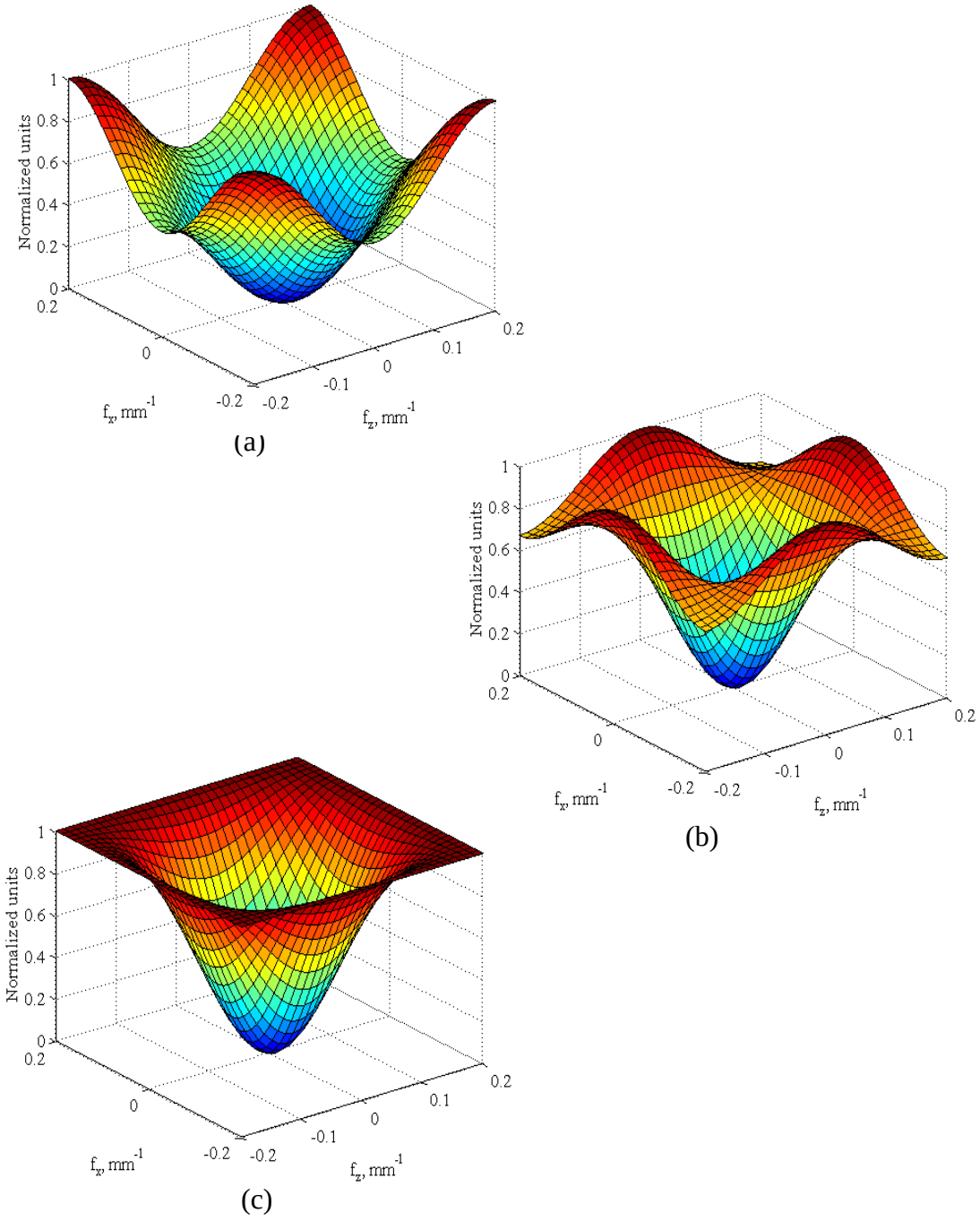

Figure 4.3: Comparison of transfer function of NDD, IR and IB2 spatial filters. Maximum spatial frequency is calculated assuming inter-electrode distance of 2.5 mm.

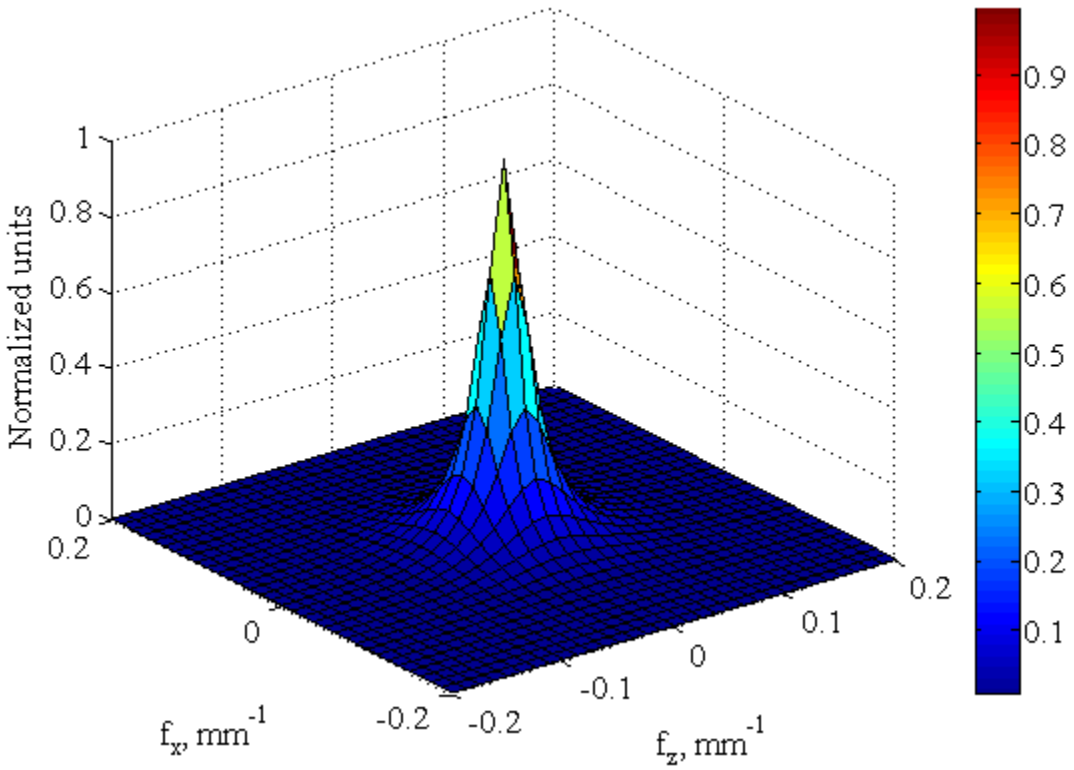

Figure 4.4: Transfer function of isotropic fat and skin layers in two-dimensional spatial frequency domain for fat thickness, t_f=3 mm, skin thickness, t_s=1 mm and conductivity ratio, R_c=20.

The transfer function of subcutaneous tissue layers depends on the properties of fat and skin only. The transfer function of the isotropic high pass filter can be represented by taking the inverse of the transfer function as:

$$H^{-1}_{fat\&skin}(\omega_x,\omega_z)=\frac{(1+R_c)\cosh(\omega_y(t_f+t_s))+(1-R_c)\cosh(\omega_y(t_f-t_s))}{2} \tag{4.8}$$

It represents the ideal characteristics of the inverse filter as a function of the fat and skin thickness and their conductivity ratio. By expanding the hyperbolic cosine function Equation (4.8) can be expressed as:

$$\begin{aligned} H^{-1}_{fat\&skin}(\omega_x,\omega_z) &= C_1\sum_{n=0}^{\infty}\frac{(\omega_y t_1)^{2n}}{(2n)!}+C_2\sum_{n=0}^{\infty}\frac{(\omega_y t_2)^{2n}}{(2n)!} \\ &= \sum_{n=0}^{\infty}\frac{C_1 t_1^{2n}+C_2 t_2^{2n}}{(2n)!}(\omega_x^2+\omega_z^2)^n \end{aligned} \tag{4.9}$$

where $C_1=\frac{1+R_c}{2}$, $C_2=\frac{1-R_c}{2}$ *and* $t_1=t_f+t_s$, $t_2=t_f-t_s$.

Implementing the binomial Newton formula the inverse transfer function can be represented as:

$$H^{-1}_{fat\&skin}(\omega_x,\omega_z)=\sum_{n=0}^{\infty}\sum_{r=0}^{n}\frac{C_1 t_1^{2n}+C_2 t_2^{2n}}{(2n)!}\frac{n!}{r!(n-r)!}\omega_z^{2r}\omega_x^{2(n-r)} \tag{4.10}$$

According to transformation theory,

$$\mathrm{F}[\delta^n(x)]\rightarrow(i\omega_x)^n$$

$$\mathrm{F}^{-1}[\omega_x^n]\rightarrow(-i)^n\delta^n(x)$$

Inverse Fourier transform of spatial frequency having nth power represents the nth derivative of delta function. The output of a system due to the input of delta function is termed as transfer function. Using this concept the inverse transfer function can be

expressed in spatial domain as:

$$H^{-1}_{fat\&skin}(x,z)=\sum_{n=0}^{\infty}\sum_{r=0}^{n}(-1)^n\frac{C_1t_1^{2n}+C_2t_2^{2n}}{(2n)!}\frac{n!}{r!(n-r)!}\left(\frac{\partial}{\partial z}\right)^{2r}\left(\frac{\partial}{\partial x}\right)^{2(n-r)} \tag{4.11}$$

Inverse Fourier transforms of spatial angular frequency, ω_x and ω_z convert the ideal inverse filter as linear combination of differential operators of even order. On a discrete grid ideal derivative operator can be approximated by discrete differential operator.

$$H^{-1}_{fat\&skin}(\omega_x,\omega_z)=\sum_{n=0}^{\infty}\sum_{r=0}^{n}(-1)^n\frac{C_1t_1^{2n}+C_2t_2^{2n}}{(2n)!}\frac{n!}{r!(n-r)!}(D_z)^{2r}(D_x)^{2(n-r)} \tag{4.12}$$

where D_x ans D_z represent the approximated discrete differential operators in spatial frequency domain along x and z directions respectively. For two-element filter mask the transfer function of the discrete differential operator can be approximated as [16]:

$$\begin{aligned} D &= \exp\left(i\pi\frac{\tilde{\omega}}{2}\right)\left[1-\exp\left(-i\pi\tilde{\omega}\right)\right] \\ &= 2i\sin\left(\pi\frac{\tilde{\omega}}{2}\right) \end{aligned} \tag{4.13}$$

where $\tilde{\omega}$ is the standardized angular wave number, which is normalized with respect to the maximum value of wave number. To meet the Nyquist theorem, at least two samples have to be taken in a wavelength. It results the maximum wave number as:

$$\omega_{\max}=\frac{2\pi}{2e} \tag{4.14}$$

$$\therefore\ \tilde{\omega}=\omega\frac{e}{\pi} \tag{4.15}$$

where e is the inter-electrode distance of the discrete grid filter, which determines the

distance between two adjacent spatial samples. Then the transfer function of discrete differential operator of order *n* becomes,

$$D^n = (2i)^n \sin^n\left(e\frac{\omega}{2}\right) \tag{4.16}$$

Introducing this approximation and truncating the series up to order *N*, the approximated transfer function of the inverse spatial discrete filter becomes,

$$H^{-1}_{fat,skin}(\omega_x,\omega_z) = \sum_{n=0}^{N}\sum_{r=0}^{n} 2^{2n}\,\alpha_n \frac{n!}{r!(n-r)!}\sin^{2r}\left(\omega_z\frac{e}{2}\right)\sin^{2(n-r)}\left(\omega_x\frac{e}{2}\right) \tag{4.17}$$

where $\alpha_n = \dfrac{C_1 t_1^{2n} + C_2 t_2^{2n}}{(2n)!}$

4.3.2 Simulation of Filter Transfer Function

From expression it is found that the behavior of the inverse spatial filter depends on the thickness of fat and skin, conductivity ratio, allowable inter-electrode distance and the order of filter. The periodicity of the filter depends on inter-electrode distance, which can be selected based on the spatial characteristics of the SEMG signal. Considering the practical limitations, the inter-electrode distance is assumed 2.5 mm, which determines that the spatial frequencies will be lower than 0.2 mm^{-1}. For the conduction velocity of 4 m/s, time frequencies will be lower than 800 Hz. Figure 4.5 shows the transfer function of ideal inverse spatial filter in spatial frequency domain. Thickness of fat and skin and conductivity ratio between this two these two layers are considered 3 mm, 1 mm and 20 respectively. The shape of the transfer function clearly demonstrates the characteristics of an isotropic high pass filter. Figure 4.6 depicts the transfer function of the

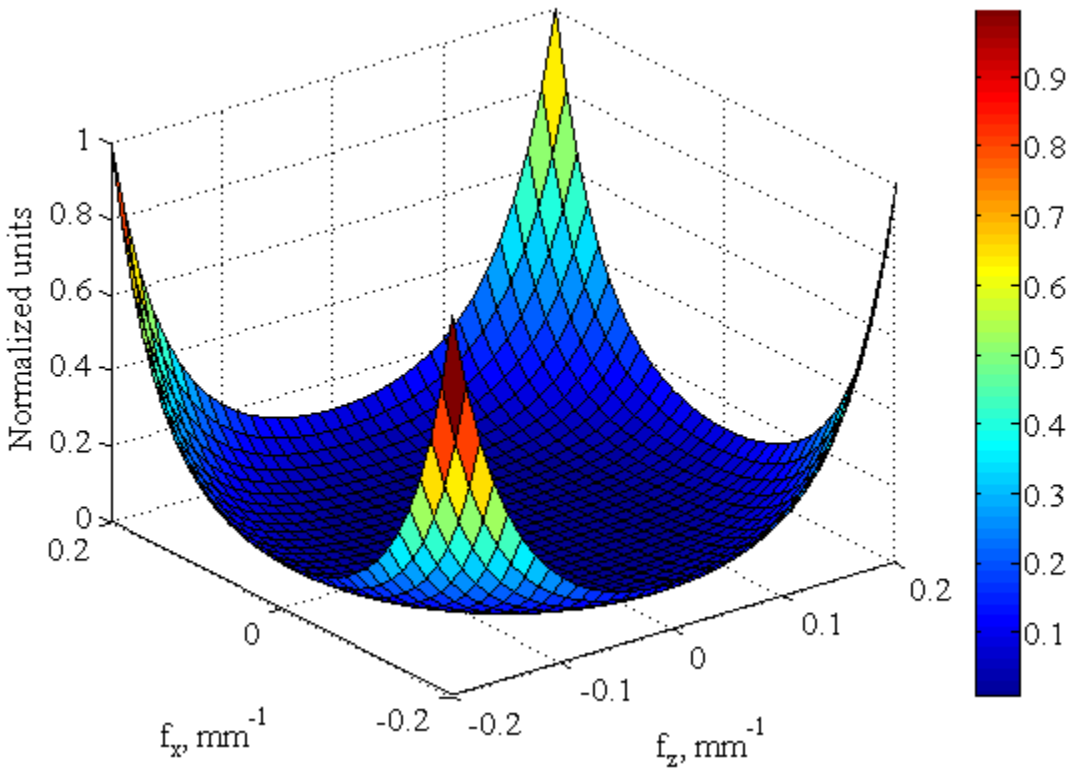

Figure 4.5: Transfer function of ideal inverse spatial filter with fat and skin layers of thickness 3 mm and 1 mm respectively and conductivity ratio R_c=20.

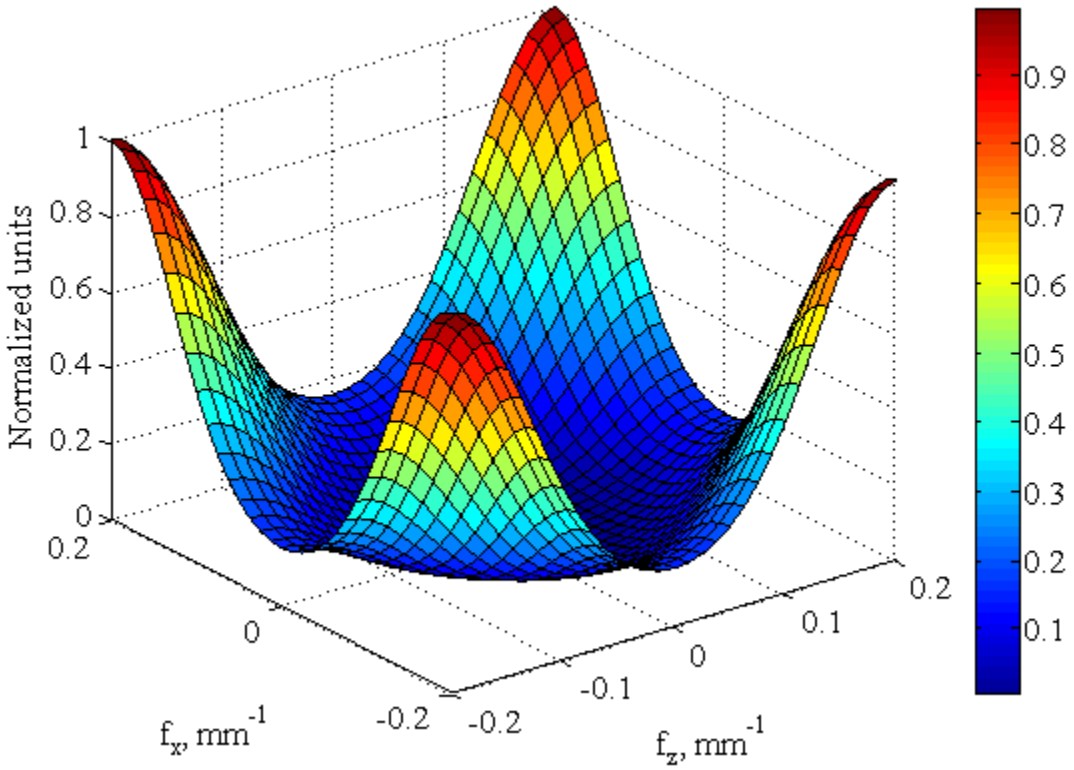

Figure 4.6: Transfer function of approximated inverse spatial filter of order three with fat and skin layers of thickness 3 mm and 1 mm respectively and conductivity ratio R_c=20.

approximated inverse spatial filter. The summation of the series of Equation (4.17) is truncated at order three. The periodicity of the transfer function is incorporated by approximating the discrete differential operators with two sinusoids in two spatial directions. The behavior of the approximated filter of different order is compared with ideal filter in Figure 4.7. The cutoff frequency of the inverse high pass filter is reduced due to approximation. But it approaches towards ideal filter with increment of filter order. The effect of fat thickness on the filter is analyzed in Figure 4.8. The increment of fat thickness increases the cutoff frequency of the ideal filter and the rate of decay coefficient is higher for layers of greater thickness. But for the case of approximated filter, this effect is not as prominent as it is for the ideal filter. It reveals one of the limitations of the approximated discrete filter.

4.3.3 Derivation of Filter Mask

The discrete filter function is approximated as a summation of factors, which are the multiplication of two discrete differential operators in two spatial frequency domains (Equation 4.12). In the spatial domain discrete differential operator, D_z and D_x can be approximated by two-element filter mask along z and x directions as:

$$d_z = \begin{bmatrix} 1 & -1 \end{bmatrix} \quad and \quad d_x = \begin{bmatrix} 1 \\ -1 \end{bmatrix} \tag{4.18}$$

The power of differential operator determines the degree of first order differential filter mask. The multiplication in spatial frequency domain corresponds convolution in space

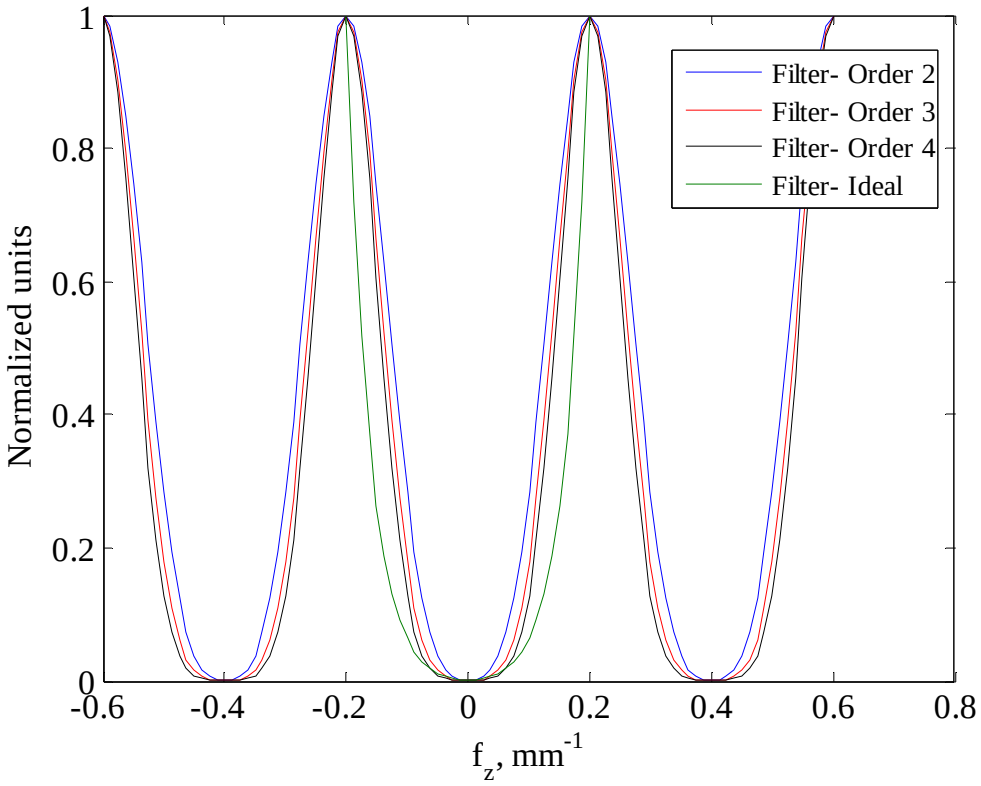

Figure 4.7: Behavior of periodic inverse spatial filters of different order with respect to the ideal characteristics of filter.

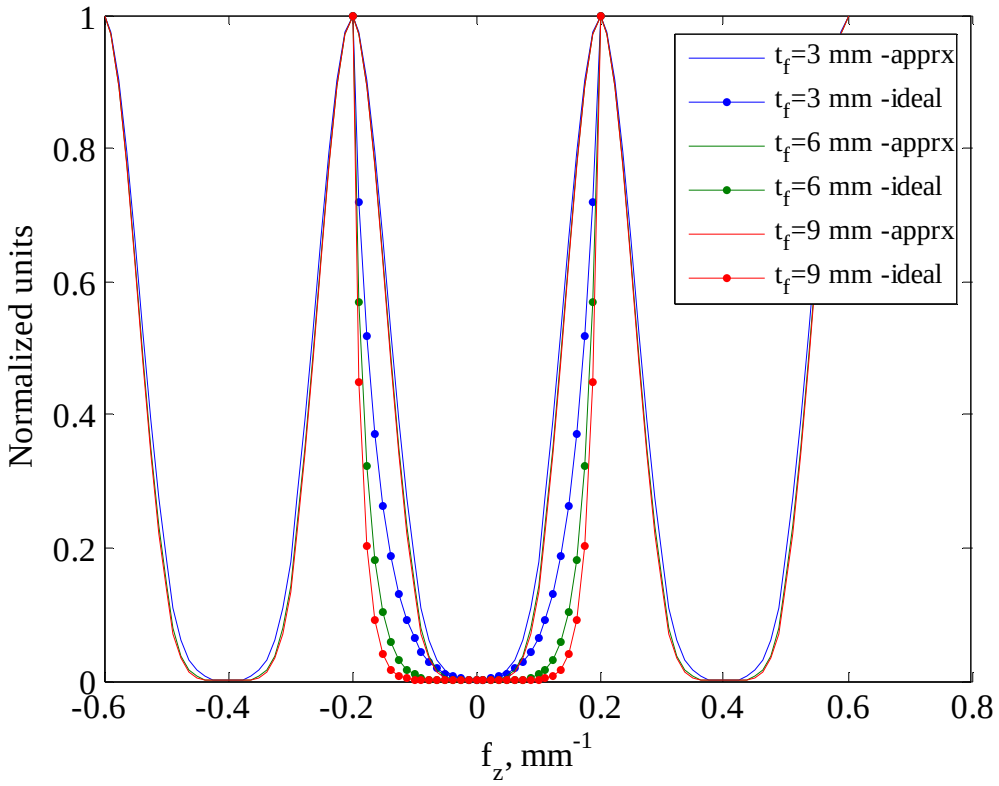

Figure 4.8: Comparison between third order approximated and ideal inverse spatial filter with the variation of fat thickness.

domain. Thus, filter mask can be obtained by taking the summation of convolution of various differential operators of different orders in the two spatial directions. In spatial domain, differential operator with different orders are calculated as follows,

$$D_z^2 = D_z \times D_z \rightarrow d_z * d_z = \begin{bmatrix} 1 & -1 \end{bmatrix} * \begin{bmatrix} 1 & -1 \end{bmatrix} = \begin{bmatrix} 1 & -2 & 1 \end{bmatrix} \quad \textit{and}$$

$$D_x^2 = D_x \times D_x \rightarrow d_x * d_x = \begin{bmatrix} 1 \\ -1 \end{bmatrix} * \begin{bmatrix} 1 \\ -1 \end{bmatrix} = \begin{bmatrix} 1 \\ -2 \\ 1 \end{bmatrix}$$

In a similar manner,

$$D_z^4 \rightarrow \begin{bmatrix} 1 & -4 & 6 & -4 & 1 \end{bmatrix} \quad \textit{and} \quad D_x^4 \rightarrow \begin{bmatrix} 1 \\ -4 \\ 6 \\ -4 \\ 1 \end{bmatrix}$$

$$D_z^6 \rightarrow \begin{bmatrix} 1 & -6 & 15 & -20 & 15 & -6 & 1 \end{bmatrix} \quad \textit{and} \quad D_x^6 \rightarrow \begin{bmatrix} 1 \\ -6 \\ 15 \\ -20 \\ 15 \\ -6 \\ 1 \end{bmatrix}$$

Different components involved in calculating the filter mask are presented in Table 4.3. The calculation is performed for the case of a third order approximated inverse spatial filter to eliminate the effect of 3 mm thick fat layer and 1 mm thick skin layer.

Table 4.3: Different components of approximated inverse spatial filter.

n	$(-1)^n \alpha_n$	r	$\frac{n!}{r!(n-r)!}$	$(d_z)^{2r} * (d_x)^{2(n-r)}$
0	1	0	1	$\begin{bmatrix} 1 \end{bmatrix}$
1	-65	0	1	$\begin{bmatrix} 1 \\ -2 \\ 1 \end{bmatrix}$
		1	1	$\begin{bmatrix} 1 & -2 & 1 \end{bmatrix}$
2	105.67	0	1	$\begin{bmatrix} 1 \\ -4 \\ 6 \\ -4 \\ 1 \end{bmatrix}$
		1	2	$\begin{bmatrix} 1 & -2 & 1 \\ -2 & 4 & -2 \\ 1 & -2 & 1 \end{bmatrix}$
		2	1	$\begin{bmatrix} 1 & -4 & 6 & -4 & 1 \end{bmatrix}$
3	-58.89	0	1	$\begin{bmatrix} 1 \\ -6 \\ 15 \\ -20 \\ 15 \\ -6 \\ 1 \end{bmatrix}$
		1	3	$\begin{bmatrix} 1 & -2 & 1 \\ -4 & 8 & -4 \\ 6 & -12 & 6 \\ -4 & 8 & -4 \\ 1 & -2 & 1 \end{bmatrix}$
		2	3	$\begin{bmatrix} 1 & -4 & 6 & -4 & 1 \\ -2 & 8 & -12 & 8 & -2 \\ 1 & -4 & 6 & -4 & 1 \end{bmatrix}$
		3	1	$\begin{bmatrix} 1 & -6 & 15 & -20 & 15 & -6 & 1 \end{bmatrix}$

The summation of all the components result following filter mask:

$$ {}^{3}M = \begin{bmatrix} 0 & 0 & 0 & -58.899 & 0 & 0 & 0 \\ 0 & 0 & -176.67 & 812.35 & -176.67 & 0 & 0 \\ 0 & -176.67 & 1624.70 & -4267.09 & 1624.70 & -176.67 & 0 \\ -58.89 & 812.35 & -4267.09 & 8969.90 & -4267.09 & 812.35 & -58.89 \\ 0 & -176.67 & 1624.70 & -4267.09 & 1624.70 & -176.67 & 0 \\ 0 & 0 & -176.67 & 812.35 & -176.67 & 0 & 0 \\ 0 & 0 & 0 & -58.899 & 0 & 0 & 0 \end{bmatrix} $$

The normalized filter mask is obtained by dividing each components of the mask with the maximum value of transfer function (Equation 4.17).

$$ {}^{3}M_{normalized} = \begin{bmatrix} 0 & 0 & 0 & -0.0016 & 0 & 0 & 0 \\ 0 & 0 & -0.0047 & 0.0217 & -0.0047 & 0 & 0 \\ 0 & -0.0047 & 0.0434 & -0.1140 & 0.0434 & -0.0047 & 0 \\ -0.0016 & 0.0217 & -0.1140 & 0.2396 & -0.1140 & 0.0217 & -0.0016 \\ 0 & -0.0047 & 0.0434 & -0.1140 & 0.0434 & -0.0047 & 0 \\ 0 & 0 & -0.0047 & 0.0217 & -0.0047 & 0 & 0 \\ 0 & 0 & 0 & -0.0016 & 0 & 0 & 0 \end{bmatrix} $$

Thus, the dimension of the mask is 7x7 with only 25 nonzero elements for a third order filter. The increment of filter order increases the order of discrete differential operator and consequently increases the dimension of mask. By varying the order of filter it is found that the transfer function of a N order filter can be represented as a matrix of dimension $(2N+1)$x$(2N+1)$ with only $2N^2+2N+1$ nonzero elements. So, the order of filter has to be selected considering the practical limitation of number of electrodes. For a third order filter weighting values of 25 electrodes need to be calculated from 7x7 dimension grid. Eliminating the effect of fat and skin, the new estimated SEMG signal for the

center point in the grid electrode can be mentioned as:

$$\varphi_{filtered}(i, j) = \sum_{k=-N}^{N} \sum_{l=-N}^{N} h_{mask}(k,l)\, \varphi_{electrode}(i-k, j-l) \tag{4.19}$$

where $h_{mask}(k,l)$ are the coefficients obtained form filter mask, $\varphi_{electrode}(i-k, j-l)$ is the measured surface potential at point (i-k, j-l) of the grid electrode array and N is the order of approximated inverse spatial filter.

4.3.4 Analysis of Grid Filter

To analyze the effect of spatial grid filter, an algorithm is developed to generate the normalized filter mask for a particular value of fat and skin thickness and order of approximation. The magnitude of mask coefficients depend on the fat thickness and the dimension of mask depends on the order of filter. To apply the filter mask, the potential distribution at different electrodes of a grid array need to be simulated. There are some limitations regarding the placement of grid electrodes at the surface of skin. The positions of all the electrodes have to be between the endplate and tendon of examined muscle [9]. Otherwise the signal will be distorted due to effect of excitation and extinction. Besides this, the electrodes have to be placed parallel to the muscle fiber and need to be symmetric in perpendicular direction of filter. Adopting these limitations, the array of single fiber action potentials is obtained at different grid points due to an excited muscle fiber located 5 mm depth inside muscle using the algorithm of generating SFAP with respect to the position of recording electrode. The effect of 3 mm fat thickness and 1 mm skin thickness is incorporated in the action potential to generate the potential distribution at skin surface. The initial position of the electrode is considered 20 mm far

away from the endplate and the inter-electrode distance is assumed 2.5 mm. Then the normalized filter mask of third order inverse spatial filter is implemented on the grid signals. Figure 4.9 shows the simulated SFAP signals at the surface of muscle and skin, which demonstrate the effect of subcutaneous fat and skin layers on the complete potential profile of center electrode. The comparison between normalized filtered signal and simulated signal at muscle surface is presented in Figure 4.10. The spatial filter can only recover the spatial effect of fat and skin. Due to this reason, both signals are normalized to observe the spatial effect of the filter. The RMS error between filtered and original signal is 4.947%, which indicates the spatial performance of the filter. One of the advantages of this filter is that it can reject the non-traveling components of the signal. Non-traveling potentials tend to become the major contribution to SEMG signal as the distance of fiber increases from the recording electrode.

Two approximations are considered while designing the algorithm of spatial filter mask. One is truncation order of the transfer function, which represents the order of spatial filter and the other one is the number of weights used to represent the first order discrete differential operator. Both approximations are involved with the dimension of grid filter. The dimension of the filer mask linearly increases with the order of filter. Using the same procedure described for third order filter, the resulting filter masks of second and fourth order filter are presented below.

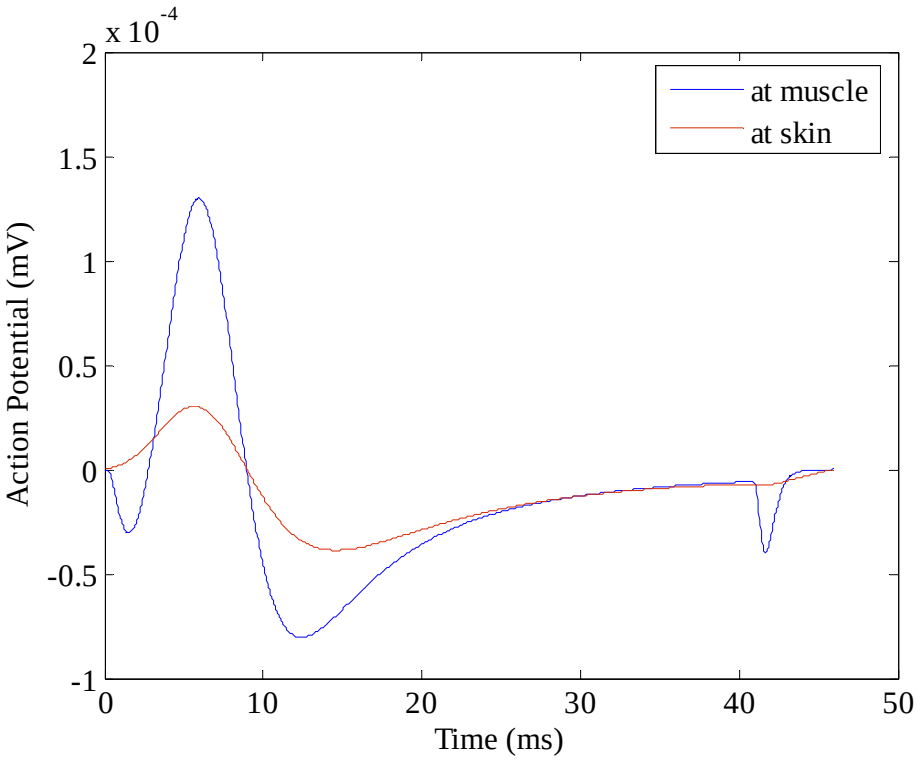

Figure 4.9: Simulated action potential generated at muscle and skin surface by a fiber at the depth of 10 mm within the muscle for the fat and skin layers of thickness 3 mm and 1 mm, conductivity ratio R_c=20.

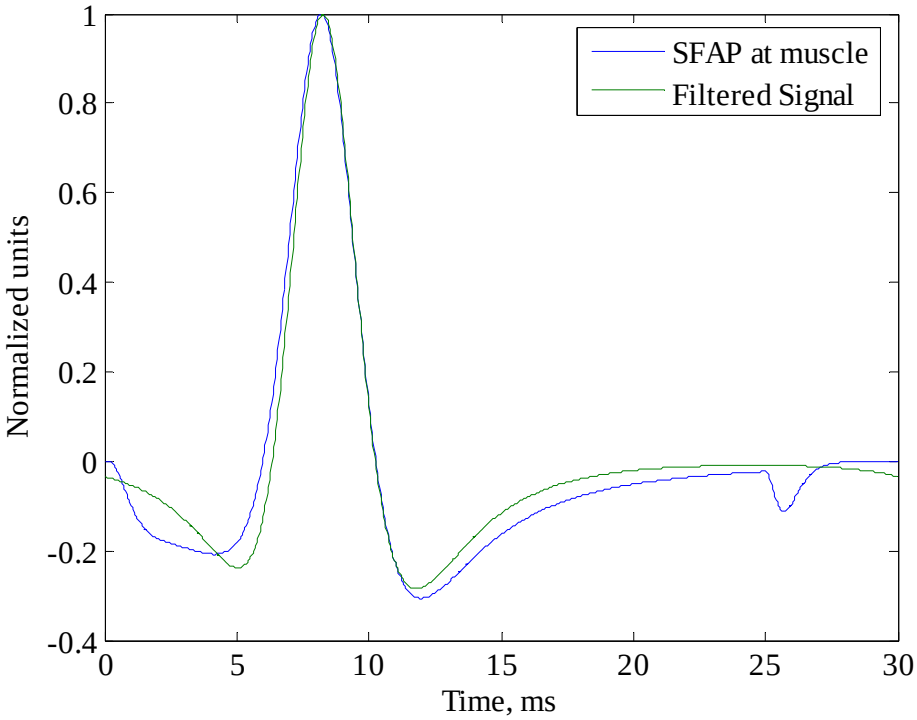

Figure 4.10: Comparison between simulated single fiber action potential at muscle surface and the spatially filtered signal obtained by implementing filter mask on the signals detected from grid electrodes placed at the surface of skin.

$$
{}^{2}M_{Normalized} = \begin{bmatrix} 0 & 0 & 0.0145 & 0 & 0 \\ 0 & 0.0290 & -0.1250 & 0.0290 & 0 \\ 0.0145 & -0.1250 & 0.3260 & -0.1250 & 0.0145 \\ 0 & 0.0290 & -0.1250 & 0.0290 & 0 \\ 0 & 0 & 0.0145 & 0 & 0 \end{bmatrix}
$$

$$
{}^{4}M_{Normalized} =
$$

$$
\begin{bmatrix} 0 & 0 & 0 & 0 & 0.0002 & 0 & 0 & 0 & 0 \\ 0 & 0 & 0 & 0.0006 & -0.0031 & 0.0006 & 0 & 0 & 0 \\ 0 & 0 & 0.0010 & -0.0093 & 0.0254 & -0.0093 & 0.0010 & 0 & 0 \\ 0 & 0.0006 & -0.0093 & 0.0495 & -0.1034 & 0.0495 & -0.0093 & 0.0006 & 0 \\ 0.0002 & -0.0031 & 0.0254 & -0.1034 & 0.1911 & -0.1034 & 0.0254 & -0.0031 & 0.0002 \\ 0 & 0.0006 & -0.0093 & 0.0495 & -0.1034 & 0.0495 & -0.0093 & 0.0006 & 0 \\ 0 & 0 & 0.0010 & -0.0093 & 0.0254 & -0.0093 & 0.0010 & 0 & 0 \\ 0 & 0 & 0 & 0.0006 & -0.0031 & 0.0006 & 0 & 0 & 0 \\ 0 & 0 & 0 & 0 & 0.0002 & 0 & 0 & 0 & 0 \end{bmatrix}
$$

The structure of the filter mask always maintains a diagonal shape for any truncation order. To justify the behavior of the grid filter, the transfer functions of different filters are simulated from mask coefficients by using Equation (4.7). The spatial resolution or inter-electrode distance is keep fixed at 2.5 mm. The simulation results presented in Figure 4.11 seem like a replica of the theoretical transfer functions of approximated spatial filter of different orders. The increment of filter order increases the dimension of filter (required number of electrodes) and approaches the characteristics of the filter towards ideal transfer function. But this improvement is very small with respect to the increment of dimension of the filter. The similarity between the theoretical transfer function, which is used to derive the filter mask and transfer function obtained from filter mask clearly validate the algorithm of designing spatial filter. The second source of approximation of using two points mask in representing discrete differentia operator

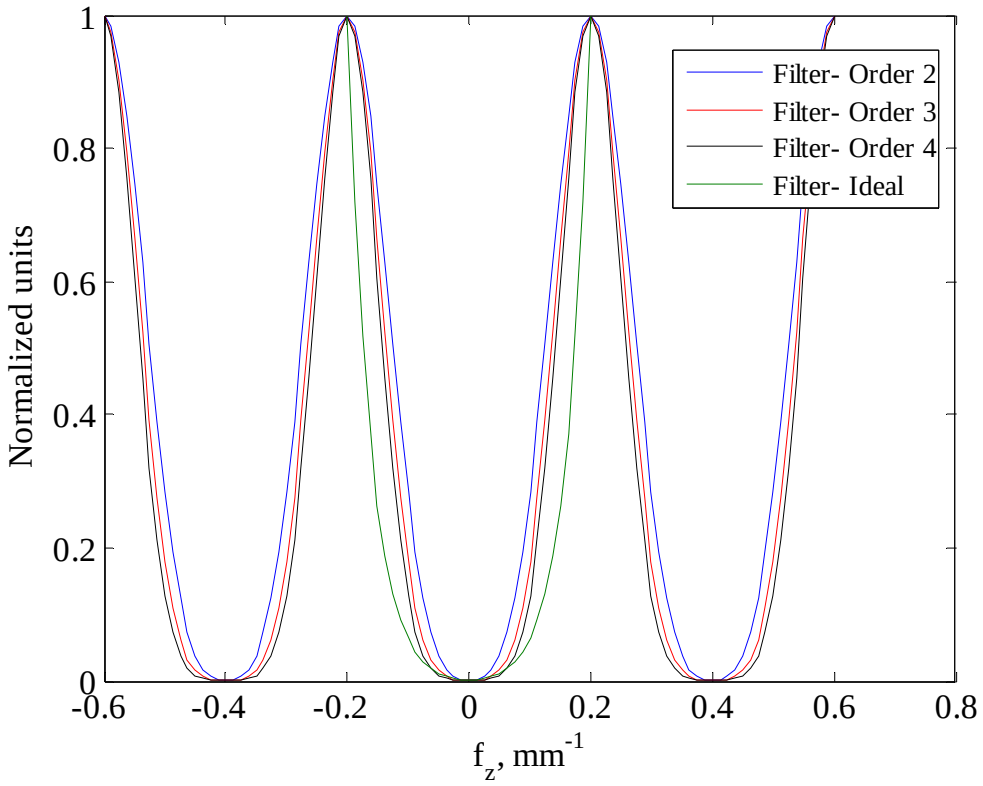

Figure 4.11: Simulated transfer functions of spatial filters of different orders obtained by using filter masks of different dimensions. The transfer function of ideal filter is included for comparison.

limits the performance of discrete filter at high frequencies regardless the order of truncation. This approximation can be improved by adopting four or six weights for the first order differential operator as [16]:

$$d = \frac{1}{24}\begin{bmatrix} -1 & 27 & -27 & 1 \end{bmatrix}$$
$$d = \frac{1}{1920}\begin{bmatrix} 9 & -125 & 2250 & -2250 & 125 & -9 \end{bmatrix} \quad (4.20)$$

But these approximations drastically increase the dimension of filter. For a third order filter, four points and six points approximation of differential operator make the dimension of filter mask 19x19 and 31x31 respectively, which are quite impractical from application point of view. This limitation influences to adopt the simplest approximation of the ideal derivative operator in generating filter mask.

4.3.5 Spatial Filter for Muscle

Same concept of designing inverse spatial filter for fat and skin layers can be adopted to eliminate the effect of anisotropic extracellular conduction medium for a certain depth inside muscle. This eventually helps to enhance the activity of deeper muscles. Lets assume that a muscle fiber is located at a depth y_1 and another muscle fiber is located at a depth y_2 from the muscle surface where $y_1 > y_2$ (Figure 4.12). Using the formula derived for multiple-layer model, the potential distribution at muscle surface can be simulated for both muscle fibers individually in spatial frequency domain. The behavior of transmembrane current is same for both cases as it is independent of the location of muscle fiber. So, the ratio between these two potentials determines the transfer

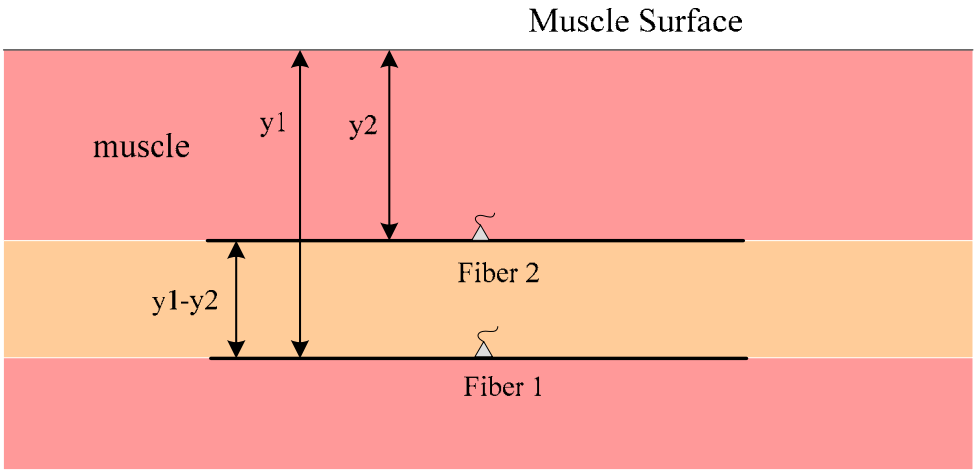

Figure 4.12: Model used to illustrate spatial filter inside muscle.

function of the anisotropic extracellular medium, which exists between these two fibers.

$$\frac{\varphi_1(\omega_x, y_1, \omega_z)}{\varphi_2(\omega_x, y_2, \omega_z)} = e^{-\omega_{ya}(y_1 - y_2)}$$

$$\therefore H_{y_1 - y_2}(\omega_x, \omega_z) = e^{-\omega_{ya}(y_1 - y_2)} \tag{4.21}$$

The transfer function depends on the thickness of the intermediate region and ratio of conductivity along z and x direction, R_a. The transfer function of the intermediate muscle layer is simulated considering y_1=10 mm and y_2=5 mm. The transfer function behaves as an anisotropic low pass filter having lower cutoff frequency along z direction (Figure 4.13). The effect of this intermediate layer can be eliminated by designing a high pass filter from the inverse of the transfer function as:

$$H^{-1}_{y_1 - y_2}(\omega_x, \omega_z) = e^{\omega_{ya}(y_1 - y_2)} \tag{4.22}$$

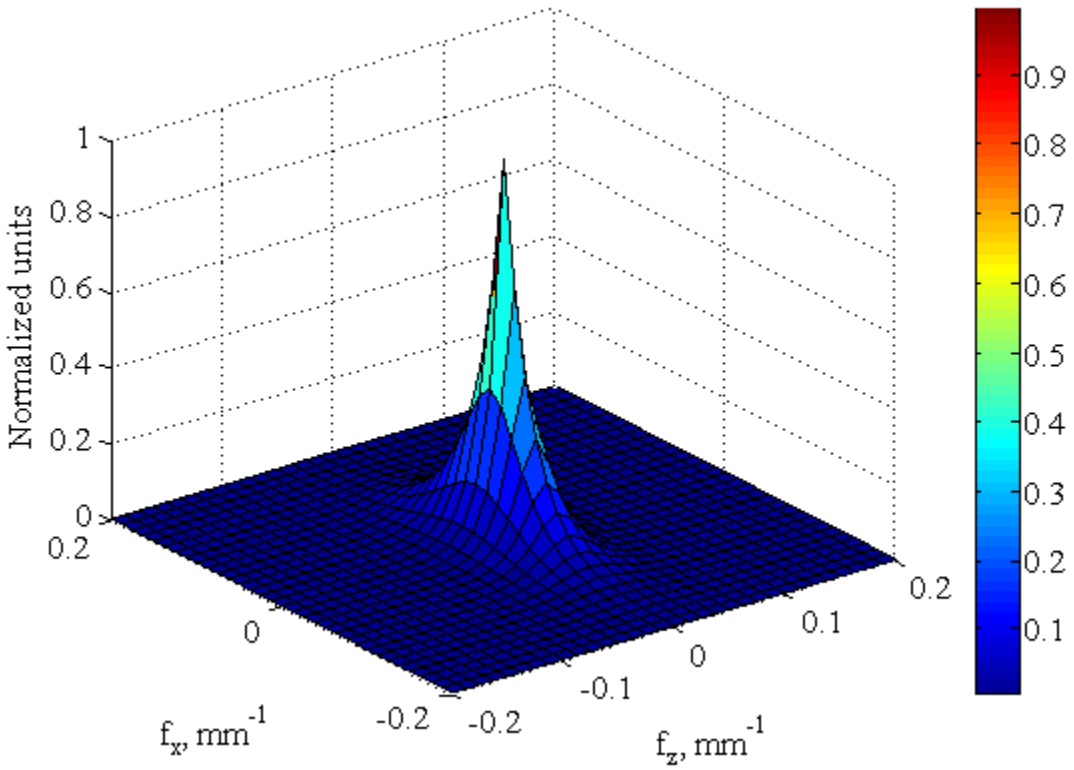

Figure 4.13: Transfer function of 5 mm thick anisotropic muscle layer in two-dimensional spatial frequency domain. The ratio of longitudinal and radial conductivity, R_a is assumed 5.24.

By expanding the exponential function,

$$H^{-1}_{y_1-y_2}(\omega_x,\omega_z)=\sum_{n=0}^{\infty}\frac{\left\{\omega_{ya}(y_1-y_2)\right\}^n}{n!}=\sum_{n=0}^{\infty}\frac{(y_1-y_2)^n}{n!}\left(\omega_x^2+R_a\omega_z^2\right)^{n/2} \tag{4.23}$$

It is quite impossible to obtain a finite series by expanding the binomial formula having a noninteger power. From the simulation result of Equation 4.23, it is found that the characteristics of third order approximated inverse filter approaches towards the ideal high pass filter if only even terms are considered by substituting *n* with *2m* (Figure 4.14).

$$H^{-1}_{y_1-y_2}(\omega_x,\omega_z)=\sum_{m=0}^{\infty}\frac{(y_1-y_2)^{2m}}{(2m)!}\left(\omega_x^2+R_a\omega_z^2\right)^m \tag{4.24}$$

This approximation eliminates the 'noninteger power' problem of expanding binomial Newton formula. Now, the approximated inverse transfer function can be written as:

$$H^{-1}_{y_1-y_2}(\omega_x,\omega_z)=\sum_{m=0}^{\infty}\sum_{r=0}^{m}\frac{(y_1-y_2)^{2m}}{(2m)!}\frac{m!}{r!(m-r)!}R_a^m\omega_z^{2m}\,\omega_x^{2(m-r)} \tag{4.25}$$

Implementing the concept of discrete differential operator the equation becomes,

$$H^{-1}_{y_1-y_2}(\omega_x,\omega_z)=\sum_{m=0}^{\infty}\sum_{r=0}^{m}(-1)^m\frac{(y_1-y_2)^{2m}}{(2m)!}\frac{m!}{r!(m-r)!}R_a^m(D_z)^{2m}(D_x)^{2(m-r)} \tag{4.26}$$

Replacing the discrete differential operator with its transfer function (Equation 4.16) and truncating the series up to order *N*, the approximated transfer function of inverse spatial discrete filter becomes,

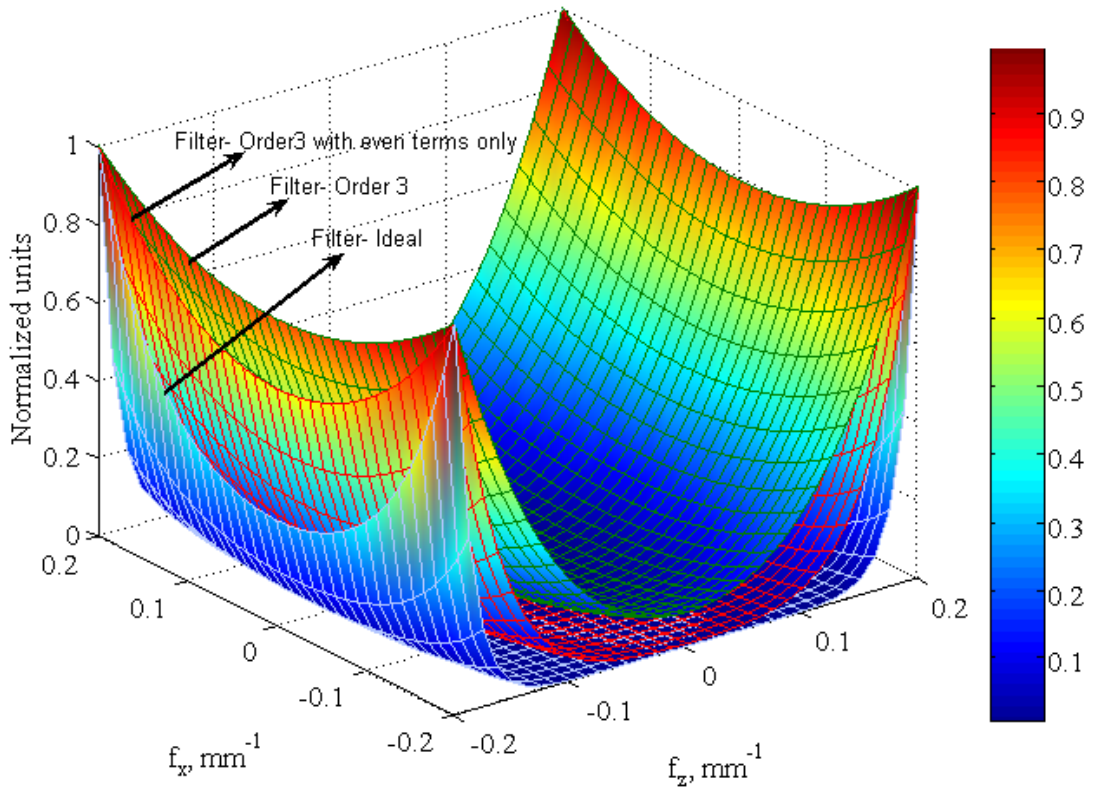

Figure 4.14: Comparison of ideal inverse spatial filter transfer function with a third order approximation for first three terms of series and first three even terms of the series by replacing *n* with *2m*.

$$H^{-1}_{y_1-y_2}(\omega_x,\omega_z)=\sum_{m=0}^{N}\sum_{r=0}^{m}2^{2m}\,\beta_m\,\frac{m!}{r!(m-r)!}\,R_a^m\sin^{2r}\left(\omega_z\frac{e}{2}\right)\sin^{2(n-r)}\left(\omega_x\frac{e}{2}\right) \quad (4.27)$$

where $\beta_n=\dfrac{(y_1-y_2)^{2m}}{(2m)!}$

Thus, the inverse spatial filter is a function of thickness of anisotropic muscle layer, whose effect need to be eliminated. Based on Equation 4.27, the approximated transfer function of third order discrete filter is simulated in Figure 4.15 maintaining the spatial resolution 2.5 mm and anisotropic conductivity ratio 5.24. The discrete spatial filter mask is calculated from the transfer function using the same procure mentioned in section 4.3.3. For a third order filter, the resulting normalized filter mask for a 5mm thick muscle layer is:

$$^{3}M_{normalized}=\begin{bmatrix} 0 & 0 & 0 & -0.0001 & 0 & 0 & 0\\ 0 & 0 & -0.0010 & 0.0024 & -0.0010 & 0 & 0\\ 0 & -0.0051 & 0.0248 & -0.0408 & 0.0248 & -0.0051 & 0\\ -0.0088 & 0.0650 & -0.1883 & 0.2659 & -0.1883 & 0.0650 & -0.0088\\ 0 & -0.0051 & 0.0248 & -0.0408 & 0.0248 & -0.0051 & 0\\ 0 & 0 & -0.0010 & 0.0024 & -0.0010 & 0 & 0\\ 0 & 0 & 0 & -0.0001 & 0 & 0 & 0 \end{bmatrix}$$

The size and shape of filter mask is same as the isotropic filter derived from fat and skin. But the values are not symmetric along x and z direction. The weighting coefficients are higher along z direction. It is obvious that the spatial widening effect plays the dominating role along the parallel direction of fiber. To analyze the application of spatial grid filter mask inside muscle, it is assumed that a 7x7 grid electrode is placed at the surface of muscle at 20 mm distant from the end plate and it has symmetry along the

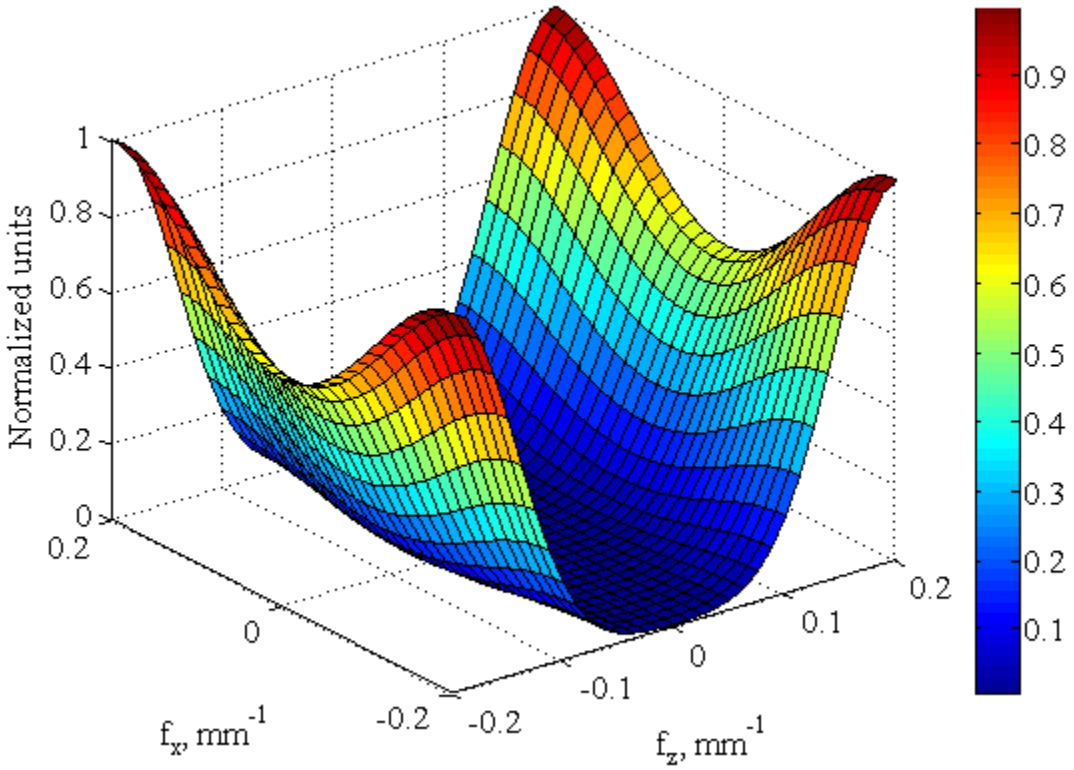

Figure 4.15: Transfer function of approximated inverse spatial filter of order three for a 5 mm thick muscle medium with R_a=5.24.

perpendicular direction of the fiber. The action potential signal is simulated in each electrode due to a muscle fiber located at 10 mm depth inside muscle considering its position with respect to the source. Then the filter mask is implemented upon the potential matrix of surface grid electrode. The output of the filter generates the single fiber action potential at the center electrode for a fiber, which is located 5 mm closer than the original fiber. Figure 4.16 shows the simulated action potential at the center electrode for a muscle fiber positioned at 10 mm and 5 mm respectively from muscle surface. Figure 4.17 illustrates the comparison between the normalized simulated signal and filtered signal for muscle fiber at 5 mm. The RMS error between these two signals is 5.425%. Moreover, it also eliminates the nontraveling signal located at the end of the SFAP profile. Thus, the spatial filtering technique can be adopted to enhance the activity of deeper muscle fibers by eliminating the effect of anisotropic muscle medium for a particular thickness.

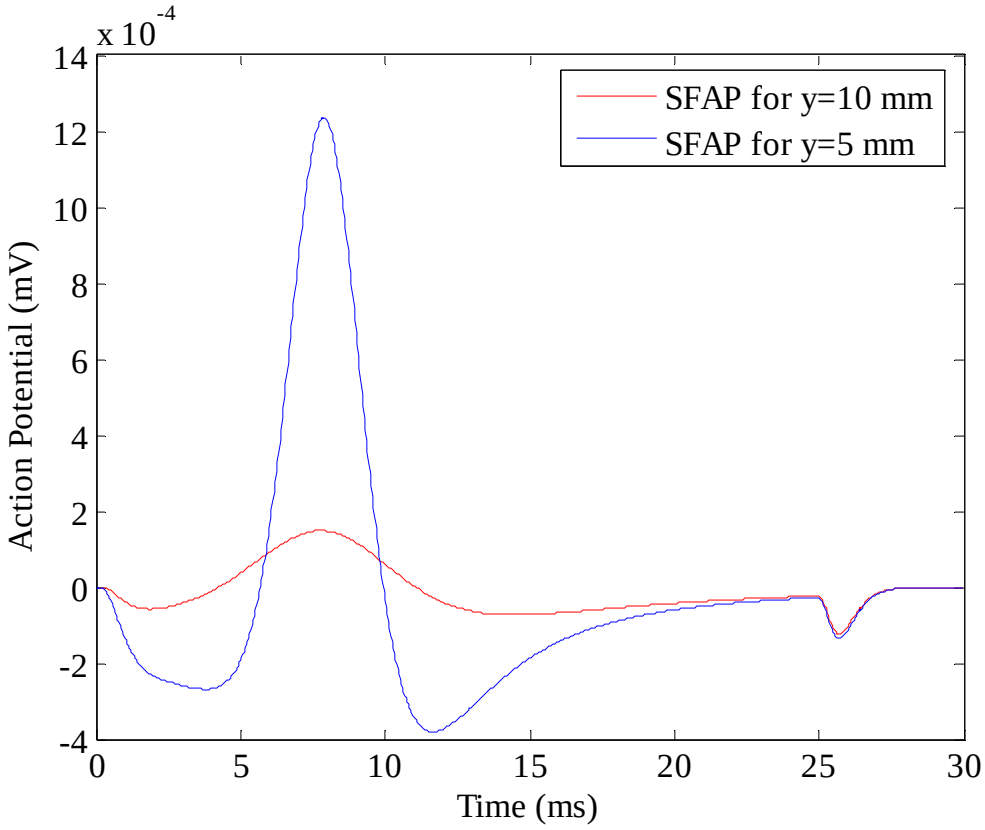

Figure 4.16: Simulated action potentials generated for a muscle located at the depth of 10 mm and 5 mm within the muscle.

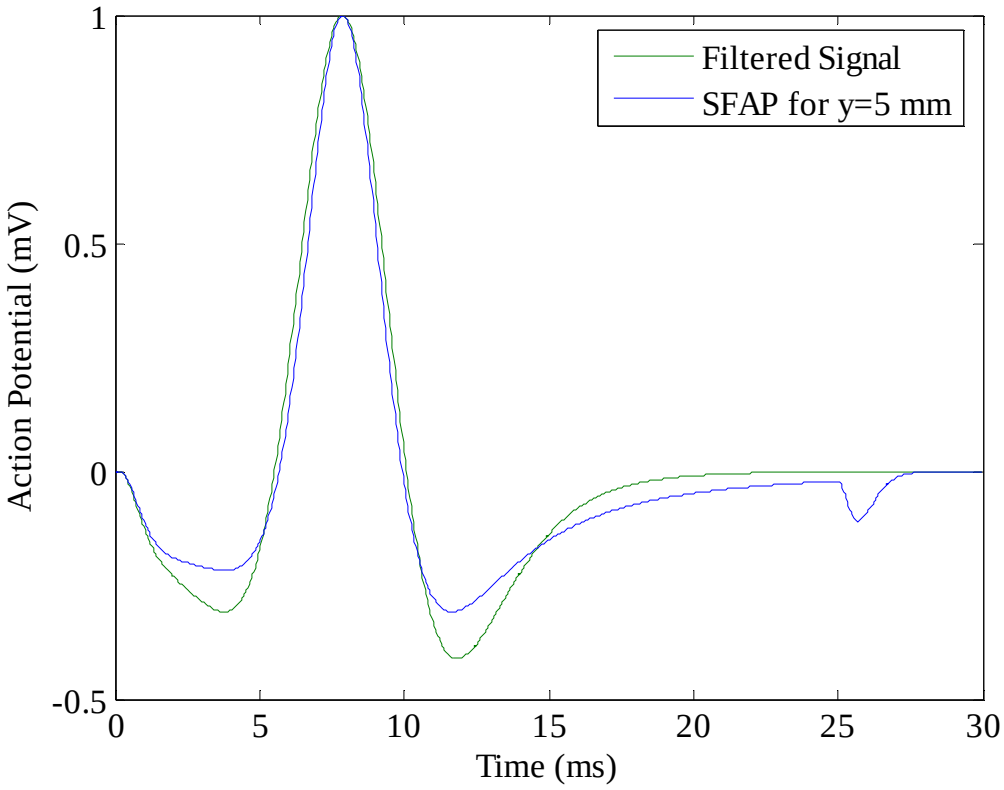

Figure 4.17: Comparison between simulated single fiber action potential for a fiber located at 5 mm depth inside muscle and the spatially filtered signal obtained by implementing filter mask on the signals of grid electrodes.

Chapter 5

Conclusion

5.1 Summary of the Work

Multi-channel SEMG technique is able to provide both classic and new information regarding the neuromuscular system in health and disease. The exploration of the possibilities of this technique relies on the precise and accurate detection of bioelectric signal generated inside muscle. That's why; numerous research activities are focused towards the quantization, decomposition, noise elimination and enhancement of SEMG signal using grid arrays. In this study, an innovation spatial filtering technique is proposed to enhance the selectivity of SEMG signal considering the effect of intermediate tissue layers between source and recording electrode. Studies have been performed on multiple-layer muscle model and two-dimensional grid electrode as an integral part of filter deign. The objectives of this study were:

- To develop an algorithm to simulate complete profile of SFAP signal at muscle surface using previously derived volume conduction model.
- To develop the multiple-layer muscle model incorporating the effect of subcutaneous fat and skin tissues in order to derive potential distribution at different layers.
- To determine the required minimum inter-electrode distance of two-dimensional

grid electrode considering spatial characteristics of SEMG signal.

- To design the two-dimensional spatial filter mask in order to eliminate the effect of isotropic fat and skin layers and enhance the activity of deeper muscles.

Based on these objectives the achievements of this work are summarized below:

From simulation, it is found that the transfer function of the extracellular medium behaves a low pass filter and its peak value shifts spatially with the position of recording electrode. The amplitude and frequency contents of SFAP signal decreases with increment of the depth of fiber inside muscle. The SFAP signal becomes biphasic to triphasic with the movement of electrodes along the parallel direction of fiber from the endplate region and the opposite situation occurs during radial movement of electrode. The spatial widening or dilation effect dominates in longitudinal direction and amplitude attenuation effect dominates in transverse direction of the fiber with movement of electrode. These findings reveal the spatiotemporal behavior of SEMG signal in two-dimensional surface grid electrode.

The activity of superficial muscles is substantially affected by thickness of fat and skin layers. The isotropic nature of fat and skin spreads the signal spatially and attenuates the amplitude of the signal severely. This effect increases with the increment of fat thickness and introduces limitation in measuring SEMG signal for obese people. As the grid electrode is placed at the surface of skin, the required minimum inter-electrode depends on the combined transfer function of the anisotropic and isotropic tissue layers. It is very

sensitive for the muscles located closer to the skin due to high rate of change of amplitude and phase of SEMG signal. Although the existence of fat and skin layers contributes some remedy in this respect, it drastically reduces the amplitude of the signal. To meet the Nyquist condition the minimum grid spacing has to be considered 2.5~3 mm to obtain the detected signal free from spatial aliasing and distortion.

The methodology of designing spatial filter electrodes is developed with an aim to invert the transfer function of fat and skin. The first order ideal differential operator is approximated with discrete differential operator having two element weights in space domain to derive the spatial filter mask for discrete grid electrodes. The developed spatial filter mask bears the characteristics of a high pass filter, as it is derived from the inversion of low pass filter. For a N order filter the dimension of diamond shaped mask is $(2N+1)\text{x}(2N+1)$ with only $2N^2+2N+1$ nonzero elements. Though the behavior of approximated filter approaches towards the ideal filter with the increment of order, it increases the dimension of filter mask, which corresponds to required number of electrodes in the grid. The optimum order of the filter is set at three considering a trade off between these two phenomena. The derived third order spatial filter has successfully compensated the spatial effect of 3 mm thick fat and 1 mm thick skin for a fiber at 5 mm depth inside muscle with 4.94% RMS error. This spatial filtering technique is extended by deriving an anisotropic filter mask to eliminate the effect of a particular thick anisotropic medium inside muscle. The transfer function of the filter exhibits higher cutoff frequency in parallel direction of fiber, as the spatial widening effect dominates in this direction. The spatial filter mask derived to negate the 5 mm thick muscle layer

successfully regenerates the SFAP signal originated by a fiber located at 5 mm depth inside muscle from the simulated signals of 7x7 grid electrodes due to a fiber located at 10 mm inside muscle with 5.425% RMS error.

5.2 Future Work

There are some limitations in proposed spatial filtering technique. Even though the derived spatial filter can successfully recover the spatial effect of the regenerated SFAP signal, it cannot fix the amplitude of the signal. That's why, normalized filter mask is used and the filtered and actual simulated signals are normalized for the comparison of spatial behavior. Another limitation is exists regarding the placement of grid electrode on the skin surface. This filter only works while the center electrode of the grid is placed just at the top of fiber in the same y-z plane. All electrodes need to be placed between the endplate and tendon of fiber.

Further steps can be taken to improve algorithm of spatial filter in order to adjust the attenuation of the signal. As the attenuation is not linear with thickness of fat and depth of muscle fiber, these two variables need to be incorporated in determining the gain of the filter. More complex spatial filtering technique can be developed incorporating the position of grid electrode as a parameter to determine grid coefficients. It will modify the shape, symmetry and values of filter mask according to the location of center electrode with respect to the endplate of the fiber.

References

1. Andreassen S, Rosenfalck A, “Ralationship of Intracellular and Extracellular Action Potentials of Skeletal Muscle Fibers,” CRC Critical Reviews in Bioengineering, vol. 6, pp. 267-306, 1981.
2. Blok J H, Dijk J P, Drost G, Zwarts M J, Stegeman D F, “A High-Density Multichannel Surface Electromyography System for the Characterization of Single Motor Units,” Review of Scientific Instruments, vol. 73, pp. 1887-1897, 2002.
3. Boisset S, Matson MS, “Quantitative Relationship Between Surface EMG and Intramuscular Electromyographic Activity in Voluntary Movement,” Amer J Phys Med, vol. 51, pp. 285-295, 1972.
4. De Luca CJ, Merletti R, “Surface Myoelectric Signal Cross talk among Muscle of the Leg,” Electroenceph Clin Neurophysiol, vol. 69, pp. 568-575, 1988.
5. DiFabio PP, “Reliability of Computerized Surface Electromyography for Determining the Onset of Muscular Activity,” Physical Therapy, vol. 67, No. 1, pp. 43-48, 1987.
6. Disselhorst-Klug C, Silny J, Rau G, “Improvement of Spatial Resolution in Surface-EMG: A Theoritical and Experimental Comparison of Different Spatial Filters,” IEEE Trans Biomed Eng, vol.44, No. 7, pp. 567-574, 1997.
7. Faina D, Rainoldi A, “Compensation of the Effect of Sub-cutaneous Tissue Layers on Surface EMG: A Simulation Study,” Medical Engineering and Physics, vol. 22. pp. 487-496, 1999.
8. Farina D, Arendt-Nielsen L, Merlitti R, Indino B, Graven-Nielsen T, “Selectivity of Spatial Filters for Surface EMG Detection From the Tibialis Anterior Muscle,” IEEE Trans Biomed Eng, vol. 50, No. 3, pp. 354-364, 2003.
9. Farina D, Cescon C, Merletti R, “Influence of Anatomical, Physical, and Detection-system Parameters on Surface EMG,” Biol. Cybern., vol. 86, pp. 445-456, 2002
10. Farina D, Merletti R, “A Novel Approach for Precise Simualtion of the EMG Signal Detected by Surface Electrode,” IEEE Trans Biomed Eng, vol. 48, No. 6, pp. 637-646, 2001
11. Farina D, Mesin L, Martina S, Merletti R, “A Surface EMG Generation Model woth Multilayer Cylindrical Description of the Volume Conductor,” IEEE Transaction on Biomedical Engineering, vol. 51, No. 3, pp. 415-426, 2004.
12. Ferdjallah M, Wertsch JJ, and Harris GF, “Effects of Surface Electrode Size on Computer Simulated Surface Motor Unit Potentials,” Electromyography and Clinical Neurophysiology, vol. 39, pp. 259-265, 1999.
13. Gootzen THJM, Stegeman DF, Van Oosterom A, “Finite Limb Dimensions and Finite Muscle Length in a Model for the Generation of Electromyographic Signals,” Electroenceph Clin Neurophysiol, vol. 81, pp. 152-162, 1991.
14. http://fourteen.apptechnc.net/~windelspecht/nervous/pages/neuromuscular_junction_jpg.htm.
15. http://www.training.seer.cancer.gov/module_anatomy/images/illu_muscle_structure.jpg.
16. Jahne B, Practical Handbook on Image Processing for Scientific and Technical Applications, 2nd Ed., CRC Press, 2004
17. Jahnke E, Emde F, Tables of Functions with Formulae and Curves, Dover Publications, New York, 1945.

18. Lapatki BG, Dijk JP, Janos IE, Zwarts MJ, Stegeman DF, " A Thin, Flexible Multielectrode Grid for High-density Surface EMG," J Appl. Physiol., vol. 96, pp. 327-336, 2004.
19. Lorente de No, "A Study of Nerve Physiology," Studies from the Rockefeller Institute for Medical Research, vol. 132, pp. 384-477, 1947.
20. Lowery M M, Stoykov N S, Taflove A, Kuiken T A, "A Multiple-Layer Finite-Element Model of the Surface EMG Signal," IEEE Transaction on Biomedical Engineering, vol. 49, pp. 446-454, 2002.
21. Lynn PA, "Direct On-line Estimation of Muscle Fiber Conduction Velocity by Surface Electromyography," IEEE Trans Biomed Eng, vol. 26, pp. 364-371, 1979.
22. Lyons K, Perry J, Gronley JK, Barnes L, Antonelli D, "Timing and Relative Intensity of Hip Extensor and Abductor Muscle Action During Level and Stair Ambulation: An EMG Study," Physical Therapy, vol. 63, pp. 1597-1605, 1983.
23. Masuda T, Miyano H, Sadoyama T, "The propagation of Motor Unit Action Potentials and Location of Neuromuscular Junction Investigated by Surface Electrode Arrays," Electroenceph Clin Neurophysiol, vol. 55, pp. 594-600, 1983.
24. Masuda T, Sadoyama T, "Topographical Map of Innervation Zones within Single Motor Units Measured with a Grid Surface Electrode," IEEE Trans Biomed Eng, vol. 35, pp. 623-628, 1988.
25. Masuda T, Sadoyama T, "Topographical Map of Innervation Zones within Single Motor Units Measured with a Grid Surface Electrode," IEEE Trans Biomed Eng, vol. 35, pp. 623-628, 1988.
26. Merletti R, Conte LL, Avignone E, Guglielminotti P, "Modeling of Surface Myoelectric Signals – Part I: Model Implementation," IEEE Trans Biomed Eng, vol. 46, No. 7, pp. 810-820, 1999
27. Nandedkar SD, Stalberg E, "Simulation of Single Muscle Fiber action Potentials," Med Biol Eng Computing, vol. 21, pp. 158-165, 1983.
28. Plonsey R, "Actions Potentials Sources and their Volume Conductor Fields," Proceedings of the IEEE, vol. 65, pp. 601-611, 1977.
29. Plonsey R, "The Active Fiber in a Volume Conductor," IEEE Trans Biomed Eng, vol. 21, pp. 371-381, 1974.
30. Rau G, Disselhorst-Klug C, "Principles of High-Spatial-Resolution Surface EMG (HSR-EMG): Single Motor Unit Detection and Application in the Diagnosis of Neuromuscular Disorder," Journal of Electromyography Kinesiology, vol. 7, pp. 233-239, 1997.
31. Reucher H, Gunter R, Silny J, "Spatial Filtering of Noninvasive Multielectrode EMG Part I. Introduction to Measuring Techniques and Applications," IEEE Trans Biomed Eng, vol. 34, pp. 98-105, 1987.
32. Roeleveld K, Stanberg A, Stalberg EV, Stegeman DE, "Motor unit size estimation of enlarged motor units with surface electromyography," Muscle & Nerve, vol. 21, pp. 878-886, 1998
33. Rosenfalck P, "Intra- and Extracellular Potential Fields of Active Nerve and Muscle Fibers," Acta Physiol. Scan., suppl. 321, 1969
34. Saladin KS, Anatomy & Physiology: The Unity of Form and Function, McGraw-Hill Companies, Inc., 2004.

35. Watson GN, A treatise of the Theory of Bessel Functions, 2nd Ed., Cambridge University Press, 1966

VITA

Mohammad Moshiur Rahman was born in Chittagong, Bangladesh, on November 23, 1977. He attended Ispahani Public Scholl in his elementary level and Chittagong College in his 11th and 12th grade of study. In 1993 he achieved Prime Minister Award for outstanding result in Secondary School Certificate examination. In 2002, he received his Bachelor's degree in Electrical and Electronic Engineering from Bangladesh University of Engineering and Technology, Bangladesh. He was awarded the university merit scholarship in junior and senior year of his undergraduate studies.

In August 2003, he joined the University of Tennessee, Knoxville (UTK), as a Masters student in the Department of Electrical and Computer Engineering. Before joining UTK, he worked in GrameenPhone Ltd., Dhaka as a system engineer in switch planning division. Prior that he served as a research and development engineer in Energypac Power Generation Ltd. Dhaka. During his Masters studies, he has worked in different research projects including "Wireless sensor design for real time acquisition of bioelectric signal", "Instrumentation of grid EMG mapping technique", "Computer muscle modeling and design of spatial grid filter" etc.